AD-A195 561 RECONSTRUCTION OF MULTIDIMENSIONAL SIGNALS FROM MULTIPLE LEVEL THRESHOLD CROSSINGS(U) MASSACHUSETTS INST OF TECH CAMBRIDGE RESEARCH LAB OF ELECTRON.. 1/2

UNCLASSIFIED A ZAKHOR JAN 88 TR-534 N00014-81-K-0742 F/G 12/1 NL

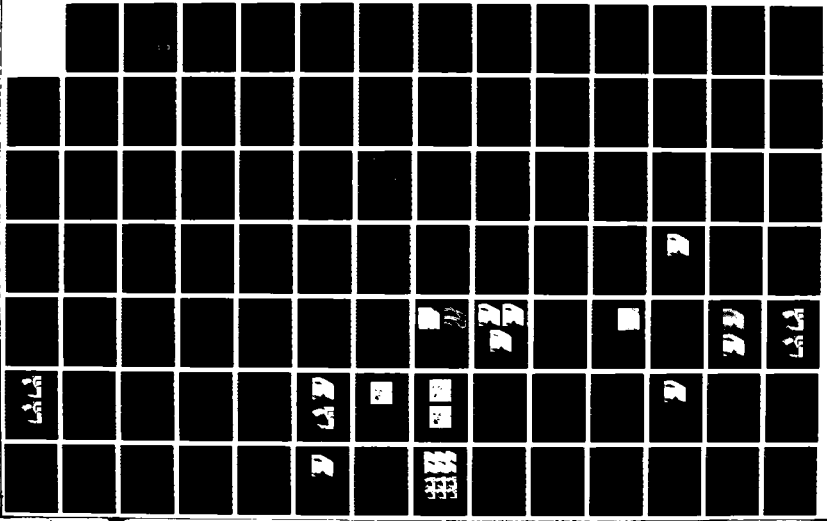

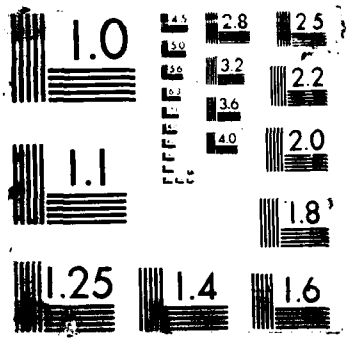
1.0
2.8
2.5
3.2
2.2
3.6
4.0
2.0
1.1
1.8
1.25
1.4
1.6

DTIC FILE COPY

(4)

AD-A195 561

Massachusetts Institute of Technology
Department of Electrical Engineering and Computer Science
Research Laboratory of Electronics
Room 36-615
Cambridge, Massachusetts 02139

Reconstruction of Multidimensional Signals from Multiple Level Threshold Crossings

Avideh Zakhor

Technical Report No. 534

January 1988

DTIC
ELECTE
MAY 25 1988
S D
H

This work has been supported in part by the Advanced Research Projects Agency monitored by ONR under Contract No. N00014-81-K-0742, in part by the National Science Foundation under Grant ECS-8407285, and in part by a Fannie and John Hertz Foundation Fellowship.

DISTRIBUTION STATEMENT A
Approved for public release;
Distribution Unlimited

UNCLASSIFIED

SECURITY CLASSIFICATION OF THIS PAGE

REPORT DOCUMENTATION PAGE

1a. REPORT SECURITY CLASSIFICATION	1b. RESTRICTIVE MARKINGS
2a. SECURITY CLASSIFICATION AUTHORITY	3. DISTRIBUTION/AVAILABILITY OF REPORT Approved for public release; distribution unlimited.
2b. DECLASSIFICATION/DOWNGRADING SCHEDULE	
4. PERFORMING ORGANIZATION REPORT NUMBER(S)	5. MONITORING ORGANIZATION REPORT NUMBER(S)
6a. NAME OF PERFORMING ORGANIZATION Research Laboratory of Electronics Massachusetts Institute of Technology 6b. OFFICE SYMBOL (If applicable)	7a. NAME OF MONITORING ORGANIZATION Office of Naval Research Mathematical & Information Scien.Div.
6c. ADDRESS (City, State and ZIP Code) 77 Massachusetts Avenue Cambridge, MA 02139	7b. ADDRESS (City, State and ZIP Code) 800 North Quincy Street Arlington, Virginia 22217
8a. NAME OF FUNDING/SPONSORING ORGANIZATION Advanced Research Projects Agency 8b. OFFICE SYMBOL (If applicable)	9. PROCUREMENT INSTRUMENT IDENTIFICATION NUMBER N00014-81-K-0742
8c. ADDRESS (City, State and ZIP Code) 1400 Wilson Boulevard Arlington, Virginia 22217	10. SOURCE OF FUNDING NOS. PROGRAM ELEMENT NO.: ; PROJECT NO.: ; TASK NO.: NR 049-506 ; WORK UNIT NO.:
11. TITLE (Include Security Classification) Reconstruction of Multidimensional Signals from Multiple Level Threshold Crossings	
12. PERSONAL AUTHOR(S) Avideh Zakhor	
13a. TYPE OF REPORT Technical 13b. TIME COVERED FROM _____ TO _____	14. DATE OF REPORT (Yr., Mo., Day) January 1988 15. PAGE COUNT 187
16. SUPPLEMENTARY NOTATION	
17. COSATI CODES FIELD / GROUP / SUB. GR.	18. SUBJECT TERMS (Continue on reverse if necessary and identify by block number)

19. ABSTRACT (Continue on reverse if necessary and identify by block number)

It has been shown theoretically that under mild conditions multidimensional signals can be recovered from one-level crossings (e.g. zero crossings). However, the accuracy with which locations of the one-level crossings need to be specified is large enough to limit the applicability of such a method in many practical situations. In this report, we will propose two major sampling strategies for reconstruction of signals from multiple-level crossings. The

In our first approach, we extend new theoretical results in multivariate polynomial interpolation theory, in order to define a variety of semi-implicit sampling strategies. These strategies, which provide sufficient conditions for recovery of multidimensional signals from non-uniform samples on lines of rational slope, are ultimately applied to the problem of reconstruction from multiple-level crossings. Although these semi-implicit results are

20. DISTRIBUTION/AVAILABILITY OF ABSTRACT UNCLASSIFIED/UNLIMITED ☒ SAME AS RPT. ☐ DTIC USERS ☐	21. ABSTRACT SECURITY CLASSIFICATION UNCLASSIFIED
22a. NAME OF RESPONSIBLE INDIVIDUAL Kyra M. Hall RLE Contract Reports	22b. TELEPHONE NUMBER (Include Area Code) (617) 253-2569 22c. OFFICE SYMBOL

DD FORM 1473, 83 APR EDITION OF 1 JAN 73 IS OBSOLETE.

UNCLASSIFIED

SECURITY CLASSIFICATION OF THIS PAGE

general enough to be used for recovery from signal crossings with arbitrary functions, they do not provide conditions for reconstruction of signals from an arbitrarily small number of thresholds. ~~In order~~ to circumvent this difficulty, ~~we propose~~ a second approach which is implicit, ~~and~~ uses algebraic geometric concepts to find conditions under which a signal is almost always reconstructible from its multi-level threshold crossings.

A problem distinct from that of uniquely specifying signals with level crossings is that of developing specific algorithms for recovering them from level crossing information, once it is known that the signals satisfy the appropriate constraints. We ~~propose~~ a variety of reconstruction algorithms are proposed for each of our two approaches, and ~~demonstrate~~ results for several images. Having proposed a variety of sampling and reconstruction strategies, we then present a preliminary investigation of their quantization characteristics. In doing so, we find that the dynamic range and bandwidth requirements for representation of signals via multiple level threshold crossings lie in between those of Nyquist and zero crossing representation. Moreover, under certain circumstances, our semi-implicit and implicit sampling strategies become identical to Nyquist sampling. This will bridge the gap between explicit, semi-implicit, and implicit sampling strategies, unify seemingly unrelated sampling schemes, and provide us with a spectrum of sampling schemes for multidimensional signals.

(mathematics)
transformations

demonstrated

Accession For
NTIS GRA&I ☑
DTIC TAB ☐
Unannounced ☐
Justification
By
Distribution/
Availability Codes
Avail and/or
Dist Special
A-1

Reconstruction of Multidimensional Signals from Multiple Level Threshold Crossings

Avideh Zakhor

B.S., California Institute of Technology (1983)

S.M., Massachusetts Institute of Technology (1985)

E.E., Massachusetts Institute of Technology (1986)

Submitted in Partial Fulfillment
of the Requirements for the
Degree of

Doctor of Philosophy

at the

Massachusetts Institute of Technology

October 1987

© 1987, Massachusetts Institute of Technology

Signature of Author _____
Dept. of Electrical Engineering and Computer Science
October 28, 1987

Certified by _____
Prof. Alan V. Oppenheim, Thesis Supervisor

Accepted by _____
Arthur C. Smith
Chairman, Electrical Engineering Department Committee
on Graduate Students, Massachusetts Institute of Technology

Reconstruction of Multidimensional Signals from Multiple Level Threshold Crossings

by

Avideh Zakhor

Submitted in partial fulfillment of the requirements for the degree of Doctor of Philosophy at the Massachusetts Institute of Technology.
September 30, 1987

Abstract

It has been shown theoretically that under mild conditions multidimensional signals can be recovered from one-level crossings (e.g. zero crossings). However, the accuracy with which locations of the one-level crossings need to be specified is large enough to limit the applicability of such a method in many practical situations. In this thesis, we will propose two major sampling strategies for reconstruction of signals from multiple-level crossings.

In our first approach, we extend new theoretical results in multivariate polynomial interpolation theory, in order to define a variety of semi-implicit sampling strategies. These strategies, which provide sufficient conditions for recovery of multidimensional signals from non-uniform samples on lines of rational slope, are ultimately applied to the problem of reconstruction from multiple-level crossings. Although these semi-implicit results are general enough to be used for recovery from signal crossings with arbitrary functions, they do not provide conditions for reconstruction of signals from an arbitrarily small number of thresholds. In order to circumvent this difficulty, we propose a second approach which is implicit, and uses algebraic geometric concepts to find conditions under which a signal is almost always reconstructible from its multilevel threshold crossings.

A problem distinct from that of uniquely specifying signals with level crossings is that of developing specific algorithms for recovering them from level crossing information, once it is known that the signals satisfy the appropriate constraints. We propose a variety of reconstruction algorithms for each of our two approaches, and demonstrate results for several images. Having proposed a variety of sampling and reconstruction strategies, we then present a preliminary investigation of their quantization characteristics. In doing so, we find that the dynamic range and bandwidth requirements for representation of signals via multiple level threshold crossings lie in between those of Nyquist and zero crossing representation. Moreover, under certain circumstances, our semi-implicit and implicit sampling strategies become identical to Nyquist sampling. This will bridge the gap between explicit, semi-implicit, and implicit sampling strategies, unify seemingly unrelated sampling schemes, and provide us with a spectrum of sampling schemes for multidimensional signals.

Thesis Supervisor: Alan V. Oppenheim
Title: Professor of Electrical Engineering, MIT.

سر بر دل آوردن گل لذ در دل برف

تاب نرم رقص ماهی در بلور آب

بوی عطر خاک باران خورده در کهسار

خواب گندمزارها در چشمهٔ مهتاب

آمدن، رفتن، دویدن

عشق ورزیدن

در غم انسان نشستن

پا بپای شادمانیهای مردم پای کوبیدن

آری، آری زندگی زیباست

زندگی آتشی دیرینه پا برجاست

گر بیفروزیش رقص شعله‌اش در هر دل پیداست

ورنه خاموشی است و خاموشی گناه ماست

Acknowledgments

I would like to express my deepest and warmest gratitude to my thesis supervisor, Prof. Alan Oppenheim for original problem suggestion, guidance and encouragement throughout the course of this thesis. His intellectual abilities, insight, friendly personality, and thrive for creating an exciting research atmosphere is simply unparalleled. I am grateful to him for being a good friend as well as an inspirational teacher.

The readability of this thesis was greatly enhanced by valuable comments from my readers, Profs. Nick Trefethen and Bruce Musicus. Nick has been particularly helpful in the initial stages of this work, and Bruce has provided many useful suggestions and improvements, as well as being a friend. I also thank Prof. Micheal Artin, Dr. Angela Vistolli, and Dr. William Ulmer of the Mathematics Dept. at MIT for helping me with the algebraic geometric results of Chapter 4. Prof. Schreiber deserves special thanks for letting me use the Autokon to generate the images in this thesis.

I acknowledge the value of several rewarding conversations with members of the Digital Signal Processing Group, Dr. David Izraelevitz, Dr. Susan Curtis, Ms. Roz Wright, Dr. Jay Kuo and my officemate Dr. Meir Feder. In particular, the results of one of the appendices of this thesis is due to a collaboration between Dr. Izraelevitz and myself. Joe Bondaryk deserves a special thank for proofreading the final draft of the thesis. Discussions with Meir have always been enjoyable no matter if they were of statistical nature or political. I thank the administrative staff at DSPG for making my stay in the group a pleasant one: Ms. Deborah Gage deserves special credit for answering my endless stream of questions, and for her dedication in running the group smoothly.

I thank Fannie and John Hertz Foundation for the generous financial support given to me during my graduate studies at MIT. I also acknowledge support from Advanced Research Projects Agency and National Science Foundation.

Many thanks go to Tina Bahadori, Elahe Sohbat, Mandana Hedayat, Julian Piot and Abeer Alwan for giving me friendship, fun and a social life. In particular, I am grateful to Tina Bahadori for helping me keep my sanity, and always making me feel better no matter what went wrong at school. Finally, I would like to thank my parents for their unbounded love, and for their patience in tolerating their daughter's long periods of absence from home during the

past ten years. I thank my mother now, as I will thank her forever for taking special interest in my education throughout my life, and it is to her that I dedicate this thesis.

Contents

1 Introduction **8**

1.1 Previous Results and Problem Formulation 13

2 Semi-Implicit Sampling Approach to Reconstruction **18**

2.1 Review of Bivariate Polynomial Interpolation Theory 19

2.2 Results in Bivariate Polynomial Interpolation Theory 23

2.2.1 Sampling Signals on Lines of Slope 1 25

2.2.2 Sampling Signals on Lines of Positive Integral Slope 31

2.2.3 Sampling Signals on Lines of Rational Slope 36

2.3 Applications of the Line-Sampling Strategy 45

2.3.1 Recovery from Crossings with Arbitrary Functions 46

2.3.2 Recovery from Projections 50

2.3.3 Recovery from Signal Values along Specific Paths 53

3 Reconstruction Algorithms for the Semi-implicit Sampling Approach **56**

3.1 Linear Least-Squares Approach 57

3.2 Recursive Approach 67

3.3 Line by Line Reconstruction Approach 72

3.3.1 Iterative Approach to Line by Line reconstruction 77

3.3.2 Application of POCS to the Iterative Algorithm 81

3.3.3 Examples of the Iterative Algorithm 84

3.4 Discussion 90

4 Implicit Approach to Reconstruction **93**

4.1 Theoretical Results 94

4.2 Reconstruction Algorithms 103

4.2.1 The Iterative Approach 106

4.2.2 Examples of the Iterative Algorithm 111

5 Preliminary Speculations on Quantization Properties **118**

5.1 Linear Least-Squares Approach 120

5.1.1 Quantization Procedures 121

5.1.2 Choice of the Number of Samples 122

5.1.3 Quantization Requirements 127

5.2 Iterative Approach 132

5.2.1 Quantization Requirements for Semi-implicit Sampling 134
5.2.2 Quantization Requirements for Implicit Sampling 138
5.3 Relationship to Nyquist Sampling 143
5.3.1 Implicit Sampling 145
5.3.2 Semi-implicit Sampling 148
5.4 Summary 152

6 Summary, Conclusions, and Future Directions of Research 155
6.1 Directions for Future Research 161

A Proof of Theorem 3.8 166

B A Bound on the Number of Finite Common Zeros Based on Polynomial Degree 170

C A Result in Algebraic Geometry 177

Chapter 1

Introduction

Signal reconstruction from partial information has been an active area of research for many years. Previous work in this area has involved developing conditions under which both one-dimensional and two-dimensional signals are uniquely specified with Fourier transform magnitude, phase, or signed-magnitude information [3,4,5,6,7]. Recently, Curtis *et.al.* considered the problem of signal reconstruction from Fourier transform sign information for multidimensional signals [8]. By exploiting the duality between space and frequency domains, they applied their result to the problem of reconstruction from zero-crossing information [9]. These zero crossing results are much less restrictive and more broadly applicable than the earlier ones based on two-dimensional extensions of one-dimensional results.

Representing signals with their zero crossings has important practical and theoretical implications. From a practical point of view, the zero-crossing results have applications in image processing and vision, where the information contained in the edges of objects is considered to be important [10]. Also, in situations where an image is clipped or otherwise distorted in such a way as to preserve zero-crossing or level-crossing information, it is possible, at least in principle, to recover the signal from its distorted version.

From a theoretical point of view, reconstruction from zero crossings is an example of *implicit*

sampling. Representation of a function by its samples or derivatives taken at preselected instants of time has received extensive attention in theory as well as in engineering practice. Sampling methods based on prespecified sampling times are referred to as *explicit*, in order to distinguish them from *implicit* methods of sampling, in which a representation is sought in terms of the instants in which the function assumes predetermined values. The idea of implicit sampling was introduced by Bond and Cahn [11], who considered representation and manipulation of one-dimensional signals by means of their real and complex zeros. Extensive work on this topic has been done by Voelcker [12], and computer simulation of these results has been reported by Sekey [13]. In addition, Bar-David [14] considered the important case of one-dimensional implicit sampling in terms of real variables alone. These results have been used to overcome distortions that are incurred either by intentional nonlinear processing or by inadvertent nonlinearities. Such nonlinearities might arise in single side-band systems, where the audio signals are typically hardlimited in order to decrease their dynamic range. Also, in magnetic tape recording, a strong higher frequency bias tone is usually added onto the signal to ensure fidelity in the presence of inherent material nonlinearity.

The majority of the research in implicit sampling has been restricted to one-dimensional problems. Indeed, the zero crossings results of Rotem and Zeevi [15] and Curtis *et.al.* [8,9] are the only examples of implicit sampling for multidimensional signals. Rotem and Zeevi's results are an extension of Logan's [16] one-dimensional result, which only deals with bandpass signals. The results due to Curtis *et.al.* however, are truly two-dimensional, since they take advantage of the fact that, in contrast to the one-dimensional case, the zero crossing contours in two or higher dimensions contain infinitely many points. These results are much less restrictive and more general than those based on the extension of one-dimensional results. However, the

accuracy with which the locations of the zero crossings need to be specified is large enough to limit their applicability in many practical situations. In effect, by representing the two-dimensional signal with zero crossings or threshold crossings, the amplitude information of the original signal is embedded in the exact location of the threshold crossings. Consequently, while the original signal can be sampled at the Nyquist rate, the threshold crossing representation may require a considerably higher, possibly infinite sampling rate to preserve the threshold crossing locations adequately. Thus, the total number of bits or the bandwidth required in the threshold crossing representation, is much higher than that required by sampling and quantizing the original signal. Therefore, the results on signal reconstruction from threshold crossings are more useful in applications in which the exact threshold crossing points are available.

It is possible, however, to view the representation of signals with threshold crossings as a trade-off between bandwidth and dynamic range, in the sense that if the available bandwidth is sufficient to preserve the threshold crossings accurately, then the dynamic range requirements are significantly reduced. On the other hand, representation of signals via their samples at the Nyquist rate can be considered as requiring minimal bandwidth and infinite dynamic range. This is because exact recovery of signals via Nyquist sampling, requires amplitude information at prespecified points, to infinite precision. Thus, the natural question which arises is whether or not there are intermediate sampling and reconstruction schemes, whose characteristics lie between these two extremes. Our objective in this thesis has been to derive sampling schemes which bridge the gap between Nyquist sampling and zero-crossing representations by enabling us to recover signals from multiple level threshold crossings. To this end, we have proposed a variety of semi-implicit and implicit sampling strategies in Chapters 2 and 4 respectively. Semi-implicit samples of a multidimensional signal are defined to be points whose coordinates are

mathematically related to each other. As we will see, some of our results on reconstruction from level crossings are general enough to be used for recovery of signals from their crossings with arbitrary functions. Possible applications of these results are for conversion of half tone images to continuous tone ones [17]. In addition, our results can also be applied to the more general problem of reconstruction from non-uniformly spaced samples. Reconstruction of functions from their samples on nonuniformly distributed locations is an important task in many applications such as machine vision [18,19], radio astronomy [20], and computed tomography [21], as well as natural sciences such as geology, meteorology, and oceanography. Several techniques based on non-harmonic Fourier series have been proposed [22,23] for reconstruction of bandlimited, one-dimensional functions, sampled at irregular intervals. These methods, however, are limited to sample sequences which have only minor deviations from uniform. Methods that have been used to perform such reconstructions for multidimensional functions include nearest-neighbor and bilinear interpolation, surface functional minimization by relaxation or gradient descent methods, and Gaussian smearing resampling. However, these methods either do not result in a minimum possible reconstruction error, or they require *a priori* knowledge about the form of the function. In fact, the only exact reconstruction strategy for the multidimensional case, proposed by Clark [24], is somewhat restrictive and its corresponding algorithm is rather heuristic. As we will see, part of our results on reconstruction from level crossings are general enough for recovery of signals from their non-uniform samples.

In summary, our objective in this thesis has been to derive semi-implicit and implicit sampling schemes, whose characteristics lie in between the Nyquist and zero-crossing representations. These strategies result in methods of reconstructing multidimensional signals from their multiple level threshold crossings, thus, providing a bridge between Nyquist reconstruction from

explicit samples at prespecified points and reconstruction via one-level crossings. As it turns out, some of these sampling techniques are general enough to be used in problems, such as reconstruction from crossings with arbitrary functions or from non-uniformly spaced samples.

The outline of this thesis is as follows. We shall begin by briefly reviewing related research on reconstruction from zero-crossings and formulating the problem of reconstruction from multi-level threshold crossings. In Chapter 2 we develop new results in bivariate polynomial interpolation theory which are ultimately used to derive semi-implicit sampling strategies for bandlimited, periodic (BLP) signals. Chapter 3 describes various reconstruction algorithms for the sampling strategies of Chapter 2. In Chapter 4, we propose a second strategy for reconstruction from multiple level threshold crossings. Although the semi-implicit approach of Chapter 2 can be applied to more general problems such as reconstruction from non-uniformly spaced samples or reconstruction from arbitrary function crossings, the results in Chapter 4 are less restrictive in the sense that they enable us to reconstruct signals from their crossings with arbitrary number of thresholds. In Chapter 5, we will present the results of a preliminary investigation of the quantization properties of the various sampling and reconstruction strategies described throughout the thesis. More specifically, we will show how quantization characteristics of reconstruction from multiple level crossings vary as a function of the number of thresholds. As we will see, the representation of two-dimensional signals, via their amplitude quantized explicit samples, is intimately related to their position quantized implicit or semi-implicit samples. Indeed, sampling and reconstruction from multiple level crossings, together with Nyquist and zero crossing sampling, provide us with a wide spectrum of signal representation with different bandwidth and dynamic range requirements. Finally, conclusions and future directions of research are included in Chapter 6.

In the remaining part of this chapter, we will briefly review the existing results on reconstruction from one-level crossings, and formulate the problem of reconstruction from multiple level threshold crossings.

1.1 Previous Results and Problem Formulation

There has been a great deal of interest in the zero crossing representation of signals in recent years. Most of the results on the unique specification of one-dimensional signals are based upon the fact that a bandlimited function is entire and is, thus, uniquely specified by its real and complex zeros to within a constant and exponential factor. An arbitrary bandlimited function is uniquely specified by its real zero crossings, if all of its zeros are real. Thus, a number of previous research efforts concentrated on identifying the conditions under which signals have only real zeros and on developing methods for modifying a signal so that all of its zeros become real [14]. Despite this, most one-dimensional, bandlimited signals encountered in practice, do not satisfy the constraints associated with these results. They are not uniquely specified by their zero crossings unless they satisfy some additional constraints, which effectively guarantee that they contain a sufficient number of zero crossings.

Although a considerable amount of theoretical work has been devoted to the problem of reconstruction of one-dimensional signals from zero crossings, much less work has been devoted to the corresponding two-dimensional problem. Logan's result has been extended to two dimensions [10,15] by requiring a one-dimensional signal derived from the original two-dimensional one to satisfy the constraints of Logan's theorem. However, the two-dimensional problem is fundamentally different from the one-dimensional one, since, in two dimensions, the zero crossings are, in general, contours rather than isolated points. Curtis and Oppenheim [9] were first to take

advantage of this fact; their main result states that for a BLP signal with a $(2N+1) \times (2N+1)$ region of support in the Fourier domain, $16N^2 + 1$ or more samples of the zero crossings are sufficient to reconstruct the signal to within a scale factor.

As shown in [9], in carrying out the above reconstruction, the locations of the zero crossings need to be specified accurate to 16 digits. Less accurate specification of the crossings results in unsuccessful reconstruction. Thus, by representing the two-dimensional signal with zero crossings or threshold crossings, the amplitude information in the original signal is embedded in the exact location of the threshold crossings. Consequently, while the original signal can be sampled at the Nyquist rate with many bits for amplitude specification, the threshold crossing representation requires a considerably higher sampling rate to preserve the threshold crossing locations adequately. Thus, it is possible to view the representation of signals with threshold crossings as a trade-off between bandwidth and dynamic range, in the sense that if the available bandwidth is sufficient to preserve the threshold crossings accurately, then the dynamic range requirements are significantly reduced. On the other hand, representation of signals via their samples at the Nyquist rate can be considered as one which requires minimal bandwidth and large dynamic range. Our main goal in this thesis is to develop intermediate sampling schemes for reconstruction from multiple level threshold crossings, so that their bandwidth and dynamic range requirements lie in between Nyquist and one-level crossing representation.

Our approach to the above problem has been to represent BLP signals in terms of polynomials. The reasons for doing so are twofold. First, BLP signals, which represent a fairly large and general class of signals, can be written as polynomials, via their Fourier series expansions. Second, since reconstruction from multiple level crossings is a special case of reconstruction from non-uniform samples, we hope to be able to use a variety of mathematical results on

polynomial interpolation theory. Consider a BLP signal

$$f(x,y) = \sum_{k_1=-N}^{N} \sum_{k_2=-N}^{N} F(k_1,k_2) e^{j2\pi(k_1 x + k_2 y)} \tag{1.1}$$

The polynomial representation of the above signal is given by:

$$\begin{aligned} g(W_1,W_2) &= f(x,y) W_1^N W_2^N \\ &= \sum_{k_1=0}^{2N} \sum_{k_2=0}^{2N} F(k_1-N, k_2-N) W_1^{k_1} W_2^{k_2} \end{aligned} \tag{1.2}$$

where

$$W_1 = e^{j2\pi x}$$

$$W_2 = e^{j2\pi y}$$

Since reconstruction of $f(x,y)$ is equivalent to finding the coefficients of the polynomial $g(W_1,W_2)$, results from multivariate polynomial interpolation theory can be applied directly to a variety of multidimensional reconstruction problems.

Unlike the univariate case, interpolation with multivariate polynomials is a non-trivial task. Whereas n arbitrary samples of an univariate (one-dimensional) polynomial of degree $n-1$ are sufficient to find its coefficients, the analogous result in dimensions higher than one does not hold, primarily because there are no *Chebychef systems* in R^s for $s \geq 2$. Chebychef systems are important in interpolation theory, and have been studied extensively by many people including Karlin [26], Karlin and Studen [27], and Krein [28]. The definition is as follows:

Definition 1.1 *A linearly independent set of continuous functions $\{u_0(x), ..., u_n(x)\}$ defined on $[a,b]$ is a Chebychef system if for any $a \leq x_0 < ... < x_n \leq b$ and $y_0, ..., y_n \in R$, there is a unique linear combination*

$$u(x) = \sum_{j=0}^{n} a_j u_j(x)$$

satisfying

$$u(x_i) = y_i \qquad\qquad i = 0, ..., n$$

Clearly, the set of n continuous functions consisting of the powers of x form a Chebychef system. Another example of a Chebychef system is

$$u_i(x) = e^{\lambda_i x} \qquad i = 0, 1, ..., n$$

where λ_i are distinct and $x \in (-\infty, +\infty)$ [29]. Chebychef systems are helpful for studying univariate interpolation. Unfortunately, as soon as we turn to multivariate interpolation, we must leave them behind, since there is no set of n universal functions which can be used for interpolation at *any* n distinct points. An implication of this result is that powers of x or y do not form a Chebychef system in R^2, and thus, bivariate polynomials are not, in general, uniquely reconstructible from their samples at arbitrary locations. Indeed, if arbitrary samples of a bivariate polynomial uniquely specified its coefficients, the problem of reconstruction from multiple level threshold crossings would have been trivial. This is because samples of our threshold contours could then be used to find the the coefficients of $g(W_1, W_2)$ or equivalently $f(x, y)$.

There are two ways out of this dilemma. One would be to study ***conditionally regular*** interpolation methods. An interpolation method is called ***regular***, if it is uniquely solvable for any selection of the points of interpolation. Conditionally regular interpolation methods are not solvable for all selection of points, but only for most of them [31]. Roughly speaking, they are uniquely solvable with probability 1. For methods of this type, if one has a concrete problem and selects the interpolation points at random, it will be extremely unlikely that the problem will be unsolvable. We will take this approach to find the sufficient conditions for reconstruction from multilevel threshold crossings in Chapter 4. The second approach is to impose certain restrictions on the locations of the interpolation points. These conditions will

guarantee that the resulting interpolation problem has a unique solution. Our approach in Chapter 2 consists of developing a series of conditions under which bivariate polynomials, or equivalently, two-dimensional signals can be uniquely recovered.

Chapter 2

Semi-Implicit Sampling Approach to Reconstruction

As we saw in secton (1.1), the polynomial representation of multidimensional signals suggests that a wide variety of multidimensional reconstruction problems can be approached via results from multivariate polynomial interpolation theory. In addition, we saw that the inherent difficulty in multivariate interpolation is the lack of existence of Chebychef systems in dimensions higher than one. In Chapter 4, we will propose conditionally regular interpolation as a possible way to circumvent this difficulty. In this chapter, however, our approach is to derive a number of theoretical results on multivariate polynomial interpolation theory by imposing constraints on the location of interpolation points. These results will ultimately be used to develop a spectrum of sampling strategies for reconstruction of multidimensional signals from non-uniformly spaced samples in general, and multiple level crossings in particular.

We will begin this chapter with a brief review of existing results in bivariate polynomial interpolation. In section (2.2), we will derive three results in multivariate interpolation theory, which become progressively more general. Utilizing polynomial representation of BLP signals, as described in the previous chapter, we apply our new theoretical results on multivariate interpolation to derive a variety of semi-implicit sampling strategies for the reconstruction of signals

from their non-uniformly spaced samples on lines of rational slope. As we will see in section (2.3), these semi-implicit sampling schemes can be applied to the problem of reconstruction from level crossings and to a variety of other problems such as reconstruction from crossings with arbitrary functions and reconstruction from projections.

2.1 Review of Bivariate Polynomial Interpolation Theory

In this section, we will review some of the existing results from bivariate polynomial interpolation theory. We will be concerned primarily with interpolation using only a function's values as opposed to its derivatives. As we mentioned earlier, our approach in this chapter involves constraining the locations of the interpolation points, in order to guarantee unique recovery of the polynomials and their associated BLP signals.

Bivariate polynomial interpolation can be done either in Π_n, the space of polynomials with total degree less than or equal to n, or in $\Pi_{(n,m)}$, the space of polynomials $p(w,z)$ with maximum degree n in w and m in z. The total degree of a polynomial $p(w,z)$ is defined to be the degree of the one-dimensional polynomial $p(w,w)$. The regions of support of the coefficients of polynomials in Π_2 and $\Pi_{(2,2)}$ are illustrated in figure (2.1). The most general result on interpolation in Π_n was derived by Gasca and Maeztu [36] in 1982. The basic idea behind their results is to choose a set of straight lines r_i in R^2, each of which is associated with a polynomial of first degree in w and z. With each line r_i, we consider a set of straight lines $r_j^{(i)}$ in such a way that the intersections determined by $r_j^{(i)}$ on r_i are the points at which the interpolation data will be given. The lines r_i and/or $r_j^{(i)}$ may appear with multiplicity greater than one, leading to derivative values as interpolation data. In general, the formulation with derivatives results in the Hermite interpolation problem, although the simplest case reduces to

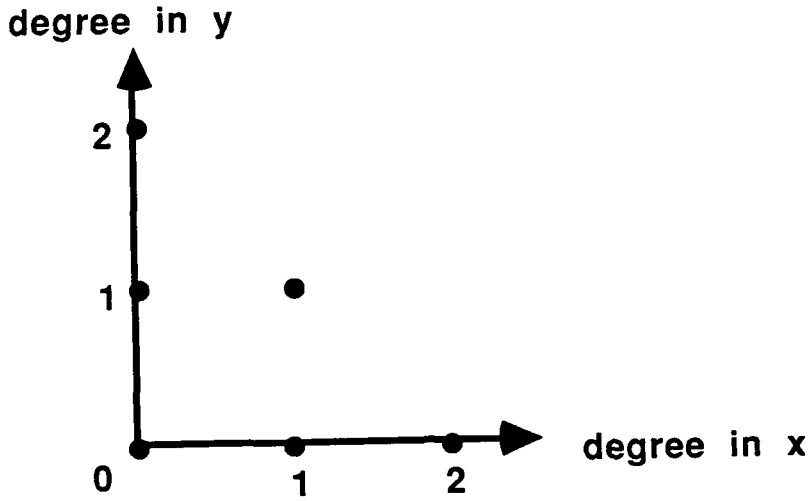

(a)

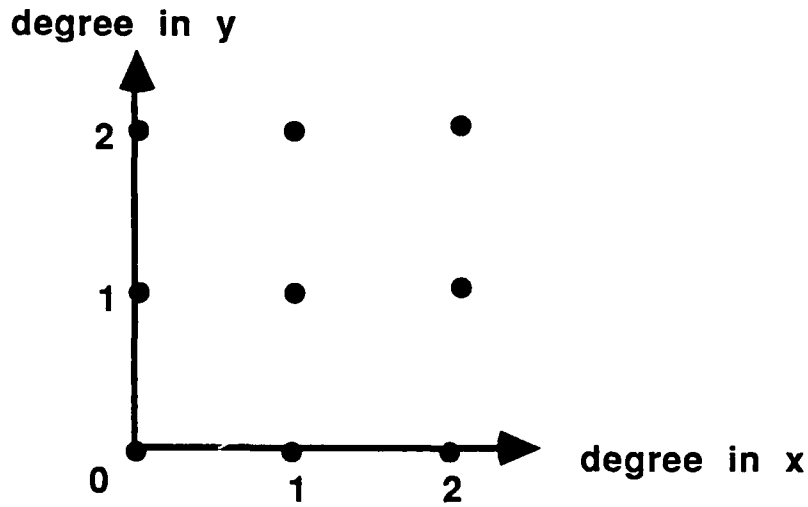

(b)

Figure 2.1: *Triangular and rectangular regions of support of polynomials in: (a)* Π_2; *(b)* $\Pi_{(2,2)}$.

Lagrange interpolation which only uses the sample values. In any case, products of lines r_i and $r_j^{(i)}$ are constructed in order to obtain a set of polynomials spanning the vector space in which the interpolation problem has a unique solution [36]. The most important consequence of the theoretical developments of Gasca and Maetzu can be stated as follows:

Theorem 2.1 (Gasca and Maetzu [36]) *Consider the distinct lines $l_0, ..., l_n$ with the set of distinct points*

$$\{(w_j^{(i)}, z_j^{(i)}) | j = 0, 1, ..., i\}$$

on l_i. If none of the interpolation points $(w_j^{(i)}, z_j^{(i)})$ are on the intersection of any two lines from $l_0, ..., l_n$, then for any data set

$$\{t_j^{(i)} \mid j = 0, ..., i;\ i = 0, 1, ..., n\}$$

there is a unique bivariate polynomial $p \in \Pi_n$ such that

$$p(w_j^{(i)}, z_j^{(i)}) = t_j^{(i)} \quad 0 \le j \le i\ ,\ 0 \le j \le n$$

The proof is included in [36,29,30], and an example of the geometric distribution of the sampling points required by this theorem for $n = 2$ is shown in figure (2.2). A special case of the above theorem was proposed earlier by Stenger [35] and Chung [32]. Their results primarily deal with the case where the interpolation points are chosen on parallel lines. The proof for the case where the interpolation lines are chosen parallel to the x axis is rather straightforward, and can be briefly outlined in the following manner. Let us denote the points on the ith line parallel to the x axis by

$$\{(w_j, z_i) \mid j = 0, 1, ..., i\}$$

We can rewrite the polynomial $p(w, z)$ as:

$$p(w, z) = q_n(z) + wq_{n-1}(z) + ... + w^{n-1}q_1(z) \tag{2.1}$$

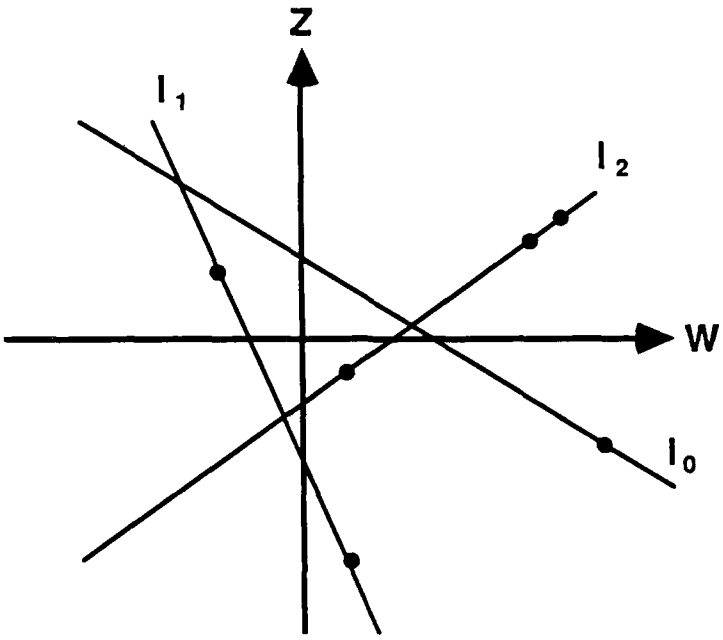

Figure 2.2: *Geometric distribution of the sampling points of Theorem (2.1) for n=2.*

where $q_k(z)$ is a polynomial of degree $k-1$ in z. In the first stage, we substitute the $n+1$ points on l_n into the above equation in order to find $q_k(z_n)$ for $1 \leq k \leq n$. Since $q_1(z)$ is a constant, its value can be determined by $q_1(z_n)$. In the second stage, the n points on l_{n-1} are used to specify $q_k(z_{n-1})$ uniquely for $2 \leq k \leq n$. Using the value of $q_2(z_n)$ from the first stage and $q_2(z_{n-1})$ from the second stage, we can uniquely specify the two coefficients of the polynomial $q_2(z)$. Similarly in the ith stage we first use the points on the $(n+1-i)$th line to find $q_k(z)$ for $1 \leq k \leq i-1$, and then use $q_i(z_l)$ for $n+1-i \leq l \leq n$ in order to find the i coefficients of $q_i(z)$. Repeating this procedure, we can uniquely determine the polynomial $q_i(z)$ for $1 \leq i \leq n$, so that $p(w,z)$ becomes completely and uniquely determined.

Most of the results in bivariate polynomial interpolation theory deal with interpolation in

Π_n, the space of polynomials of total degree less than or equal to n. The only existing result on interpolation in $\Pi_{(n,m)}$, the space of polynomials $p(w,z)$ of maximum degree n in w and m in z, deals with the case where the interpolation points are on a nonuniform rectangular grid and can be stated as follows:

Theorem 2.2 (Non-uniform Rectangular Sampling [29,32,33,34]) *Given a set of points*

$$\{(w_i, z_j) | i = 0, ..., n; \quad j = 0, ..., m;\}$$

and data

$$\{t_{ij} | i = 0, ..., n; \quad j = 0, ..., m;\}$$

there exists a unique bivariate polynomial

$$p(w,z) = \sum_{i=0}^{n} \sum_{j=0}^{m} a(i,j) w^i z^j$$

such that

$$p(w_i, z_j) = t_{ij} \qquad i = 0, ..., n; \qquad j = 0, ..., m;$$

The proof is straightforward and is given in many references including [29,32,33,34]. Intuitively, for a fixed value of $j = j_0$, the points $(w_0, z_{j_0}), ..., (w_n, z_{j_0})$ can be used to find the coefficients $a(0, j_0), ..., a(n, j_0)$. Repeating this procedure, we can find all the coefficients of $p(w,z)$. An example of the geometric distribution of the sampling points required by this theorem for $n = 2$ and $m = 1$ is shown in figure (2.3). Applying the above theorem to equations (1.2) and (1.1), we conclude that samples of a two-dimensional BLP signal on a non-uniform rectangular grid shown in figure (2.3) can be used to reconstruct it uniquely.

2.2 Results in Bivariate Polynomial Interpolation Theory

As we saw in Theorem (2.1) of the previous section, one way to interpolate in Π_n, the space of polynomials of total degree n, is to choose $n+1$ distinct lines $l_0, ..., l_n$, and select the

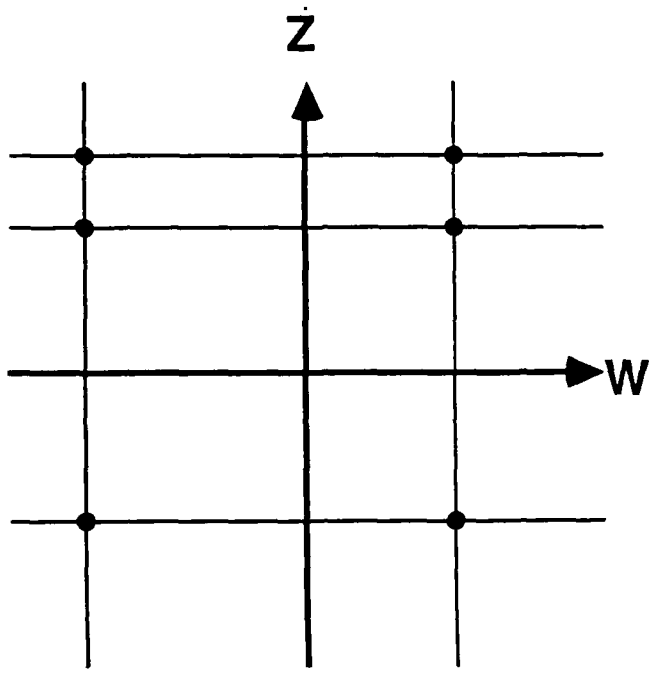

Figure 2.3: *Geometric distribution of the sampling points of Theorem (2.2) for* $n = 2$ *and* $m = 1$.

interpolation points from these lines. More specifically, if we choose $i + 1$ points on l_i, the ith line, then the interpolation problem is guaranteed to have a unique solution. Since in most signal processing applications, the support regions of the Fourier coefficients of the two-dimensional signals under consideration are rectangular, we are primarily interested in interpolation in the space of polynomials whose coefficients have rectangular rather than triangular region of support. Thus, it seems natural to extend the theorems of the previous section from Π_n, the space of polynomials of maximum degree n in w and z, to $\Pi_{(n,n)}$, the space of polynomials of maximum degree n in w and maximum degree n in z. As we will see in this section, generalization of Theorem (2.1) provides us with a spectrum of powerful sampling schemes for two-dimensional BLP signals. More specifically, the extension of Theorem (2.1) in section

(2.2.1) implies that if we choose N distinct lines of slope 1 in an image with a $N \times N$ region of support in the Fourier domain, then $2i + 1$ arbitrary samples on the ith line are sufficient for reconstruction of the image. In section (2.2.2), we generalize this result to the case where all the sampling lines have fixed positive integer slopes. Finally, in section (2.2.3) we will use a modified version of Bezout's theorem to generalize the results of section (2.2.2) to the case where our sampling lines have different rational slopes. Unlike the constructive proofs of sections (2.2.1) and (2.2.2), the algebraic geometric approach of section (2.2.3) will not provide an algorithmic procedure for the actual reconstructions.

The theoretical results of this section are applied to the problem of reconstruction from threshold and sine-wave crossings and a variety of other reconstruction problems in section (2.3). The actual reconstruction algorithms and their numerical properties are discussed at length in Chapters 3 and 5.

2.2.1 Sampling Signals on Lines of Slope 1

In this section, we will extend Theorem (2.1) of section (2.1) to the case where the interpolation is done in $\Pi_{(n,n)}$, the space of polynomials of maximum degree n in x and maximum degree n in y. This is because, in most signal processing applications, we are usually interested in images with square support in the Fourier domain. While Theorem (2.1) can be applied to these signals, since many of the coefficients which correspond to a triangular support are zero, the required number of interpolation points exceeds the number of unknown Fourier coefficients.

Our first result on interpolation in $\Pi_{(n,n)}$ enables us to choose the interpolation points on lines which pass through the origin. It can be stated in the following manner:

Theorem 2.3 *Let $l_0, ..., l_n$ be distinct lines with l_i, the ith line, defined by*

$$z = \alpha_i w \qquad \alpha_i \neq 0 \tag{2.2}$$

and consider arbitrary distinct points on l_i given by

$$\{(w_j^{(i)}, z_j^{(i)}) \mid j = 0, ..., 2i\} \tag{2.3}$$

where the ordering of the lines is arbitrary. If none of the interpolation points is equal to $(0,0)$, *the common intersection of all lines, then for any data set*

$$\{t_j^{(i)} \mid 0 \leq j \leq 2i; 0 \leq i \leq n\} \tag{2.4}$$

there is a unique bivariate polynomial of the form

$$p(w,z) = \sum_{i=0}^{n}\sum_{j=0}^{n} a(i,j) w^i z^j \tag{2.5}$$

such that

$$p(w_j^{(i)}, z_j^{(i)}) = t_j^{(i)} \quad 0 \leq j \leq 2i; \quad 0 \leq i \leq n \tag{2.6}$$

Proof: Substituting the equation of the *kth* line, l_k into $p(w,z)$ we get

$$\begin{aligned} p(w, \alpha_k w) &= \sum_{i=0}^{n}\sum_{j=0}^{n} a(i,j) w^i (\alpha_k w)^j \\ &= \sum_{i=0}^{2n} b_i^{(k)} w^i \end{aligned} \tag{2.7}$$

where

$$b_i^{(k)} = \begin{cases} \displaystyle\sum_{m=0}^{i} a(i-m, m)\alpha_k^m & 0 \leq i \leq n \\ \displaystyle\sum_{m=i-n}^{n} a(i-m, m)\alpha_k^m & n \leq i \leq 2n \end{cases} \tag{2.8}$$

For an arbitrary integer $s \geq -1$, we can split the summation in equation (2.7) in the following manner:

$$\sum_{i=s+1}^{2n-s-1} b_i^{(k)} w^i = p(w, \alpha_k w) - \sum_{i=0}^{s} b_i^{(k)} w^i - \sum_{i=2n-s}^{2n} b_i^{(k)} w^i \tag{2.9}$$

Setting $s = -1$, using the $2n+1$ points of l_n, we can uniquely determine $b_i^{(n)}$ for $0 \leq i \leq 2n$. In particular, considering equation (2.8), the values of $b_0^{(n)}$ and $b_{2n}^{(n)}$ enable us to determine $a(0,0)$, $a(n,n)$, and $b_{2n}^{(j)}$ for $0 \leq j \leq n-1$. This is because, from equation (2.8), we have:

$$b_0^{(k)} = a(0,0) \tag{2.10}$$

$$b_{2n}^{(k)} = a(n,n)\alpha_k^n \tag{2.11}$$

Similarly, by setting $s = 0$ in equation (2.9) and using the $2n-1$ points on l_{n-1}, we can uniquely specify $b_i^{(n-1)}$ for $1 \le i \le 2n-1$. This can be done because the determinant

$$\begin{vmatrix} x_0 & x_0^2 & \cdot & \cdot & \cdot & x_0^{2n-1} \\ x_1 & x_1^2 & \cdot & \cdot & \cdot & x_1^{2n-1} \\ & \cdot & \cdot & \cdot & \cdot & \cdot \\ & \cdot & \cdot & \cdot & \cdot & \cdot \\ x_{2n-2} & x_{2n-2}^2 & \cdot & \cdot & \cdot & x_{2n-2}^{2n-1} \end{vmatrix} \tag{2.12}$$

is non-zero as long as the x_i's are different from each other and from zero. Now we can utilize the values of $b_1^{(n)}$ and $b_1^{(n-1)}$ together with equation (2.8) to find $a(0,1)$ and $a(1,0)$. More specifically, from equation (2.8) we have:

$$b_1^{(k)} \;=\; \alpha_k a(0,1) \;+\; a(1,0) \tag{2.13}$$

Letting $k = n, n-1$ in the above equation, we can uniquely specify $a(0,1)$, $a(1,0)$ and hence b_1^k for $0 \le k \le n-2$.

In a similar manner, the values of $b_{2n-1}^{(n)}$ and $b_{2n-1}^{(n-1)}$ can be used to find $a(n,n-1)$ and $a(n-1,n)$ and hence $b_{2n-1}^{(k)}$. More specifically from equation (2.8) we get:

$$b_{2n-1}^{(k)} \;=\; \alpha_k^n a(n-1,n) \;+\; \alpha_k^{n-1} a(n,n-1) \tag{2.14}$$

The determinant of the above system of equations for $k = n, n-1$ is given by

$$\begin{vmatrix} \alpha_{n-1}^n & \alpha_{n-1}^{n-1} \\ \alpha_n^n & \alpha_n^{n-1} \end{vmatrix} \;=\; -\alpha_{n-1}^{n-1}\alpha_n^{n-1} \begin{vmatrix} \alpha_{n-1} & 1 \\ \alpha_n & 1 \end{vmatrix} \tag{2.15}$$

Taking into account that $\alpha_k \neq 0$, the above determinant is guaranteed to be non zero. Thus the coefficients $a(n,n-1)$ and $a(n-1,n)$ can be specified uniquely.

Repeating the above procedure for $s = 1, \ldots, 2n-1$, we can find all the coefficients $a(i,j)$. More specifically, at the *sth* stage, we know $b_{2n-s}^{(k)}$ and $b_s^{(k)}$ for $0 \le k \le n$ and using the $2(n-s)-1$ points of the line l_{n-s-1}, we can find $b_i^{(n-s-1)}$ for $s+1 \le i \le 2n-s-1$. These values will enable us to uniquely specify the coefficients

$$\{a(i,j) \mid i+j \;=\; s+1, 2n-s-1\}$$

and hence $b_{2n-s-1}^{(k)}$ and $b_{s+1}^{(k)}$ for $0 \le k \le n-s-2$. Consequently we can completely and uniquely determine all the coefficients of $p(w,z)$. □

Thus, our proof not only shows that the appropriate set of interpolation points on lines passing through the origin results in a unique solution, but also provides us with a recursive method to find the coefficients. The geometrical distribution of the interpolation points required by this theorem for $n = 2$ is shown in figure (2.4).

We will now use Theorem (2.3) to define a sampling strategy for BLP signals of the form given by equation (1.1). Since $g(W_1, W_2)$ of equation (1.2) is a bivariate polynomial of maximum degree $2N$ in W_1 and maximum degree $2N$ in W_2, invoking Theorem (2.3), we can reconstruct

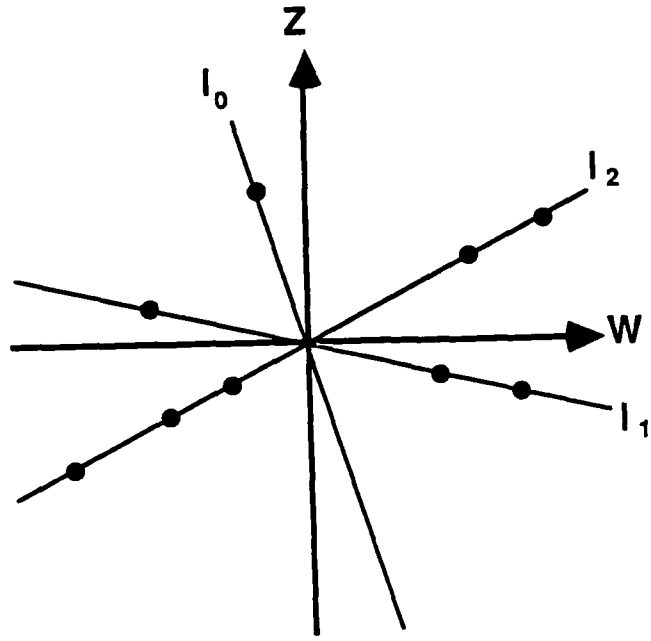

Figure 2.4: *Geometric distribution of the sampling points of Theorem (2.3) for $n = 2$.*

it by choosing our sampling points along $2N + 1$ distinct lines given by:

$$W_2 = \alpha_i W_1 \qquad 0 \leq i \leq 2N \tag{2.16}$$

where

$$W_1 = e^{j2\pi x}$$

$$W_2 = e^{j2\pi y}$$

If we let

$$\alpha = e^{j2\pi\beta}$$

then the lines in the $W_1 - W_2$ plane, given by equation (2.16), will correspond to lines of the

form

$$y = x + \beta_i \tag{2.17}$$

in the $x - y$ plane. Putting all of this together, we get:

Corollary 2.1 *Consider a bandlimited, continuous time, periodic signal $f(x, y)$ with period one in the x and y directions and Fourier series representation*

$$f(x,y) = \sum_{n1=-N}^{N} \sum_{n2=-N}^{N} F(n_1, n_2) e^{j2\pi x n_1} e^{j2\pi y n_2} \tag{2.18}$$

Let $l_0, ..., l_{2N}$ be distinct lines in the $x - y$ plane with l_i, the ith line, given by

$$y = x + \beta_i \tag{2.19}$$

and the set of arbitrary distinct samples on l_i given by

$$\{(x_j^{(i)}, y_j^{(i)}) \mid 0 \le j \le 2i\} \tag{2.20}$$

Then, for any data set

$$\{t_j^{(i)} \mid 0 \le j \le 2i \ ; \ 0 \le i \le 2N\} \tag{2.21}$$

we can reconstruct $f(x, y)$ uniquely.

An example of the geometric distribution of the sampling points required by this theorem for $N = 1$ is shown in figure (2.5). Figure (2.5a) shows three sampling lines of unit slope in the periodically extended version of a BLP signal, and figure (2.5b) shows how sampling lines "wrap around" one period of the signal. From Corollary (2.1) we can conclude that the set of points on lines of slope one given by:

$$\{(x_j^{(i)}, y_j^{(i)}) \mid y_j^{(i)} = x_j^{(i)} + \beta^{(i)}, \ 0 \le i \le 2, \ 0 \le j \le 2i\}$$

are sufficient to guarantee the unique reconstruction of the signal.

As we will see in section (2.3), Corollary (2.1) can be applied to the problem of reconstruction of multidimensional signals from threshold crossings by choosing the interpolation points to be the intersections of level crossings and the sampling lines.

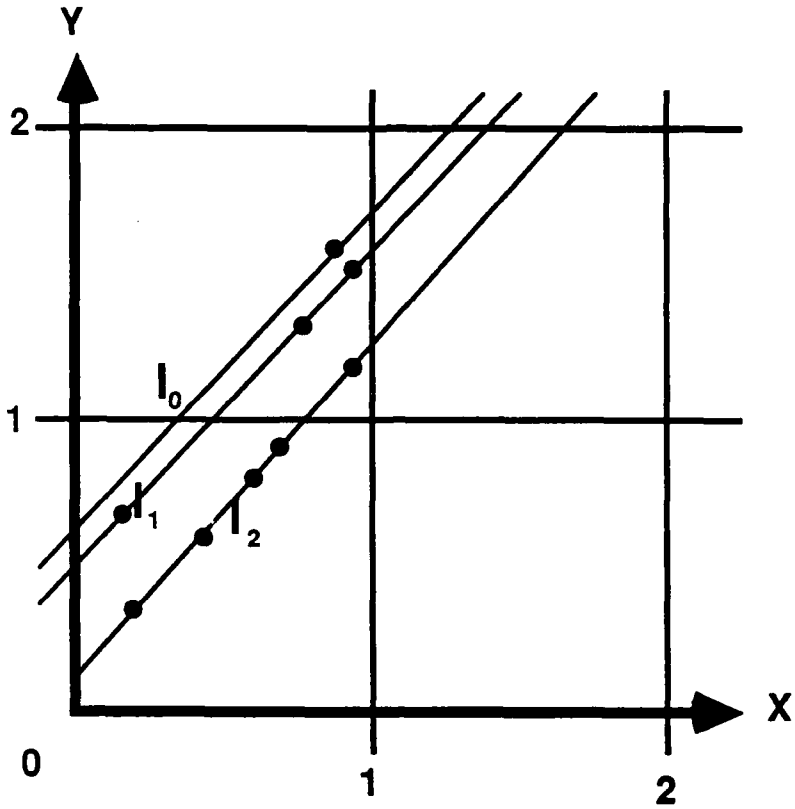

(a)

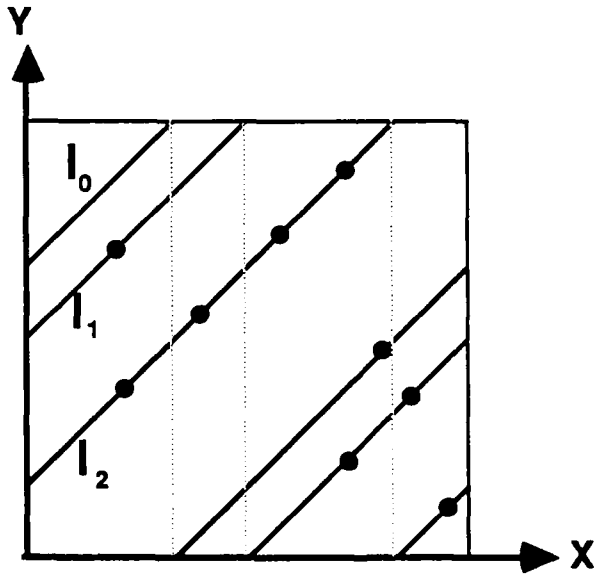

(b)

Figure 2.5: *Geometric distribution of the sampling points of Corollary (2.1) for $N = 1$. (a) The sampling lines are shown in the periodically extended version of the BLP signal; (b) The sampling lines are shown to wrap around one period of the signal.*

2.2.2 Sampling Signals on Lines of Positive Integral Slope

In this section, we will generalize Theorem (2.3) to the case where our interpolation points are chosen on curves of the form $z = \alpha w^m$ as opposed to straight lines passing through origin. Thus the results in the previous section become a special case of the ones we will derive in this section. A generalized version of Theorem (2.3), can be stated in the following manner:

Theorem 2.4 *Let $c_0, ..., c_p$ be distinct curves with c_i, the ith curve given by*

$$z = \alpha_i w^m \qquad\qquad \alpha_i \neq 0$$

where $m \leq n$ is an arbitrary positive integer, p is an integer satisfying

$$\sum_{i=0}^{p} [(m+1)n - 2mi + 1] \geq (n+1)^2$$

and

$$\{(w_j^{(i)}, z_j^{(i)}) | j = 0, ..., (m+1)n - 2mi; \} \tag{2.22}$$

is a set of distinct points on l_i. If none of the interpolation points defined by (2.22) are equal to $(0,0)$, the common intersection of all the curves, then for any data set

$$\{t_j^{(i)} | j = 0, ..., (m+1)n - 2mi;\ i = 0, ..., p; \}$$

there is a unique bivariate polynomial of the form

$$p(w,z) = \sum_{i=0}^{n} \sum_{j=0}^{n} a(i,j) w^i z^j$$

such that

$$p(w_j^{(i)}, z_j^{(i)}) = t_j^{(i)} \qquad j = 0, ..., (m+1)n - 2mi \qquad i = 0, ..., n$$

The proof is included in Appendix (A). The proof not only shows that interpolation points on curves of the form $z = \alpha w^m$ result in a unique solution, but also provides a recursive method to find the coefficients. It is worthwhile to mention that unlike Theorem (2.3), the number of interpolation points used by Theorem (2.4) might be larger than the number of unknown coefficients. More specifically, it can be shown that the number of sampling curves,

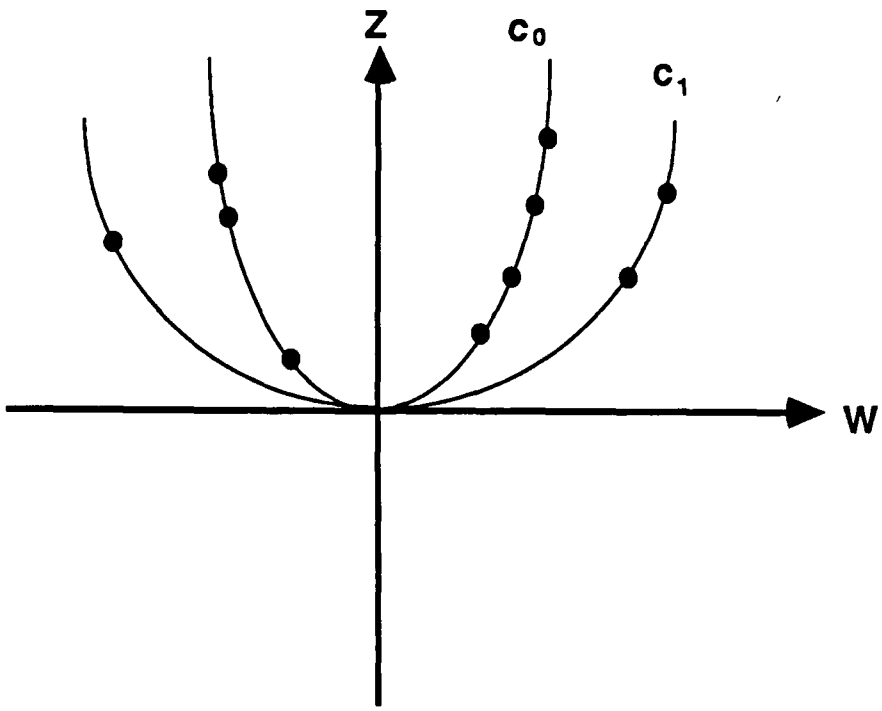

Figure 2.6: *Geometric distribution of the sampling points of Theorem (2.4) for $n = 2$ and $m = 2$.*

$p + 1$, is given by

$$p + 1 = \lceil \frac{n+1}{m} \rceil$$

where $\lceil k \rceil$ is defined to be the smallest integer equal to or larger than k. Thus, the number of interpolation points is equal to the number of coefficients only when $n + 1$ is divisible by m. The geometrical distribution of the interpolation points required by the above theorem for $n = 2$, $m = 2$ is shown in figure (2.6).

We will now use Theorem (2.4) to define a generalized sampling strategy for BLP signals of the form given by equation (1.1). Since $g(W_1, W_2)$ in equation (1.2) is a bivariate polynomial of maximum degree $2N$ in W_1 and maximum degree $2N$ in W_2, invoking Theorem (2.4), we can

reconstruct it by choosing our sampling points along $2N+1$ distinct lines given by

$$W_2 = \alpha_i W_1^m \qquad 0 \le i \le 2N \tag{2.23}$$

where

$$W_1 = e^{j2\pi x}$$

$$W_2 = e^{j2\pi y}$$

If we let

$$\alpha = e^{j2\pi\beta}$$

then the lines in the $W_1 - W_2$ plane given by equation (2.16) will correspond to lines of the form

$$y = mx + \beta_i \tag{2.24}$$

in the $x - y$ plane. Putting all of this together, we get:

Corollary 2.2 *Consider a bandlimited, continuous time, periodic signal $f(x,y)$ with period one in the x and y coordinates and Fourier series representation*

$$f(x,y) = \sum_{n1=-N}^{N} \sum_{n2=-N}^{N} F(n_1,n_2) e^{j2\pi x n_1} e^{j2\pi y n_2} \tag{2.25}$$

Let $l_0, \ldots, l_p$ be distinct lines in the $x - y$ plane with l_i, the ith line, given by

$$y = mx + \beta_i \tag{2.26}$$

where $m \le 2N$ is an arbitrary positive integer, p is an integer satisfying

$$\sum_{i=0}^{p} [2N(m+1) - 2mi + 1] \ge (2N+1)^2$$

and the set of arbitrary distinct samples on l_i is given by

$$\{(x_j^{(i)}, y_j^{(i)}) \mid 0 \le j \le 2(m+1)N - 2mi\} \tag{2.27}$$

Then, for any data set

$$\{t_j^{(i)} \mid 0 \le j \le 2(m+1)N - 2mi \; ; \; 0 \le i \le p\} \tag{2.28}$$

we can reconstruct $f(x,y)$ uniquely.

Two examples of the geometric distribution of the sampling points required by this result for $N = 1$ are shown in figure (2.7). In the first example, the slope of the sampling lines is 1, and the distribution of the points is identical to that of Corollary (2.1). In the second example, the slope of the sampling lines is 2, and the number of interpolation points exceeds the number of Fourier coefficients. In general, the distribution of samples required by Corollary (2.2) varies as a function of the slope of the sampling lines, providing us with a spectrum of sampling techniques. For instance, if our signal has 5×5 region of support in the Fourier domain, any one of the following sampling sets can be used to reconstruct it uniquely.

1. The set of 25 points on lines of slope one given by

$$\{(x_j^{(i)}, y_j^{(i)}) \mid y_j^{(i)} = x_j^{(i)} + \beta^{(i)},\ 0 \le i \le 5,\ 0 \le j \le 4N + 1 - 2i\}$$

2. The set of 29 points on lines of slope two given by

$$\{(x_j^{(i)}, y_j^{(i)}) \mid y_j^{(i)} = 2\, x_j^{(i)} + \beta^{(i)},\ 0 \le i \le 2,\ 0 \le j \le 6N - 4i + 1\}$$

3. The set of 28 points on lines of slope three given by

$$\{(x_j^{(i)}, y_j^{(i)}) \mid y_j^{(i)} = 3\, x_j^{(i)} + \beta^{(i)},\ 0 \le i \le 1,\ 0 \le j \le 8N - 6i + 1\}$$

4. The set of 34 points on lines of slope four given by

$$\{(x_j^{(i)}, y_j^{(i)}) \mid y_j^{(i)} = 4\, x_j^{(i)} + \beta^{(i)},\ 0 \le i \le 1,\ 0 \le j \le 10N - 8i + 1\}$$

5. The set of 25 points on a line of slope 5 given by

$$\{(x_j^{(i)}, y_j^{(i)}) \mid y_j^{(i)} = 5\, x_j^{(i)} + \beta^{(i)},\ i = 0,\ 0 \le j \le 12N - 10i + 1\}$$

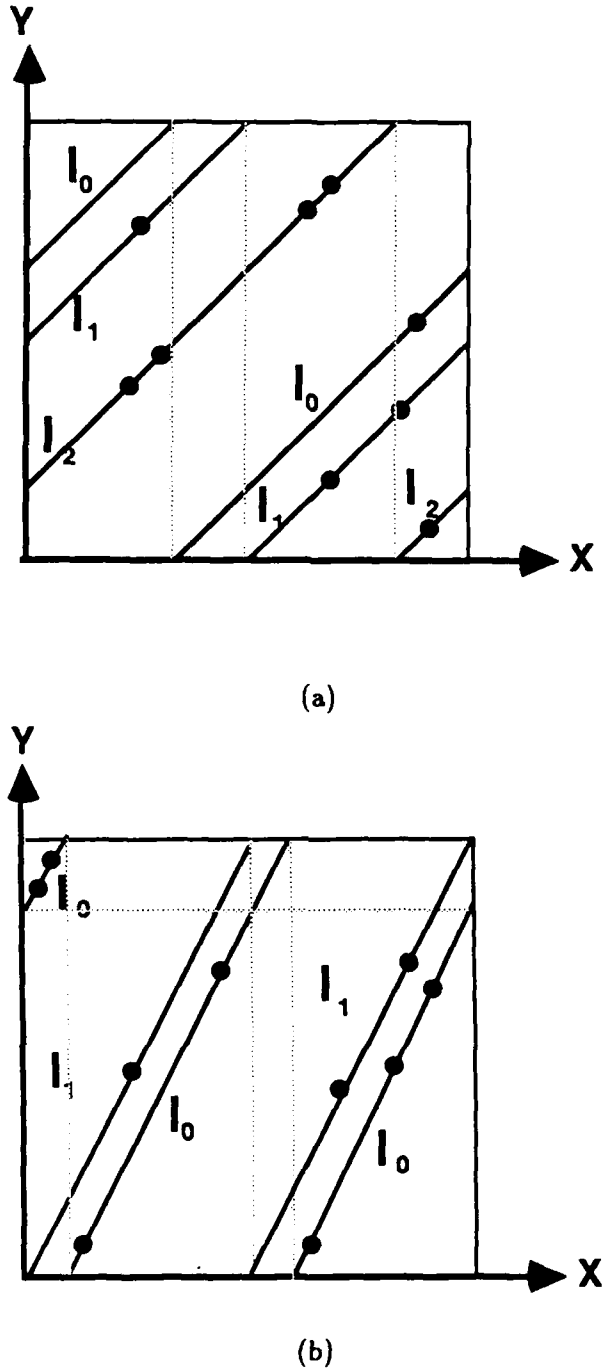

Figure 2.7: *Geometric distribution of the sampling points of Corollary (2.2) for* $N = 1$ *and: (a)*$m = 1$*; (b)*$m = 2$.

Note that for cases (1) and (5), the number of unknown Fourier coefficients is equal to the number of interpolation points whereas, for cases (2), (3) and (4), we need more samples than coefficients. As we will see in section (2.3), the results derived in this section can be applied to the problem of reconstruction from level crossings by choosing the intersection of sampling lines and threshold contours as our interpolation points.

2.2.3 Sampling Signals on Lines of Rational Slope

In the previous two sections, we found sufficient conditions for reconstruction of multidimensional BLP signals from their samples on lines with fixed positive integer slopes. In this section, we use a modified version of Bezout's theorem to derive a more general result on bivariate interpolation. This result is then applied to find the sufficient conditions for sampling BLP signals along lines with different rational slopes. Furthermore, our algebraic geometric approach enables us to determine the sampling conditions under which the reconstruction problem is guaranteed to have infinitely many solutions.

As we will see, the theoretical results developed in this section are more general than the ones in the previous sections. In fact, one can show that all the theorems of sections (2.2.1) and (2.2.2) are special cases of the results in this section. However, unlike the constructive proofs of the previous sections, the algebraic geometric approach does not provide us with an algorithmic procedure for the actual reconstructions.

Let us begin with the important concept of *irreducibility*. A bivariate polynomial is said to be irreducible over complex numbers, if it cannot be factored into polynomials of smaller degree with complex coefficients. Thus, two irreducible polynomials have no common factors unless the

one with smaller total degree is a factor of the other one. Bezout's theorem is concerned with the number of common zeros of two bivariate polynomials and can be stated in the following manner:

Theorem 2.5 (Bezout [37,38]) *If two bivariate polynomials of total degree r and s given by:*

$$p(x,y) = \sum_{i=0}^{r}\sum_{j=0}^{r-i} a(i,j)x^i y^j$$

$$q(x,y) = \sum_{i=0}^{s}\sum_{j=0}^{s-i} b(i,j)x^i y^j$$

have no common factors of degree greater than zero, then they have at most rs common zeros.

In this theorem, the total degree of a polynomial in two variables is defined in terms of the sum of the degrees in each variable. That is, the total degree of the two-dimensional polynomial $p(x,y)$ is equivalent to the degree of the one-dimensional polynomial $p(x,x)$. Since we are primarily interested in signals with rectangular Fourier domain support, we need to modify Bezout's theorem in order to find a tighter upper bound on the number of common zeros of two polynomials whose coefficients have rectangular regions of support. The modified Bezout's theorem originally derived by Zakhor and Izraelivitz [39] can be stated in the following way:

Theorem 2.6 (Modified Bezout's Theorem [39]) *Consider two bivariate polynomials $p(x,y) \in \Pi_{(N_x,N_y)}$ and $q(x,y) \in \Pi_{(M_x,M_y)}$ of the form*

$$p(x,y) = \sum_{i=0}^{N_x}\sum_{j=0}^{N_y} a(i,j)x^i y^j$$

$$q(x,y) = \sum_{i=0}^{M_x}\sum_{j=0}^{M_y} b(i,j)x^i y^j$$

If p and q have no common factors of degree greater than zero, then they have at most $N_xM_y + M_xN_y$ common zeros.

The proof is included in Appendix (B). Theorem (2.6) implies that if a polynomial $p(x,y) \in \Pi_{(N_x,N_y)}$ with maximum degrees N_x in x and N_y in y, has more than $N_xM_y + M_xN_y$ common zeros with an irreducible polynomial $q(x,y) \in \Pi_{(M_x,M_y)}$ with maximum degrees M_x in x and M_y in y, then $q(x,y)$ must be a factor of $p(x,y)$. This consequence of Theorem (2.6) can be used to derive the most general theorem of this chapter:

Theorem 2.7 *Let $c_0, c_1, ..., c_p$ be distinct bivariate irreducible polynomials with the maximum degrees of c_i in w and z given by $m_w^{(i)}$ and $m_z^{(i)}$ and p being an integer satisfying either of the following two conditions:*

$$n_w < \sum_{i=0}^{p} m_w^{(i)} \tag{2.29}$$

$$n_z < \sum_{i=0}^{p} m_z^{(i)} \tag{2.30}$$

Define A_i to be the set of

$$S(i) \equiv m_z^{(i)}(n_w - \sum_{k=0}^{i-1} m_w^{(k)}) \; + \; m_w^{(i)}(n_z - \sum_{k=0}^{i-1} m_z^{(k)}) \; + \; 1$$

points on c_i given by

$$A_i \; = \; \{(w_j^{(i)}, z_j^{(i)}) \mid c_i(w_j^{(i)}, z_j^{(i)}) \; = \; 0, \; 0 \le j < S(i)\} \tag{2.31}$$

If none of the interpolation points given by (2.31) are on the intersections of two or more of the c_i's, then for any data set

$$\{t_j^{(i)} \mid 0 \le i \le p, \; 0 \le j < S(i)\}$$

there is a unique bivariate polynomial of the form

$$p(w,z) \; = \; \sum_{i=0}^{n_w} \sum_{j=0}^{n_z} a(i,j) w^i z^j$$

such that

$$p(w_j^{(i)}, z_j^{(i)}) \; = \; t_j^{(i)} \quad 0 \le i \le p, \; 0 \le j < S(i)\} \tag{2.32}$$

Proof: To show that there is a unique polynomial which satisfies (2.32), we have to show that there are no polynomials in $\Pi_{(n_w,n_z)}$ which vanish at all the interpolation points $\cup A_i$. Suppose, on the contrary, that there is a polynomial $q(w,z) \in \Pi_{(n_w,n_z)}$ which vanishes at all the interpolation points.

Since q has $m_w^{(0)} n_z + n_w m_z^{(0)} + 1$ common zeros with c_0, by the modified version of Bezout's theorem, c_0 must be a factor of $q(w,z)$. That is

$$q(w,z) = c_0(w,z) q^{(1)}(w,z)$$

where $q^{(1)}(w,z)$ is a polynomial of maximum degree $n_w - m_w^{(0)}$ in w and $n_z - m_z^{(0)}$ in z. Furthermore, since by hypothesis, none of the interpolation points on c_1 are on c_0 and $q(w,z)$ has $1 + m_z^{(1)}(n_w - m_w^{(0)}) + m_w^{(1)}(n_z - m_z^{(0)})$ common zeros with c_1, it must be true that the same number of common zeros with c_1. Taking into account the irreducibility of c_1, by modified version of Bezout's theorem, c_1 must be a factor of $q^{(1)}(w,z)$ and hence $q(w,z)$.

Repeating the above argument for $c_2, \ldots, c_{p-1}$, we get:

$$q(w,z) = c_0(w,z) \ldots c_{p-1}(w,z)\ q^{(p)}(w,z)$$

where $q^{(p)}(w,z)$ has maximum degree $n_w - \sum_{i=0}^{p-1} m_w^{(i)}$ in w and maximum degree $n_z - \sum_{i=0}^{p-1} m_z^{(i)}$ in z and has $1 + m_w^{(p)}(n_z - \sum_{k=0}^{p-1} m_z^{(k)}) + m_z^{(p)}(n_w - \sum_{k=0}^{p-1} m_w^{(k)})$ common zeros with c_p. Since c_p is irreducible, by modified version of Bezout's theorem, it must be a factor of $q^{(p)}(w,z)$. This contradicts our hypothesis since by inequalities (2.32) and (2.29), the degree of c_p in either w or z, is larger than that of $q^{(p)}(w,z)$. □

The above theorem is the generalized version of Theorems (2.3) and (2.4). More specifically, if c_i is an irreducible polynomial of the form

$$z = \alpha_i w^l \tag{2.33}$$

then Theorem (2.7) simply reduces to Theorem (2.4) for positive integer values of l, and to Theorem (2.3) for $l = 1$. This is because polynomials of the form given by equation (2.33) are known to be irreducible. An example of the distribution of sampling points required by Theorem (2.7) for $n_w = n_z = 2$, $m_w^{(0)} = m_z^{(0,1)} = 1$ and $m_w^{(1)} = 2$ is shown in figure (2.8).

There are two classes of irreducible polynomials which are particularly useful in deriving sampling strategies for multidimensional periodic signals of the form given by equation (1.1). These two classes of polynomials in W_1 and W_2 are of the form:

$$W_2^{M_y} = \alpha W_1^{M_z} \quad , \quad M_z > 0, \quad M_y > 0 \tag{2.34}$$

$$W_2^{M_y} W_1^{M_x} = \alpha \ , \quad M_x > 0, \ \ M_y > 0 \tag{2.35}$$

where M_y and M_x are positive integers which are relatively prime with respect to each other. Using the fact that W_1 and W_2 of equation (1.1) are related to x and y, the signal coordinates, via

$$W_1 = e^{j2\pi x}$$

$$W_2 = e^{j2\pi y}$$

and letting

$$\alpha = e^{j2\pi\beta}$$

the curves in the $W_1 - W_2$ plane given by equations (2.34) and (2.35) correspond to lines of the form

$$M_y y = \beta + M_x x \ , \quad M_x, \ M_y > 0 \tag{2.36}$$

$$M_y y + M_x x = \beta \ , \quad M_x, \ M_y > 0 \tag{2.37}$$

in the $x - y$ plane. Geometrically, equations (2.36) and (2.37) correspond to lines with positive and negative rational slopes respectively. Therefore, lines with positive and negative rational slopes in the $x - y$ domain correspond to irreducible bivariate polynomials in the $W_1 - W_2$ plane. We can use this fact, together with Theorem (2.7) to define the following sampling strategy:

Corollary 2.3 *Consider a bandlimited, continuous time, periodic signal $f(x, y)$ with period one in x and y direction and Fourier series representation:*

$$f(x, y) = \sum_{n1=-N}^{N} \sum_{n2=-N}^{N} F(n_1, n_2) e^{j2\pi x n_1} \ e^{j2\pi y n_2} \tag{2.38}$$

Let $l_0, ..., l_p$ be distinct lines in the $x - y$ plane with l_i, the ith curve given by

$$M_y^{(i)} y = M_x^{(i)} x + \beta_i \tag{2.39}$$

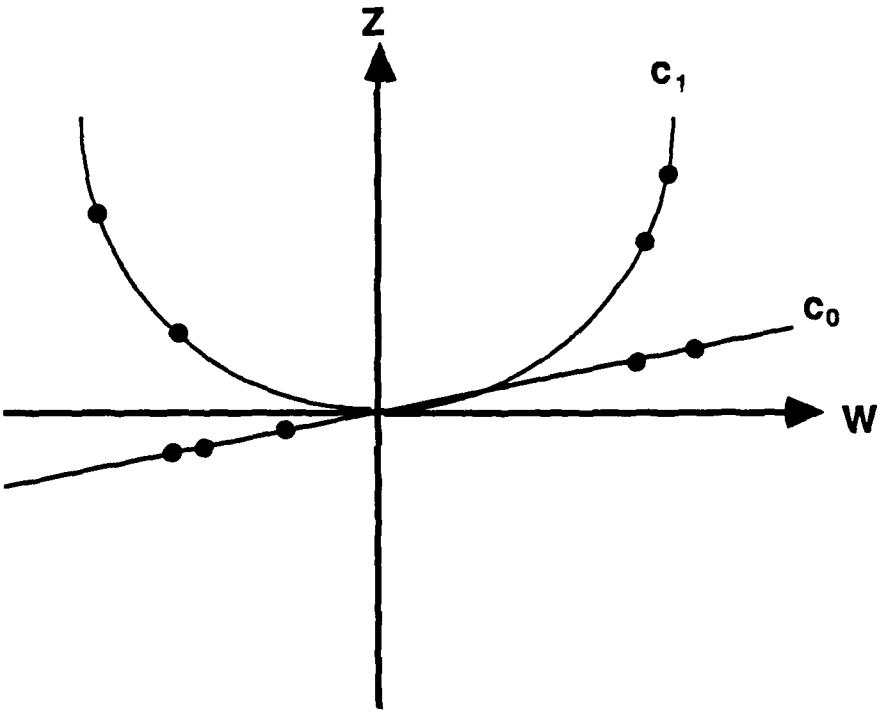

Figure 2.8: *Geometrical distribution of the sampling points of Theorem (2.7) for* $n_w = n_z = 2$.

where $M_x^{(i)}$ *and* $M_y^{(i)}$ *are positive or negative integers which are relatively prime with respect to each other. Let p be an integer satisfying either one of the following:*

$$2N < \sum_{i=0}^{p} \left| M_x^{(i)} \right| \tag{2.40}$$

$$2N < \sum_{i=0}^{p} \left| M_y^{(i)} \right| \tag{2.41}$$

Suppose that the set of

$$S(i) = \left| M_y^{(i)} \right| (2N - \sum_{k=0}^{i-1} \left| M_x^{(k)} \right|) + \left| M_x^{(i)} \right| (2N - \sum_{k=0}^{i-1} \left| M_y^{(k)} \right|) + 1$$

arbitrary distinct samples on l_i*, is given by*

$$\{(x_j^{(i)}, y_j^{(i)}) \mid 0 \le i \le p, \quad 0 \le j < S(i)\} \tag{2.42}$$

If none of the interpolation points given by equation (2.42) are on the intersection of two or more of the c_i*'s, then for any data set*

$$\{t_j^{(i)} \mid 0 \le j < S(i)\} \tag{2.43}$$

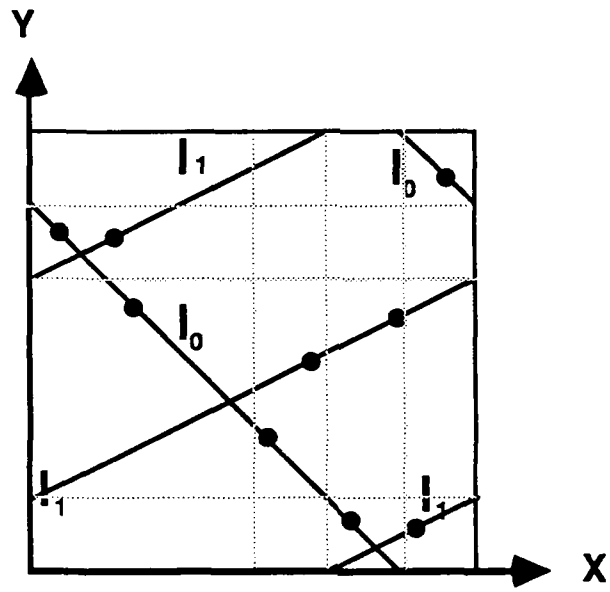

Figure 2.9: *Geometric distribution of the sampling points of Corollary (2.3) for $N = 1$.*

we can reconstruct $f(x, y)$ uniquely.

An example of the geometric distribution of the sampling points required by this theorem for $N = 1$ and $M_x^{(0)} = -1$, $M_y^{(0)} = 1$, $M_x^{(1)} = 1$, $M_y^{(1)} = 2$ is shown in figure (2.9). The above result is more general than our previous results in the sense that Corollary (2.1) becomes a special case of it when

$$M_x^{(i)} = M_y^{(i)} = 1 \quad , \quad \forall i$$

and Corollary (2.2) becomes its special case when

$$M_y^{(i)} = 1 \quad , \quad \forall i$$

$$M_x^{(i)} = m > 0 \quad , \quad \forall i$$

All the theorems we have discussed so far, provide us with sufficient conditions for unique recovery of polynomials or their associated BLP signals. We can use arguments similar to the proof of Theorem (2.7) to find conditions under which the reconstruction problem will have infinitely many solutions:

Theorem 2.8 *Let $c_0, c_1, \ldots, c_p$ be distinct bivariate polynomials with the maximum degrees of c_i in w and z given by $m_w^{(i)}$ and $m_z^{(i)}$ where p is an integer satisfying the following two inequalities:*

$$n_w > \sum_{i=0}^{p} m_w^{(i)} \tag{2.44}$$

$$n_z > \sum_{i=0}^{p} m_z^{(i)} \tag{2.45}$$

Suppose that we choose $S(i)$, an arbitrary number of interpolation points, on the ith curve, c_i. Then for any data set

$$\{t_j^{(i)} \mid 0 \le i \le p,\ 0 \le j < S(i)\}$$

there are an infinite number of bivariate polynomials of the form

$$p(w,z) \;=\; \sum_{i=0}^{n_w}\sum_{j=0}^{n_z} a(i,j) w^i z^j$$

such that

$$p(w_j^{(i)}, z_j^{(i)}) \;=\; t_j^{(i)} \qquad 0 \le i \le p,\ 0 \le j < S(i) \tag{2.46}$$

Proof: The proof is similar to the proof of Theorem (2.7). To show that there are an infinite number of polynomials which satisfy (2.46), it is sufficient to show that there is at least one polynomial of maximum degree $< n_w$ in w and $< n_z$ in z which vanishes at all the interpolation points defined by the theorem. The most obvious choice for this polynomial is

$$q(w,z) \;=\; \prod_{i=0}^{p} c_i(w,z)$$

Since by inequalities (2.44) and (2.45), the maximum degree of $q(w,z)$ is less than n_w in w and less than n_z in z, there exists infinite number of polynomials in $\Pi_{(n_w,n_z)}$ which satisfy (2.46). □

Translating the above result to the signal domain via our usual transformations:

$$W_1 \;=\; e^{j2\pi z}$$

$$W_2 = e^{j2\pi y}$$

and assuming the irreducible curves of the above corollary to be of the form shown in equations (2.34) and (2.35), we arrive at the following result:

Corollary 2.4 *Consider a bandlimited, continuous time, periodic signal $f(x,y)$ with period one in x and y direction and Fourier series representation:*

$$f(x,y) = \sum_{n1=-N}^{N} \sum_{n2=-N}^{N} F(n_1,n_2) e^{j2\pi x n_1} e^{j2\pi y n_2} \tag{2.47}$$

Let $l_0, ..., l_p$ be distinct lines in the $x-y$ plane with l_i, the ith curve given by

$$M_y^{(i)} y = M_x^{(i)} x + \beta_i \tag{2.48}$$

where $M_x^{(i)}$ and $M_y^{(i)}$ are positive or negative integers which are relatively prime with respect to each other. Let p be an integer satisfying the below two inequalities:

$$2N > \sum_{i=0}^{p} \left| M_x^{(i)} \right| \tag{2.49}$$

$$2N > \sum_{i=0}^{p} \left| M_y^{(i)} \right| \tag{2.50}$$

Suppose that we choose $S(i)$, an arbitrary number of interpolation points on the ith line l_i. Then, for any data set

$$\{t_j^{(i)} \mid 0 \le j < S(i)\} \tag{2.51}$$

there are infinitely many functions of the form given by equation (2.47) such that:

$$f(x_j^{(i)}, y_j^{(i)}) = t_j^{(i)} \qquad 0 \le i \le p, \quad 0 \le j \le S(i)$$

In terms of sampling multidimensional periodic signal, the above theorem implies that unless the number of interpolation lines and their respective slopes are chosen carefully, we might encounter situations where the interpolation problem has non unique solutions.

To summarize this section, we have derived a variety of results on multivariate polynomial interpolation in $\Pi_{(n,n)}$. Exploiting the polynomial representation of multidimensional BLP signals, we applied these results to the problem of reconstruction from non-uniformly spaced

samples. More specifically, our results provide us with sufficient conditions for the unique reconstruction of signals from their samples on various lines of positive or negative rational slopes. A summary of all the theorems and corollaries of the last two sections is included at the end of this chapter. In the next section, we will apply these results to a variety of multidimensional reconstruction problems.

2.3 Applications of the Line-Sampling Strategy

In section 2.2, we found sufficient conditions under which samples of a multidimensional signal can be used to uniquely specify it. More specifically, the theoretical results of the previous section provide us with a variety of distributions of sampling points along lines of positive or negative rational slope which result in unique recovery of a signal. Although our main motivation for deriving these semi-implicit sampling strategies has been the problem of reconstruction from multiple level threshold crossings, they can also be applied to a variety of other reconstruction problems with non-uniformly spaced samples in areas such as machine vision [18,19], radio astronomy [20] and computed tomography [21], as well as natural sciences such as geology, meteorology, and oceanography. These problems can be divided into the following three categories:

1. Recovery of signals from their crossings with arbitrary functions. A special case of this problem is reconstruction of signals from their single or multiple level threshold crossings. Another special case is reconstruction of signals from their crossings with periodic functions, which has potential applications in the conversion of halftone images to continuous tone ones.

2. Recovery of signals from their projections. Applications of this problem include such diverse fields as X-ray tomography, transmission electron microscopy and radio astronomy.

3. Recovery of signals whose values are known along certain paths, curves or contours. This problem arises frequently in the area of machine vision, where depth or distance information is available on the zero crossing contour of the convolution of the image with the Laplacian of a Gaussian.

Although the main focus of this thesis is the problem of reconstruction from multiple level threshold crossings, in this section, we will briefly describe the way our semi-implicit schemes of section (2.2) can be applied to some of these other problems.

2.3.1 *Recovery from* Crossings with Arbitrary Functions

In reconstructing signals from their crossings with arbitrary functions, the intersections of sampling lines with the crossing contours are used as interpolation points. The steps involved in the reconstruction of BLP signals from their multiple level crossings can be summarized as follows:

1. Find the level crossing contours associated with the thresholds.

2. Find a set of sampling lines with rational slopes whose intersections with the crossing contours satisfies the distributions required by Corollaries (2.1), (2.2) or (2.3).

3. Use the intersections to find the coefficients of the polynomial associated with the signal or equivalently the Fourier coefficients of the signal.

In Chapter 3, we will propose a variety of techniques for carrying out the third step of the above

description, and show examples of reconstruction from level crossings. As we will see, the major difficulty in applying the above procedure to actual reconstruction problems is that, in general, we are not guaranteed to get enough intersections between sampling lines and threshold contours to satisfy the distribution requirements of Corollaries (2.1), (2.2) or (2.3). Of course, as will be seen in section (3.4), we can find guidelines which help us choose the slope and position of our sampling lines in an "optimal" fashion so that the number of intersections of sampling lines with the threshold contours is maximized. However, the problem still remains that for small number of thresholds, n_t, we might not be able to find any set of sampling lines which satisfy our theoretical requirements. Indeed, this becomes our main motivation for deriving the less restrictive results of Chapter 4. Meanwhile, we can make a few observations for the more general problem of reconstruction from crossings with arbitrary functions. As it turns out, for certain class of functions such as sinusoids, the number of intersections of sampling lines with function crossings of the signal becomes signal independent. As an example, consider the eye picture shown in figure (2.10) and its sinusoid crossings with the function:

$$h(x,y) \;=\; A\;(\;1+\;cos(2\pi(px+qy))) \tag{2.52}$$

shown in figure (2.11). As seen, the above sinusoid assumes its maximum value $2A$ and minimum value 0 on equidistant lines of slope $-\frac{p}{q}$. Thus, if we impose the condition

$$0 \;=\; [h(x,y)]_{min} \;<\; f(x,y) \;<\; [h(x,y)]_{max} \;=\; 2A\;,\;\;\forall(x,y) \tag{2.53}$$

on the amplitude of our signal, then between every two neighboring parallel lines where $h(x,y)$ assumes its minimum and maximum values, there exists a contour of crossings of $h(x,y)$ and our signal $f(x,y)$. Since, the intensity of the eye picture lies in the range $[0,256]$, to satisfy inequality (2.53), the value of A for the crossings shown in figure (2.11) was chosen to be 128.

If we now sample these sinusoid crossings of our signal along lines of rational slope $\frac{n}{m}$ given by

$$l: \quad y = \frac{n}{m}x + \beta \tag{2.54}$$

we are guaranteed to get exactly $2\lceil pm + qn \rceil$ samples. As shown in figure (2.11), each sample on line l is located between the two intersections of the sampling line with two lines at which $h(x, y)$ assumes its maximum and minimum values.

We can use the above example, together with the distribution requirements of Corollaries (2.1), (2.2) and (2.3), to find the exact number of sinusoids needed for recovery of a signal via a given set of sampling lines. For instance, suppose that we are interested in sampling crossings of a sinusoid with a $(2N+1) \times (2N+1)$ BLP signal along lines of rational slope $\frac{n}{m}$ where n and m are relatively prime with respect to each other. Invoking Theorem (2.7) we realize that for this sampling strategy the maximum number of samples needed on any of the sampling lines is $2N(n+m)+1$. Since the number of intersections of a sinusoid with period $\frac{1}{p}$ in the x direction and $\frac{1}{q}$ in the y direction with a line of slope $\frac{n}{m}$ is $2\lceil pm + qn \rceil$, in order to satisfy the sampling requirements of Theorem (2.7), we must have

$$2(pm + qn) \geq 2N(m + n) + 1$$

or

$$(pm + qn) > (m + n)N \tag{2.55}$$

A necessary condition for satisfying the above inequality is that at least one of the quantities p or q must be greater than N. This in turn implies that using the semi-implicit sampling strategies of this chapter a BLP signal can be uniquely reconstructed from its crossings with a sinusoid only if the frequency of the sinusoid lies outside the bandwidth of the signal. More

Figure 2.10: *The original eye picture with* 31×31 *region of support in the Fourier domain.*

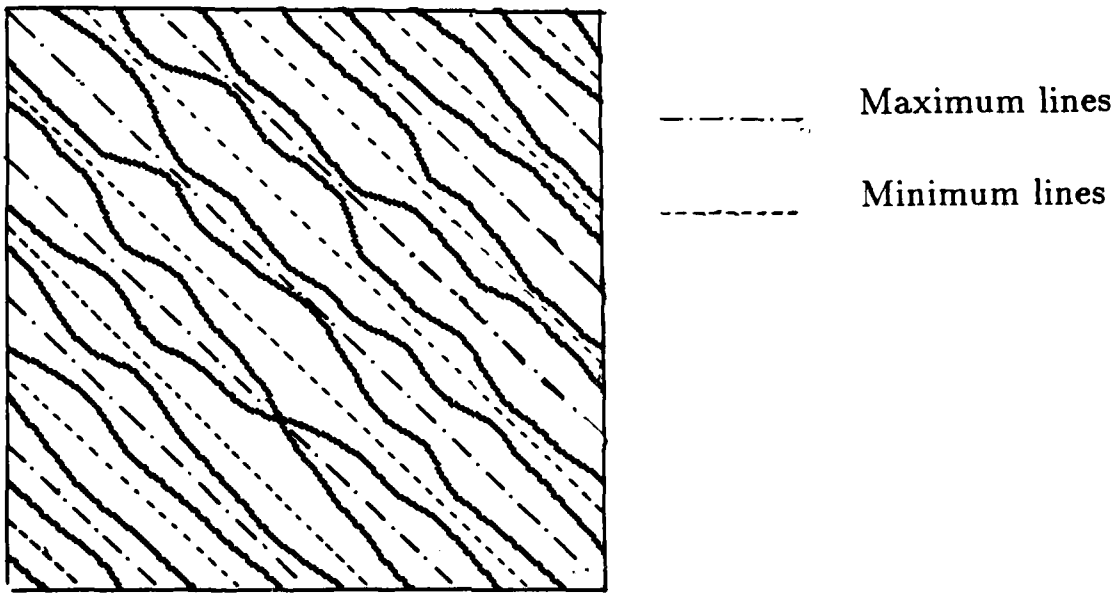

Figure 2.11: *Sinusoid crossings of the original eye picture. The lines at which the sinusoid assumes its maximum and minimum values are also shown.*

generally, reconstruction of an $(2N+1) \times (2N+1)$ signal from samples of its crossings with L sinusoids along lines of slope $\frac{n}{m}$ is possible if and only if:

1. The maximum and minimum values of each sinusoid is larger and smaller than the maximum and minimum values of the signal under consideration.

2. The periods of the sinusoids along x and y directions given by $\frac{1}{p_i}$ and $\frac{1}{q_i}$ satisfy:

$$\sum_{i=1}^{L}(p_i m \ + \ q_i n) \ > \ (m+n)N \tag{2.56}$$

An important practical application of reconstruction from crossings with periodic functions is recovery of contone images from halftone images [17]. The halftone process has been used for more than a century for converting continuous tone pictures into regular patterns of black and white dots which can then be printed. The size of each dot is related to the tone at that same place in the original image being reproduced. Mathematically speaking, the halftone version of a continuous tone image can be obtained by comparing the value of the signal with a two-dimensional periodic function and producing a white or black pixel on a high contrast medium depending on whether the signal value is higher or lower than that of the periodic function. Thus, if the period of the thresholding function is a sinusoid satisfying the inequality (2.55), we can be guaranteed unique reconstruction of the continuous tone image by sampling the halftone image along lines of slope $\frac{n}{m}$. A few examples of such reconstructions are shown in Chapter 3.

2.3.2 Recovery from Projections

Another major application of the theoretical results of section (2.2) is in the area of reconstruction of multidimensional signals from their projections. In this section, we will show that

the one-projection theorem due to Mersereau and Oppenheim [45] is a special case of Theorem (2.4) and can be generalized to situations with an arbitrary number of projections.

Consider a bandlimited two-dimensional signal of order M and bandwidth W whose Fourier transform is given by [45]:

$$F(\omega_1, \omega_2) = \frac{\pi^2}{W^2} \sum_{m=0}^{M-1} \sum_{n=0}^{M-1} f(\frac{m\pi}{W}, \frac{n\pi}{W}) e^{-j\frac{\pi}{W}(m\omega_1 + n\omega_2)} b_W(\omega_1, \omega_2) \tag{2.57}$$

where

$$b_W(\omega_1, \omega_2) = \begin{cases} 1 & |\omega_1| < 1, \ |\omega_2| < 1 \\ 0 & elsewhere \end{cases} \tag{2.58}$$

The key result in recovering signals from their projections is the projection slice theorem, which essentially relates the one-dimensional Fourier transform of a projection of a signal to a slice of its two-dimensional Fourier transform. In many applications, the only available information for reconstructing a signal is samples of the slices of its two-dimensional Fourier transform. The one-projection theorem of Mersereau and Oppenheim ([45]) basically states that M^2 samples on one slice of the two-dimensional transform is sufficient for unique reconstruction of the signal, provided the angle of the projection is chosen to be a *critical angle*. To prove the one-projection theorem for the special case where the projection angle is given by $\theta = \tan^{-1} M$, let

$$Z_1 = e^{-j\frac{\pi}{W}\omega_1}$$

$$Z_2 = e^{-j\frac{\pi}{W}\omega_2}$$

in equation (2.57). Then, the Fourier transform shown in equation (2.57) can be written as a polynomial in terms of Z_1 and Z_2:

$$F(Z_1, Z_2) = \frac{\pi^2}{W^2} \sum_{m=0}^{M-1} \sum_{n=0}^{M-1} Z_1^m Z_2^n$$

Thus, invoking Theorem (2.4), M^2 samples on a line of the form:

$$Z_2 = Z_1^M$$

in the $Z_1 - Z_2$ domain, or equivalently

$$\omega_2 = M\omega_1$$

in the $\omega_1 - \omega_2$ plane are sufficient for unique recovery of the coefficients of $F(\omega_1, \omega_2)$. Exploiting the fact that Theorem (2.4) is a special case of Theorem (2.7), we can generalize this result to reconstruction from an arbitrary number of slices with rational slopes. More specifically, we have:

Corollary 2.5 *Consider a signal whose Fourier transform is given by equation (2.57). Let $s_0, \ldots s_p$ be distinct slices in the ω_1, ω_2 plane with s_i the ith slice given by:*

$$P_2^{(i)}\omega_2 = P_1^{(i)}\omega_1$$

where $P_2^{(i)}$ and $P_1^{(i)}$ are positive or negative integers which are relatively prime with respect to each other. Let L be the smallest integer such that either one of the following is satisfied:

$$M - 1 < \sum_{i=0}^{L} |P_1^{(i)}|$$

$$M - 1 < \sum_{i=0}^{L} |P_2^{(i)}|$$

Suppose that the set of

$$Q(i) = |P_2^{(i)}|(M - 1 - \sum_{k=0}^{i-1} |P_1^{(k)}|) + |P_1^{(i)}|(M - 1 - \sum_{k=0}^{i-1} |P_2^{(k)}|) + 1$$

arbitrary distinct samples on s_i, is given by

$$\left\{(\omega_1^{(i)}(j), \omega_2^{(i)}(j) \mid 0 \leq j < Q(i)\right\}$$

Then, if none of the interpolation points is equal to $(\omega_1, \omega_2) = (0, 0)$, coefficients of $F(\omega_1, \omega_2)$, or equivalently our original signal can be uniquely reconstructed from the samples of the Fourier transform of the signal.

We will not investigate the consequences of the above result experimentally, simply because it is not directly related to the main focus of this thesis, which is reconstruction from multiple level threshold crossings.

2.3.3 Recovery from Signal Values along Specific Paths

In many reconstruction applications, the value of a signal is known along certain contours, paths or curves and it is necessary to recover the signal from this information. Clearly, our results of previous sections can be applied to these situations by using the intersections of sampling lines and the contours as interpolation points.

As an example, consider the surface interpolation problem which arises frequently in machine vision. Computational theories of structure from motion [40] and stereo vision [41] only specify the computation of three dimensional surface information at special points in the image. Yet, the visual perception is clearly of complete surfaces. To account for this, a computational theory for interpolating surfaces from visual information has been proposed by many researchers [18]. More specifically, if we view the human early visual system as a symbolic manipulator, we can consider visual processing as a series of transformations from one representation to another [42,43]. The first transformation is from images to a description called the *primal sketch* of those locations at which the image irradiances change. These locations can be found by finding the zero crossings of the convolution of the original image with the Laplacian of a Gaussian. Next, primal sketch descriptions of several images are matched, either by the stereo or motion computation, to obtain a description of the surface information at the zero crossings. This representation is called the raw $2\frac{1}{2}D$ sketch. Finally, the raw $2\frac{1}{2}D$ sketch is

interpolated to obtain complete surface descriptions, called the full $2\frac{1}{2}D$ sketch [44]. Since the input representations for the interpolation step consist of explicit surface information such as distance or relative distance along the zero crossings of the convolved image, the intersections of our sampling lines with the zero crossing contours of the convolved image can be used as interpolation points for finding the polynomial associated with the surface under consideration. Under these circumstances, the theoretical results of section (2.2), provide us with a variety of sufficient conditions for interpolating the distance values on selected points of the zero crossing contour of the convolved image.

To summarize this chapter, we have developed a variety of results on interpolation of polynomials in $\Pi_{(n,n)}$. These results ultimately have been used to derive a variety of semi-implicit sampling strategies for reconstruction of multidimensional signals from their crossings with arbitrary functions, their non-uniformly spaced samples, and their projections. A summary of all the theorems and corollaries derived in this chapter are included in table (2.1). In the next chapter, we will propose reconstruction algorithms for the specific problem of reconstruction from multiple level threshold crossings.

Theorem or Corollary Number	Reference for proof	Region of Support	Description
Theorem (2.1)	Gasca and Maetzu [36]	triangular	polynomial interpolation with $n+1$ lines and $i+1$ samples on the ith line
Theorem (2.2)	[29,32,33,34]	rectangular	polynomial interpolation with non-uniform rectangular sampling
Theorem (2.3)	section (2.2.1)	rectangular	polynomial interpolation with $n+1$ lines through the origin and $2i+1$ samples on the ith line
Corollary (2.1)	Theorem (2.3)	rectangular	recovery of BLP signals from their samples on lines of unit slope
Theorem (2.4)	appendix (A)	rectangular	polynomial interpolation from samples on curves of the form $z = \alpha w^m$
Corollary (2.2)	Theorem (2.4)	rectangular	recovery of BLP signals from samples on lines of positive integer slope
Theorem (2.5)	Bezout [37,38]	triangular	upper bound on the number of common zeros of two polynomials
Theorem (2.6)	appendix (B)	rectangular	upper bound on the number of common zeros of two polynomials
Theorem (2.7)	section (2.2.3)	rectangular	polynomial interpolation with samples on irreducible curves
Corollary (2.3)	Theorem (2.7)	rectangular	recovery of BLP signals from their samples on lines of rational slope
Theorem (2.8)	section (2.2.3)	rectangular	necessary conditions for unique interpolation of polynomials
Corollary (2.4)	Theorem (2.8)	rectangular	necessary conditions for unique reconstruction of BLP signals
Corollary (2.5)	Theorem (2.7)	rectangular	recovery of bandlimited signals of a given order from an arbitrary number of projections

Table 2.1: *Summary of the theorems and corollaries of Chapter 2.*

Chapter 3

Reconstruction Algorithms for the Semi-implicit Sampling Approach

In Chapter 2, we derived a spectrum of semi-implicit sampling strategies for a variety of multidimensional reconstruction problems. Our main goal in this chapter is to derive reconstruction algorithms for these sampling schemes. Although most of the examples in this chapter are related to the problem of reconstruction from multiple level threshold crossings, the majority of our proposed algorithms can also be applied to the other reconstruction problems described in section (2.3).

Our first approach to signal reconstruction, which involves solving a linear system of equations, is included in section (3.1). Although this approach has the potential of being numerically stable, it is computationally intensive and requires large amounts of storage. Our second approach which is described in section (3.2), is recursive and is based on the proofs of Theorems (2.3) and (2.4). The recursive algorithm requires less storage and computation. However, since it computes the coefficients recursively, small errors in the initial steps of the algorithm are propagated and magnified in the final steps of the algorithm. Thus, as we expect, unless the interpolation problem at hand is extremely well conditioned, the recursive algorithm does not result in satisfactory reconstruction. In section (3.3), we will derive a line by line reconstruction

algorithm which is somewhat similar to the recursive algorithm of section (3.2), but is free of its numerical instabilities. The basic idea behind line by line reconstruction is to recover the one-dimensional signal associated with each of the sampling lines and then to interpolate the original signal from these one-dimensional functions. We will propose two strategies for the former part of the algorithm. The first strategy is non-iterative; It can be used for a variety of reconstruction problems utilizing the semi-implicit sampling strategy The second strategy, which is iterative, can only be applied to the problem of reconstruction from function crossings. In addition, the number of interpolation points required for each of these two line by line reconstruction strategies exceeds the theoretical requirements of Chapter 2. The main features of the iterative algorithm are its robustness, speed, and low storage requirements.

For all the reconstruction examples of this chapter, the location of crossings are specified to 16 digits. The quantization issues of some of the reconstruction methods described in this chapter will be investigated further in Chapter 5.

3.1 Linear Least-Squares Approach

The most straightforward approach to the reconstruction of signals via the semi-implicit sampling strategy is to solve a linear system of equations. Thus, in reconstructing a $(2N+1) \times (2N+1)$ BLP signal from n_t thresholds, we must first find a set of sampling lines whose intersections with the threshold contours satisfy the theoretical requirements of Chapter 2, Then these $M > N^2$ samples are used to solve the following linear system of equations:

$$\sum_{k_1=-N}^{N} \sum_{k_2=-N}^{N} F(k_1,k_2) e^{j2\pi(k_1 x_j + k_2 y_j)} = t_i \quad 1 \le i \le n_t, \quad 1 \le j \le M$$

The required number of reconstruction samples depends on the sampling lines and is at least as large as the number of Fourier coefficients. As we will see in section (5.1.2), increasing the

number of reconstruction samples improves the condition number of the reconstruction problem at hand.

Examples of reconstruction of the 31×31 eye picture shown in figure (2.10) from 8 of its level crossings are shown in figures (3.1) and (3.2). Figure (3.1) shows the 8 level non-uniform amplitude quantized version of figure (2.10) and the threshold contours associated with these levels. Since the intensity value of the original picture lies between 0 and 256, the thresholds were also chosen in this range. Figure (3.2), shows the reconstructed versions of the original eye picture, via different sets of sampling lines. More specifically, 31 sampling lines of unit slope were used for the reconstruction shown in figure (3.2a), 11 sampling lines of slope 3 were used for the reconstruction shown in figure (3.2b), and 15 sampling lines with slopes $1, 2, \pm\frac{1}{2}, \pm 3, \pm\frac{1}{3}, \pm 4, \pm\frac{1}{4}, 5$ were used for the reconstruction shown in figure (3.2c). In all the above examples, the distributions obtained from the intersections of sampling lines and threshold contours satisfied the theoretical requirements of Theorems (2.3), (2.4), and (2.3). To improve the robustness, we used *all* the intersections of sampling lines and threshold contours as reconstruction samples, and applied QR decomposition [1] to solve the overdetermined linear systems of equations associated with each example. More specifically, the number of samples used for reconstructions shown in figures (3.2a), (3.2b), and (3.2c) were 1475, 1266, and 1548 respectively.

Robustness of the linear least-squares approach is highly dependent upon the actual algorithm used for solving the overdetermined system of equations. Of the many algorithms available, we chose the QR decomposition primarily for stability reasons. Unfortunately, the most stable algorithms, such as QR, are also very computation intensive. For instance, solving an $m \times p$ overdetermined system of equations requires mp^2 floating point operations (flops).

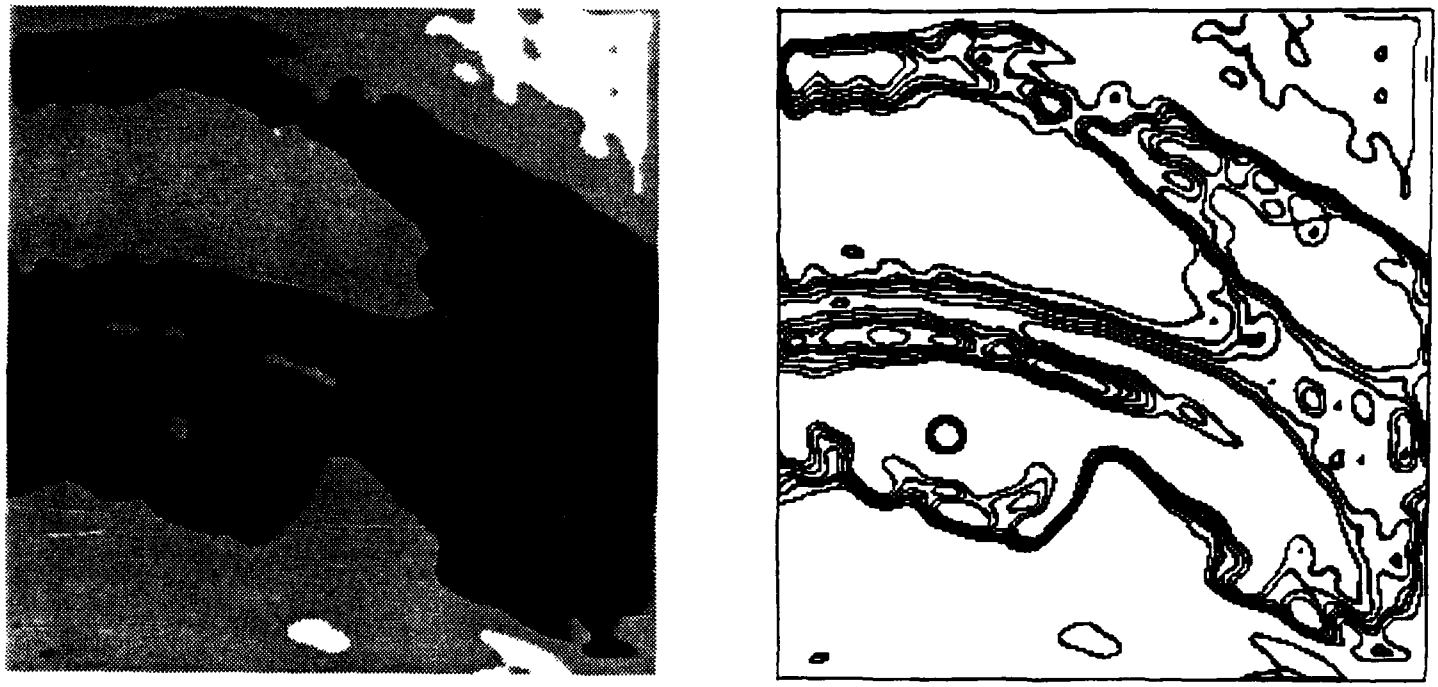

(a) (b)

Figure 3.1: *(a) 8 level non uniform amplitude quantized version of the original eye picture; (b) Threshold contours associated with the 8 level crossings.*

Thus, assuming that the number of interpolation points used is of the same order of magnitude as the number of unknown Fourier series coefficients, for an image with $N \times N$ region of support in the Fourier domain, the number of flops required by the QR decomposition algorithm is proportional to N^6. The other major drawback of the linear least-squares approach is its storage requirements. The storage required for an image with $N \times N$ region of support in the Fourier domain is N^4. Indeed, storage was our main limiting factor in terms of the largest image we could process using the QR decomposition.

One way to get around the storage problem is to use iterative algorithms such as the conjugate gradient method. In these algorithms, the $M \times N^2$ matrix associated with the M

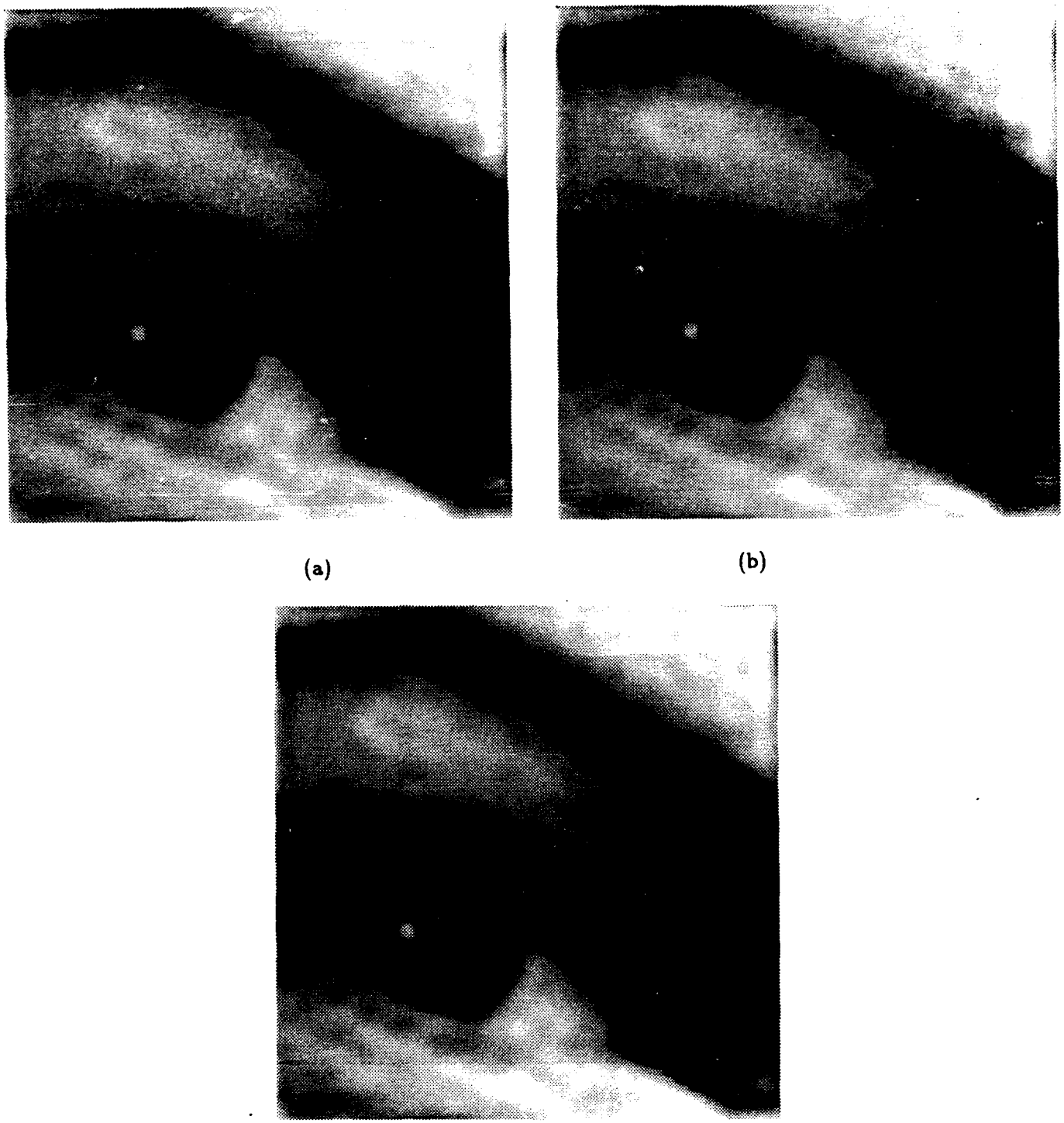

Figure 3.2: *Reconstructed version of the original eye picture via QR decomposition from intersections of 8 level crossings with: (a) 31 lines of unit slope, (b) 11 lines of slope 3, (c) 15 lines of slopes* $1, 2, \pm\frac{1}{2}, \pm 3, \pm\frac{1}{3}, \pm 4, \pm\frac{1}{4}, 5$.

samples of a signal with $N \times N$ region of support in the Fourier domain need not be stored, since in each step of the iteration we only need to multiply it implicitly by a vector. The conjugate gradient algorithm needs to operate on symmetric matrices. Thus, in order to solve the overdetermined system of equations given by:

$$A\,\vec{x} = \vec{b}$$

we need to premultiply both sides of the above equation by A^T to get:

$$A^T\,A\,\vec{x} = A^T\,\vec{b}$$

Since the condition number of $A^T A$ is the square of the condition number of A, and the convergence rate of the algorithm is proportional to the condition number of $A^T A$ [1], if our original interpolation problem is slightly ill-conditioned (i.e., A has rather large condition number), then it will take many iterations before the algorithm converges. Thus, the conjugate gradient approach is only appropriate for situations where our interpolation problem is well-conditioned. Geometrically speaking, this corresponds to the situation in which our samples are more or less evenly distributed in the image. We have found experimentally that reconstruction of images from multiple level threshold crossings via the conjugate gradient algorithm is unsuccessful, when the number of thresholds is small. As an example, consider figure (3.3b) which shows the reconstructed version of the original eye picture from 8 of its thresholds crossings on lines of slope 1 via the conjugate gradient algorithm. The intersections of threshold crossings and the sampling lines are shown in figure (3.3a). As is apparent, the quality of reconstruction in various areas of the image is highly dependent on the density of the available crossings in the region.

Although the conjugate gradient algorithm does not perform satisfactorily for reconstruction

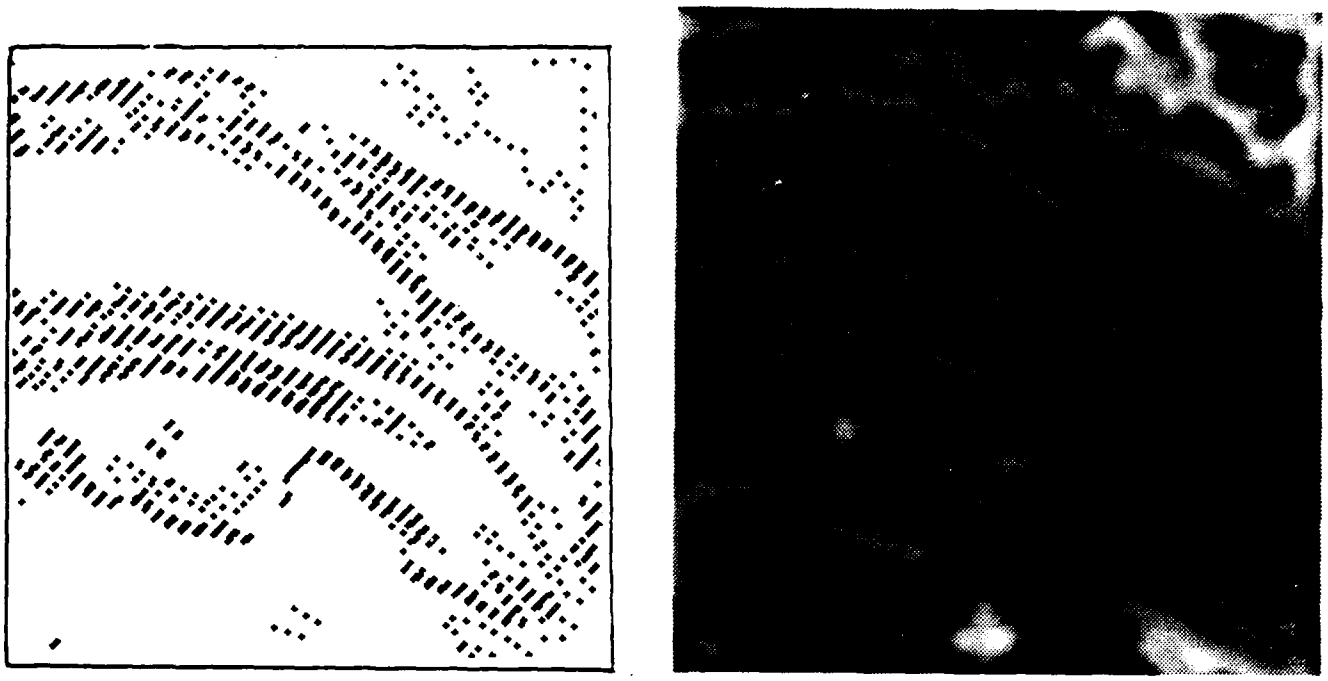

(a) (b)

Figure 3.3: *(a) Intersections of lines of unit slope with the 8 level crossings shown in figure (3.1b); (b) Reconstructed version of the eye picture via the conjugate gradient algorithm using the intersections of 8 level crossings with lines of unit slope.*

from level crossings, it can be used successfully for reconstruction problems in which the samples are evenly distributed across the image. Recall from section (2.3.1) that the sinusoid crossings of BLP signals lie in between parallel equidistant lines at which the sinusoid assumes its maximum and minimum values. Thus, we would expect the conjugate gradient algorithm to perform satisfactorily for the problem of reconstruction from sinusoid crossings[1]. Figure (3.4) shows the one bit amplitude quantized version of the original 31×31 eye picture with the sinusoidal function

[1]Note that even distribution of the samples results in stable reconstruction of the signal *plus sinusoid*, and not necessarily the signal itself. For instance, if the dynamic range of the sinusoid is much larger than that of the signal, we would expect the quality of reconstruction of the signal by itself to be rather poor.

$$128\{1 + cos[2\pi(16x + 16y)]\}$$

Figure (3.5) shows the reconstructed version of the eye picture via the conjugate gradient algorithm with 20 iterations. The reconstruction samples were chosen to be a subset of all the intersections of the 31 lines of unit slope with the crossings, satisfying the minimum distribution requirements of Corollary (2.1).

Our second example involves reconstruction of the 63×63 picture shown in figure (3.6) which will be referred to as *cman*. One bit amplitude quantized version of the sum of original cman picture and the sinusoidal function:

$$128\{1 + cos[2\pi(32x + 32y)]\}$$

is shown in figure (3.7). Its reconstructed versions via the conjugate gradient algorithm with 20 iterations are shown in figure (3.8). Figure (3.8a) was reconstructed from all the intersections of 63 equidistant lines of slope one with sinusoid crossings, whereas a smaller subset of the intersections satisfying the theoretical requirements of Theorem (2.3) were chosen for reconstruction of figure (3.8b). Thus, all the sampling lines in the former case have 64 points, whereas in the latter case there are sampling lines with as few points as 1 or 3. Indeed, the artifacts shown in figure (3.8b) are due to the fact that some sampling lines contain many fewer interpolation points than other lines. To summarize this section, we have proposed the application of two major least-squares algorithms for solving the linear system of equations associated with our reconstruction problem. The QR decomposition approach is extremely robust and can be used for a variety of reconstruction problems including the ones in which the samples are not evenly distributed across the image. The drawback of the QR decomposition approach is that it is computationally intensive and its storage requirements are rather large. The conjugate gra-

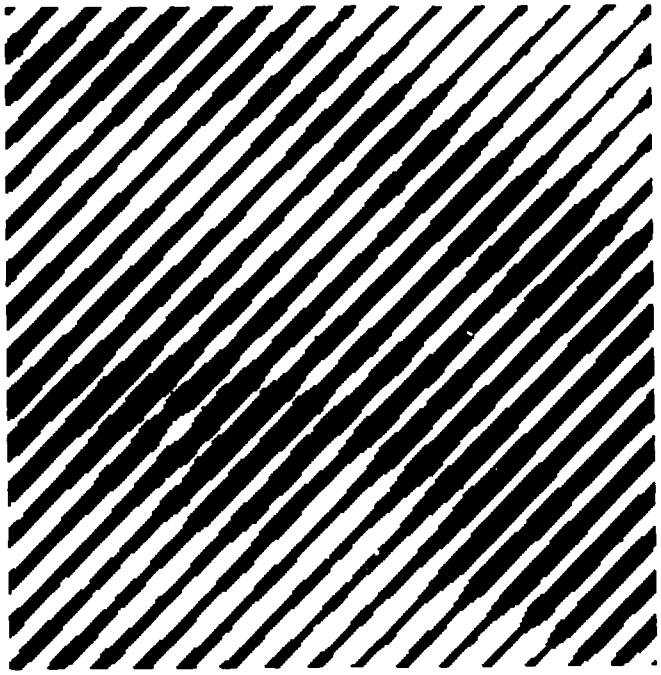

Figure 3.4: *One bit amplitude quantized version of the sum of the original eye picture and* $128(1 + cos(2\pi(16x + 16y)))$.

Figure 3.5: *Reconstruction of the eye picture from its sinusoid crossings via the conjugate gradient algorithm. Reconstruction samples were chosen from a subset of all the intersections of lines of unit slope with the crossings, satisfying the minimum distribution requirements of Theorem (3.6).*

Figure 3.6: *The original cman picture with* 63×63 *Fourier coefficients.*

Figure 3.7: *One bit amplitude quantized version of the sum of the original cman picture and* $128(1 + cos(2\pi(32x + 32y)))$.

(a)

(b)

Figure 3.8: *Reconstruction of the cman picture from its sinusoid crossings via the conjugate gradient algorithm. All the intersections of sampling lines of unit slope with the sinusoid crossings were used for reconstruction shown in (a), and a subset of them for (b).*

dient algorithm needs less storage and converges rather quickly for well conditioned problems such as reconstruction from sinusoid crossings. However, its slow convergence properties for ill conditioned problems limits .ts applicability to reconstruction from multiple level threshold crossings.

3.2 Recursive Approach

As mentioned in Chapter 2, although the algebraic geometric results of section (2.2.3) are considerably more general than those of sections (2.2.1) and (2.2.2), the inherent advantage of the results in the latter sections lies in the existence of recursive algorithms to carry out the reconstruction proposed by their theoretical results[2]. These algorithms are essentially based on the constructive proofs of Theorems (2.3) and (2.4) which provide us with sufficient conditions for unique recovery of BLP signals from their samples on lines with fixed positive integer slope. These proofs are constructive in the sense that unique recovery is shown by actually deriving a reconstruction strategy. Since detailed description of the recursive algorithms are included in Chapter 2 and Appendix (A), we will briefly describe the recursive algorithm based on the proof of Theorem (2.3) and show a few examples of reconstruction.

Theorem (2.3) of section (2.2.1) provides us with the distribution of points on lines passing through the origin, which results in unique recovery of polynomials

$$p(w,z) = \sum_{i=0}^{n} \sum_{j=0}^{n} a(i,j)\, w^i\, z^j \tag{3.1}$$

More specifically, it states that for unique reconstruction of a polynomial of the above form, we

[2]It might also be possible to derive a recursive proof for the results of section (2.2.3). However, since such a proof would be considerably more complex than the algebraic geometric one, and its resulting recursive algorithm is likely to be rather unstable (for reasons which we will discuss in this section), we have decided not to presue the recursive approach for the theoretical results of section (2.2.3).

need $n+1$ lines $l_0, ..., l_n$

$$z = \alpha_i w \qquad \alpha_i \neq 0$$

with $2i + 1$ points on the ith line. Defining the variables $b_i^{(k)}$ associated with the kth sampling line in terms of its slopes α_k and the polynomial coefficients $a(i,j)$ in the following way:

$$b_i^{(k)} = \begin{cases} \sum_{m=0}^{i} a(i-m,m)\alpha_k^m & , \ 0 \leq i \leq n \\ \sum_{m=i-n}^{n} a(i-m,m)\alpha_k^m & , \ n \leq i \leq 2n \end{cases} \tag{3.2}$$

we conclude that samples on the kth line satisfy:

$$\sum_{i=s+1}^{2n-s-1} b_i^{(k)} w^i = p(w, \alpha_k w) - \sum_{i=0}^{s} b_i^{(k)} w^i - \sum_{i=2n-s}^{2n} b_i^{(k)} w^i \tag{3.3}$$

The recursive algorithm essentially consists of $2n+1$ steps corresponding to $s = -1, ..., 2n-1$ in the above equation. More specifically, at the sth stage, the algorithm uses the computed values of $b_{2n-s}^{(k)}$ and $b_s^{(k)}$ for $0 \leq k \leq n$, together with the $2(n-s)-1$ samples on the line l_{n-s-1}, in order to find $b_i^{(n-s-1)}$ for $s+1 \leq i \leq 2n-s-1$ by solving a linear system of equations indicated by equation (3.3). These values are then used in equation (3.2) to find the coefficients $\{a(i,j) \mid i + j = s+1, 2n-s-1\}$ by solving a second set of linear equations. Finally, the coefficients $\{a(i,j) \mid i + j = s+1, 2n-s-1\}$ are used to find $b_{2n-s-1}^{(k)}$ and $b_{s+1}^{(k)}$ for $0 \leq k \leq n-s-2$ via equation (3.2) for the next step of the algorithm.

From the above description, we see that the polynomial coefficients are found recursively and that the coefficients found in initial steps are used to compute the ones in the later stages. Thus, as we might expect, small errors in finding the coefficients in the initial steps are propagated and magnified in the final steps of the algorithm. Indeed, this turns out to be a major source of instability for the recursive algorithm.

Since BLP signals can be expressed as polynomials, the above recursive algorithm can be used for reconstructing signals from their samples on lines of unit slope. In applying this algorithm to the problem of reconstruction from multiple level crossings, we have found that unless the interpolation points are more or less evenly distributed across the image, the algorithm fails to recover the signal successfully. For instance, the algorithm is unsuccessful in reconstructing the 31×31 eye picture of figure (2.10) from its 8 level crossings shown in figure (3.1b), even though it is capable of reconstructing it from its sinusoid crossings shown in figure (3.4). This is because, as we mentioned earlier, the sinusoid crossings of the signal are almost uniformly distributed across the image. The reconstructed version of the eye picture from its crossings with $128\{1 + cos[2\pi(16x + 16y)]\}$ is shown in figure (3.9). The reconstruction samples were chosen to be a subset of all the intersections of 31 equidistant lines of unit slope with the crossings, satisfying the minimum required distribution of Theorem (2.3).

The reconstructed version of the cman picture from its sinusoid crossings shown in figure (3.7), is shown in figure (3.10). The reconstruction samples were chosen to be a subset of the intersections of 63 equidistant lines of unit slope and the sinusoid crossings, satisfying the distribution requirements of Theorem (2.3). Notice that unlike reconstruction via conjugate gradient algorithm shown in figure (3.8b), there are no artifacts in figure (3.10) due to unequal number of samples on different sampling lines. This indicates that the recursive algorithms are somewhat more stable than the conjugate gradient algorithm. In fact, the recursive algorithm described in this section is robust enough for reconstruction from sinusoid crossings of larger images such as the one shown in figure (3.11). Figure (3.11) which will be referred to as *vegas*, has 127×127 Fourier coefficients. Its crossings with $128\{1 + cos[2\pi(64x + 64y)]\}$ are shown in figure (3.12) and its reconstructed version is shown in figure (3.13). The reconstruction

samples were chosen as a subset of the all the intersections of 127 equidistant lines of slope one with the sinusoid crossings, satisfying the minimum distribution requirements of Theorem (2.3).

Finally, let us briefly discuss the efficiency and storage requirements of the recursive algorithm, described in this section. As we mentioned earlier, to find the coefficients of a polynomial given by equation (3.1), the recursive algorithm goes through $2n+1$ steps and in each step it has to solve two Van der Monde systems of linear equations. More specifically, in the kth step, the size of these systems are $(2n-k)\times(2n-k)$ and $(k+2)\times(k+2)$. Although there are ways of solving a $p\times p$ Van der Monde system of equations with $O(p^2)$ flops, these methods are usually unstable. Stable techniques, on the other hand, require $O(p^3)$ floating point operations. Thus the total number of operations required for reconstruction of a signal with $N\times N$ region of support in the Fourier domain is of the order of $O(N^4)$. Furthermore, the storage requirements of the recursive algorithm is of the order of N^2.

Comparing characteristics of the recursive algorithm with the QR decomposition we find that the latter requires more computation and space but is also more stable. However, as we saw in figures (3.8b) and (3.10), the recursive approach is more stable than the iterative approach of the conjugate gradient algorithm. Furthermore, the recursive algorithm can only be used for reconstruction from samples on lines of integer slope with all the lines having equal slopes, whereas the linear least-squares approaches of section (3.1) are capable of reconstructing from samples on lines with different positive or negative rational slopes. However, the least-squares and recursive methods are similar, in the sense that they can both be used for the more general problem of reconstruction from non-uniformly distributed samples, as opposed to the specific problem of reconstruction from level crossings. As we will see in the next section, this is not

Figure 3.9: *Reconstructed version of the eye picture via the recursive algorithm from its sinusoid crossings. The reconstruction samples were chosen to be a subset of all the intersections of 31 equidistant lines of unit slope with the crossings, satisfying the minimum required distribution of Theorem (3.6).*

Figure 3.10: *Reconstructed version of the cman picture from its sinusoid crossings via the recursive algorithm. The reconstruction samples were chosen to be a subset of all the intersections of 63 equidistant lines of unit slope with the crossings, satisfying the minimum required distribution of Theorem (3.6).*

Figure 3.11: *The original vegas picture with* 127×127 *region of support in the Fourier domain.*

the case for the iterative version of our line-by-line reconstruction algorithm.

3.3 Line by Line Reconstruction Approach

As we saw in the previous section, the major drawback of the recursive approach to reconstruction is its numerical instability, which is a direct consequence of computing the Fourier coefficients recursively. More specifically, the recursive algorithm finds the coefficients in the kth step by using the value of the coefficients it has computed in the first $(k-1)$ steps. Thus, as we might expect, small errors in computing the coefficients in the initial steps are propagated and magnified in the final steps of the algorithm.

Our main goal in this section is to propose a new algorithm, similar in style to the recursive

Figure 3.12: *One bit amplitude quantized version of the sum of vegas picture and* $128\{1 + cos[2\pi\ (64x + 64y)]\}$.

Figure 3.13: *Reconstructed version of the vegas picture from its sinusoid crossings via the recursive algorithm. The reconstruction samples were chosen to be a subset of all the intersections of 127 equidistant lines of unit slope with the crossings, satisfying the minimum required distribution of Theorem (3.6).*

approach, which is free of its numerical instabilities. The line by line reconstruction strategy we are going to describe in this section exploits the fact that the one-dimensional signal obtained by sampling our two-dimensional signal along a line with rational slope is bandlimited and periodic. More specifically, consider a two-dimensional, BLP signal with $(2N+1) \times (2N+1)$ region of support in the Fourier domain given by

$$f(x,y) = \sum_{k_1=-N}^{N} \sum_{k_2=-N}^{N} F(k_1,k_2)\, e^{j2\pi x k_1}\, e^{j2\pi y k_2}$$

If it is sampled along the line:

$$my = nx + \beta$$

the one-dimensional signal is periodic and has $2N(m+n)+1$ Fourier series coefficients. Thus $2N(m+n)+1$ samples of this one-dimensional signal will enable us to uniquely specify it[3]. Since our semi-implicit line sampling strategy of Chapter 2 consists of using points on lines of various rational slopes, an obvious way to recover a two-dimensional signal would be to

1. Reconstruct each of the one-dimensional signals corresponding to the sampling lines separately.

2. Recover the two-dimensional signal using the one-dimensional ones.

We now need to address a few issues with regard to the above reconstruction strategy. The first issue is whether or not the sampling distribution proposed by the theoretical results of Chapter 2 provide us with enough interpolation points to recover the one-dimensional signal associated with each of the sampling lines. As it turns out, the sampling requirements of the above line by line reconstruction scheme are more stringent than those of Corollary (2.3),

[3]The fact that the one-dimensional signal associated with a sampling line with rational slope is bandlimited and periodic was originally shown by Merseraeu [2].

which is the most general result of Chapter 2. For instance, in situations where all of the sampling lines have integer slopes p, the theoretical results of Chapter 2 require $2(p+1)N - 2pi$ interpolation points on the ith line, whereas the above line by line reconstruction strategy needs $2(p+1)N$ samples on *all* the lines. In other words, for line by line reconstruction, the number of samples required on each of the lines is equal to the maximum number of points required by Theorem (2.4) on *any* one of them. Since the line by line approach requires more samples than the minimum specified by the theoretical results of Chapter 2, we would expect that, for the problem of reconstruction from level crossings, more thresholds are needed to generate these samples. Indeed, as we will see in the examples of this section, while the eye picture of figure (2.10) can be reconstructed from samples of its 8 level crossings via the linear least-squares approach, 14 level crossings are needed for its line by line reconstruction.

The second issue which needs to be addressed has to do with the recovery of the two-dimensional signal under consideration, once all the one-dimensional signals associated with the sampling lines have been reconstructed. In situations where all the nodes of the $(2N+1) \times (2N+1)$ square grid of the two-dimensional signal are located on the sampling lines, the value of the signal on the grid can be computed easily from the one-dimensional signals. Equally spaced sampling lines of unit slope is an example of such a situation. For the more general case, we can proceed as follows:

1. Use the one-dimensional signals to find their intersections with $(2N+1)$ equally spaced horizontal or vertical lines. For the most general sampling scenario, described by Corollary (2.3), we can show that each horizontal or vertical line intersects our sampling lines in at least $(2N+1)$ points. More specifically, if inequality (2.40) of Corollary (2.3) is satisfied, then each of the $(2N+1)$ horizontal lines intersect our sampling lines at $(2N+1)$ points;

On the other hand, if inequality (2.41) is satisfied, then each of the $(2N+1)$ vertical lines intersect our sampling lines at $(2N+1)$ points.

2. Since the one-dimensional signal associated with each horizontal or vertical line is a BLP signal with $(2N+1)$ Fourier coefficients, they are reconstructible from their $(2N+1)$ samples, obtained in the previous step.

3. For each of the horizontal or vertical lines, find the values of the signal on $(2N+1)$ equally spaced points. These $(2N+1)$ points on each of the $(2N+1)$ horizontal or vertical lines correspond to samples of the two-dimensional signal on a $(2N+1) \times (2N+1)$ square grid.

The third issue we need to address is the recovery of the one-dimensional signals associated with the sampling lines. As we mentioned earlier, the sampling requirements of line by line reconstruction could be more stringent than those required by the theoretical results of Chapter 2. Since the one-dimensional signal along the ith sampling line:

$$l_i : \qquad m_i\, y \;=\; n_i\, x \;+\; \beta_i$$

is bandlimited and periodic with $2N(m_i + n_i) + 1$ Fourier harmonics, theoretically speaking, $2N(m_i + n_i) + 1$ samples of it are sufficient to reconstruct it uniquely. We can find its Fourier series coefficients by solving a $(2N(m_i+n_i)+1) \times (2N(m_i+n_i)+1)$ linear system of equations, or use Lagrange interpolation to compute its samples. An example of reconstruction of the original eye picture shown in figure (2.10) from intersections of 14 of its threshold crossings with lines of unit slope is shown in figure (3.14). In this example, the one-dimensional signals associated with the sampling lines were found by solving linear systems of equations.

For the specific problem of reconstruction from level crossings, we can propose an iterative algorithm which uses *all* the intersections of the level crossings with sampling lines to reconstruct

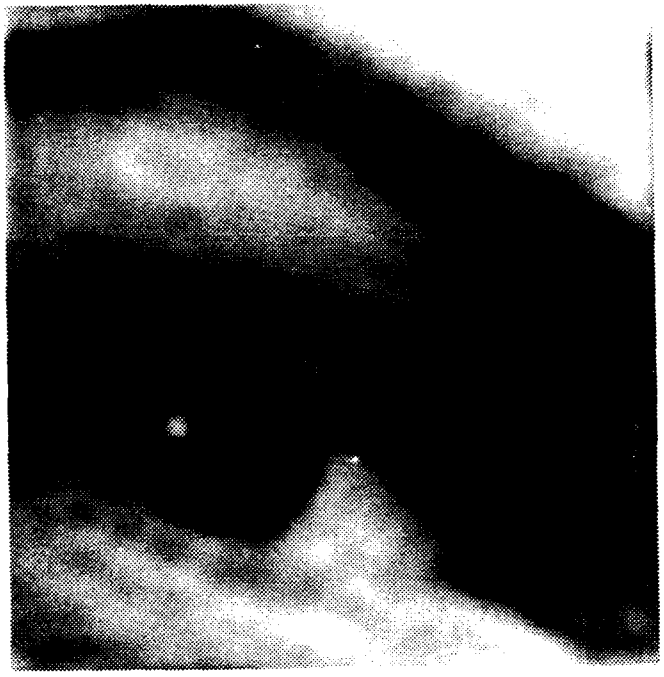

Figure 3.14: *Reconstruction of the original eye picture from intersections of lines of unit slope with 14 of its level crossings. Non-iterative line by line reconstruction was used.*

the one-dimensional signals associated with the sampling lines. We will devote the remaining part of this section to this iterative algorithm.

3.3.1 Iterative Approach to Line by Line reconstruction

In this section, we will describe an iterative algorithm for the reconstruction of one-dimensional signals, associated with sampling lines, from their intersections with level crossings. As we will see, similar to the least-squares and recursive approaches of sections (3.1) and (3.2), the iterative approach can be applied both to the specific problem of reconstruction from function crossings and to the more general problem of reconstruction from non-uniformly distributed samples.

The basic idea behind iterative reconstruction is to iterate between space and frequency domains by imposing appropriate constraints on the signal in each domain. The frequency domain constraint is due to the fact that the one-dimensional signal, obtained by sampling our two-dimensional signal along a line with rational slope, is bandlimited and periodic. The space domain constraint can be derived using the level crossing information. More specifically, if the locations of all the crossings of a one-dimensional, continuous, BLP signal $g(z)$ with p thresholds $t_1 < t_2 \ldots < t_p$ are known, and the signal is known to be in the range $[t_0, t_{p+1}]$, then for any arbitrary z_0, we can deduce the range into which $g(z_0)$ falls. That is, given z_0, we can find i such that

$$t_i \leq g(z_0) \leq t_{i+1}$$

The above process is shown pictorially in figure (3.15). In order to derive the range information for any point on a one-dimensional signal, we need a minimum of two samples corresponding to two different thresholds. This has to do with the fact that the samples, corresponding to one threshold, are incapable of resolving the sign ambiguity of the one-dimensional signal under consideration.

Using the above ideas, we propose the following algorithm for reconstructing a one-dimensional, continuous, BLP signal, $g(z)$ with period 1 and $2N+1$ Fourier harmonics from *all* of its level crossings with thresholds $t_1, \ldots, t_p$:

1. Deduce the range of intensity for $M > 2N+1$ equally spaced points

$$0, \frac{1}{M}, \frac{2}{M}, \ldots, \frac{M-1}{M}$$

That is, for each of the above points, find the threshold t_i such that the actual value of g at that point is larger than t_i and smaller than t_{i+1}. Thus, if $t_l(n)$ and $t_u(n)$ denote the

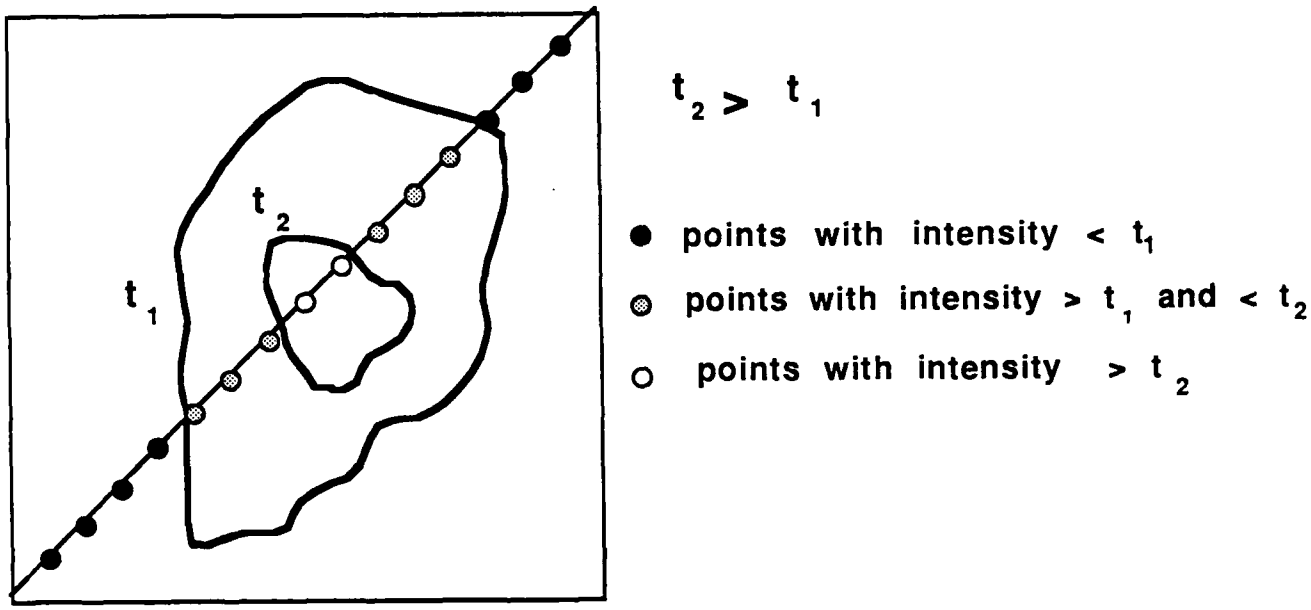

(a)

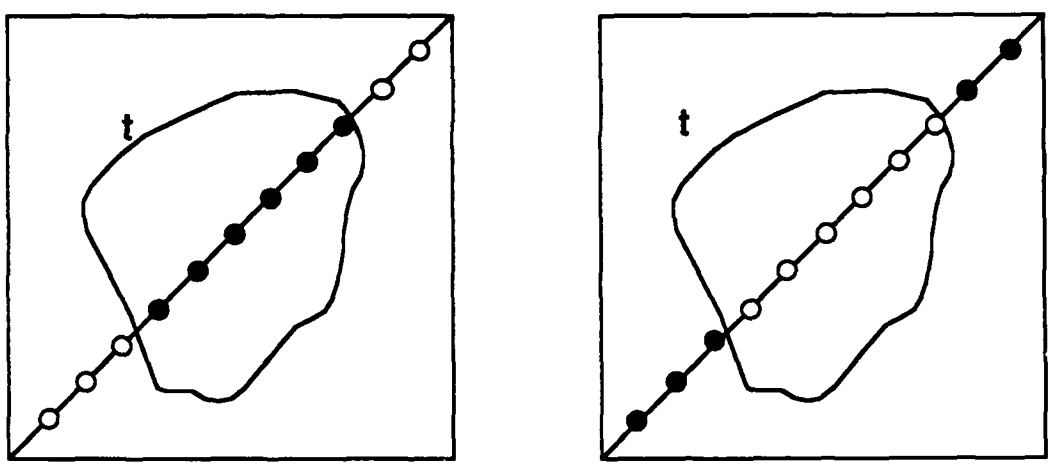

points with intensity > t

points with intensity < t

(b)

Figure 3.15: *(a) Deriving the space domain constraint for recovery of a one-dimensional signal via the iterative algorithm; (b) Ambiguous range information via samples of the contour associated with one threshold.*

lower and upper bound for the nth point, we have:

$$t_l(n) \leq g(\frac{n}{M}) \leq t_u(n) \quad , \quad n = 0, ..., M-1 \tag{3.4}$$

2. Let $g^{(l)}(\frac{n}{M})$ denote the value of g in the lth iteration at the point $\frac{n}{M}$. Then, the initial guess becomes:

$$g^{(0)}(\frac{n}{M}) = \frac{t_l(n) + t_u(n)}{2} \quad , \quad n = 0, ..., M-1$$

As we will see later, the convergence of the algorithm is independent of the initial guess.

3. Take the discrete Fourier transform (DFT) of g in the lth step:

$$G^{(l)}(k) = DFT\ [\ g^{(l)}(\frac{n}{M})\ ] \quad , \quad 0 \leq n, k < M$$

4. Impose the bandlimited constraint:

$$\tilde{G}^{(l+1)}(k) = \begin{cases} G^{(l)}(k) & , \quad 0 \leq k \leq N \quad , M-N \leq k < M \\ 0 & , \quad elsewhere \end{cases}$$

5. Take the inverse discrete Fourier transform (DFT^{-1}) of $\tilde{G}^{(l+1)}(k)$:

$$\tilde{g}^{(l+1)}(\frac{n}{M}) = DFT^{-1}[\tilde{G}^{(l+1)}(k)] \quad , \quad 0 \leq k, n < M$$

6. Impose the space domain constraint:

$$g^{(l+1)}(\frac{n}{M}) = \begin{cases} \tilde{g}^{(l+1)}(\frac{n}{M}) & , \quad t_l(n) \leq \tilde{g}^{(l+1)}(\frac{n}{M}) \leq t_u(n) \\ t_l(n) & , \quad \tilde{g}^{(l+1)}(\frac{n}{M}) < t_l(n) \\ t_u(n) & , \quad \tilde{g}^{(l+1)}(\frac{n}{M}) > t_u(n) \end{cases} \tag{3.5}$$

7. If all the M points of $\tilde{g}^{(l+1)}(\frac{n}{M})$ satisfy the space domain constraint to within some acceptable error, then we are done. Otherwise go to step (3) and repeat steps (3) through (7).

As far as convergence of the above algorithm goes, we can show that the mean square error between the unknown signal, which satisfies the space and frequency domain constraints, and the solution obtained via successive iterations decreases. Furthermore, as we will see in the next section, we can apply the theory of projection onto convex sets (POCS) to prove that the algorithm is guaranteed to converge to a solution, which satisfies both the space and frequency domain constraint, if such a solution exists.

3.3.2 Application of POCS to the Iterative Algorithm

We could use the theory of projection onto convex sets to establish the convergence of our algorithm. As we will see, our algorithm is a special case of a more general iterative scheme discussed extensively in the literature [46,47]. By generalizing our algorithm, we can not only establish its convergence, but also find ways of improving its convergence properties. The basic theorem describing the general iterative method can be stated as follows:

Theorem 3.1 (Youla and Webb [46]) *Let H be a Hilbert space with elements $f, g, ..., etc$, a zero vector ϕ and an inner product (x, y). Furthermore, let C_0, the intersection of closed, convex subsets $C_1, ..., C_m$ of H be given by:*

$$C_0 = \cap_{i=1}^{m} C_i$$

be non-empty. Consider the composition operator

$$T = T_m T_{m-1} ... T_1$$

where

$$T_i = 1 + \lambda_i (P_i - 1)$$

and P_i is a projection operator onto C_i. Then, for every $x \in H$ and every choice of relaxation constants $\lambda_1, ..., \lambda_m$ in the interval:

$$0 < \lambda_i < 2 \quad , \quad 1 \leq i \leq m$$

the sequence $\{T^n x\}$ converges weakly to a point in C_0. If H is finite dimensional, the convergence is strong. In addition, if one of the C_i's say C_m, is finite dimensional, by setting

$$\lambda_m = 1$$

we are guaranteed of strong convergence even though H might be infinite dimensional.

Before we proceed to apply the above result to our reconstruction problem, let us briefly go over a few definitions. The sequence $\{f_k\}$ is said to converge strongly to f if

$$\lim_{k\to\infty} \| f_k - f \| = 0$$

The sequence $\{f_k\}$ is said to converge weakly to f if

$$\lim_{k\to\infty} (f_k, g) = (f, g) \quad \forall g \in H$$

Finally, the *projection*

$$h \equiv P_i f$$

of f onto C_i is the element which satisfies

$$\min_{y\in C_i} \| f - y \|^2 = \| f - h\|^2$$

Our iterative algorithm is essentially a special case of Theorem (3.1) where the Hilbert space H is the finite dimensional space of all M point real sequences and the inner product between two M point sequences $x(n)$ and $y(n)$ is given by:

$$(x, y) = \sum_{n=0}^{M-1} x(n)y(n)$$

The convex, closed subsets of H, are given by C_1 and C_2. C_1 is the set of all M point real, bandlimited sequences whose DFT is 0 in the range $N < k < M - N$, and C_2 is the set of all M point real sequences, $y(n)$, which satisfy the space domain constraint derived from the level crossing information as described in the first step of our algorithm. That is:

$$t_l(n) \leq y(n) \leq t_u(n) \qquad 0 \leq n < M \tag{3.6}$$

Note that for C_2 to be closed, it is necessary to define it exactly the way it is shown above. For instance, if in inequality (3.6), the $\leq$ were replaced with $<$, then C_2 would not be closed. P_1 is the bandlimiting operator which projects onto the set C_1, and P_2 is the projection operator which imposes the space domain constraint and projects onto C_2. Thus, our iterative algorithm is nothing but a successive application of the operator $T = P_1 P_2$ to an arbitrary initial condition, which we chose in the second step of the algorithm. Therefore, taking into account the fact that H is a finite dimensional vector space, and applying Theorem (3.1) with

$$\lambda_1 = \lambda_2 = 1$$

we can conclude that our iterative algorithm converges strongly to an element in the set C_0, which in this case, is the set of M point real sequences which satisfy both the space and frequency domain constraints. It is worthwhile to mention that, since M is finite, there might be many M point real sequences in the set C_0. However, in the limit as $M \to \infty$, the set C_0 will contain exactly one sequence, as long as the number of samples on a given line exceeds the number of Fourier coefficients of the one-dimensional signal associated with the line (because of the uniqueness of Fourier series). Under these circumstances, H will not be finite dimensional; thus one might begin to worry whether strong convergence is guaranteed any longer. However, as it is mentioned in Theorem (3.1), since at least one of our convex closed subsets, namely C_1, is finite dimensional, we are still guaranteed of strong convergence as long as we set

$$\lambda_1 = 1$$

Theorem (3.1) not only outlines the conditions under which our iterative algorithm, described earlier in this section, converges, but also generalizes our algorithm by introducing the relaxation parameters λ_1 and λ_2. We can control the convergence properties of our algorithm

by adjusting the values of the λ's. We speak of under-relaxation or over-relaxation, depending on whether $0 < \lambda < 1$ or $1 < \lambda < 2$ respectively. With $\lambda = 2$, we have another special case, referred to by Motzkin and Schoenberg [48] as the reflection method. Values of λ outside the interval $(0, 2]$ disrupt convergence.

Convergence of the generalized iterative algorithm depends on the "angle" formed at the intersection of the projection sets, C_1 and C_2; a wide angle between the sets results in a faster convergence than situations where the sets intersect at a smaller angle. In general, one can expect that the smaller the intersection of the sets is, the smaller the angle at which they intersect will be, resulting in slower convergence. There are many ways to accelerate the convergence of this type of iterative algorithm. The simplest such technique is over-relaxation, which essentially consists of choosing the relaxation parameter between 1 and 2; this has the effect of "opening up" a small angle of intersection between sets. As we will see in the next section, for the particular problem of reconstruction from level crossings, convergence rates do not present serious enough problems for us to seek other means of accelerating convergence.

3.3.3 Examples of the Iterative Algorithm

An example of reconstruction of the original 31×31 eye picture of figure (2.10) via the iterative algorithm is shown in figure (3.16). Intersections of 14 level crossings with 32 lines of unit slope were used to recover the one-dimensional signal associated with the sampling lines. Although our theoretical results of Chapter 2 only require 31 sampling lines, to be able to use the FFT with a power of 2 for interpolation from one-dimensional signals to the square grid, we chose 32 equally spaced sampling lines. Thus samples of the two-dimensional signal

Figure 3.16: *Reconstructed version of the original eye picture from intersections of lines of unit slope with 14 level crossings via the iterative algorithm.*

on a 32×32 grid coincided with equally spaced points on the sampling lines. The relaxation parameters were chosen to be $\lambda_1 = \lambda_2 = 1$, and the number of equally spaced points on the sampling lines, M, was chosen to be 64.

The main reason for choosing such a large number of thresholds in the above example is that the number of crossings on a given line must be larger than the number of Fourier harmonics of the one-dimensional signal associated with that line. However, even if this condition is satisfied, there might still be many one-dimensional, BLP signals satisfying the space and frequency domain constraints, as long as M is finite. Thus, unique reconstruction, via the iterative algorithm, is possible only in the limit as $M \to \infty$, if the number of crossings on each line is greater than or equal to the number of Fourier series coefficients of the one-dimensional

signal associated with the line. Since in practice, M can not be infinite, the solution obtained by the iterative algorithm is only an approximate one, regardless of the number of crossings used for reconstruction. Therefore, the question which arises naturally is the way reconstruction quality is degraded as the number of crossings is decreased below the number of Fourier series coefficients of the one-dimensional signal to be recovered. We will answer this question more quantitatively in Chapter 5. In this section, however, we will only show two examples of reconstruction where the number of crossings on the sampling lines are smaller than the number of Fourier coefficients of the one-dimensional signal associated with the sampling line. Figure (3.17a) shows the reconstructed version of the eye picture from 4, 6 and 8 thresholds, via the iterative algorithm for $M = 64, 128$. Similar to the previous example, we chose 32 equidistant sampling lines, and 20 iterations for each one-dimensional reconstruction. The relaxation parameters were chosen to be $\lambda_1 = 1$, $\lambda_2 = 1.75$. Our second example shown in figure (3.17b) deals with the reconstruction of the 63×63 cman picture from 4, 6 and 8 thresholds with $M = 128, 256$. We used 64 equidistant sampling lines of unit slope, the number of iterations for each line was 20, and the relaxation parameters were chosen to be $\lambda_1 = 1$, $\lambda_2 = 1.75$.

As seen in both of the above examples, increasing the number of thresholds affects the quality of reconstruction in a more substantial way than increasing M. We have found experimentally that if the sixth step of the algorithm dealing with projection onto the space domain is modified in the following way:

$$g^{(l+1)}(\frac{n}{M}) = \begin{cases} \tilde{g}^{(l+1)}(\frac{n}{M}) & , \quad t_l(n) \leq \tilde{g}^{(l+1)}(\frac{n}{M}) \leq t_u(n) \\ \frac{t_l(n) + t_u(n)}{2} & , \quad otherwise \end{cases} \tag{3.7}$$

the algorithm converges in fewer steps than the case where relaxation parameters are used

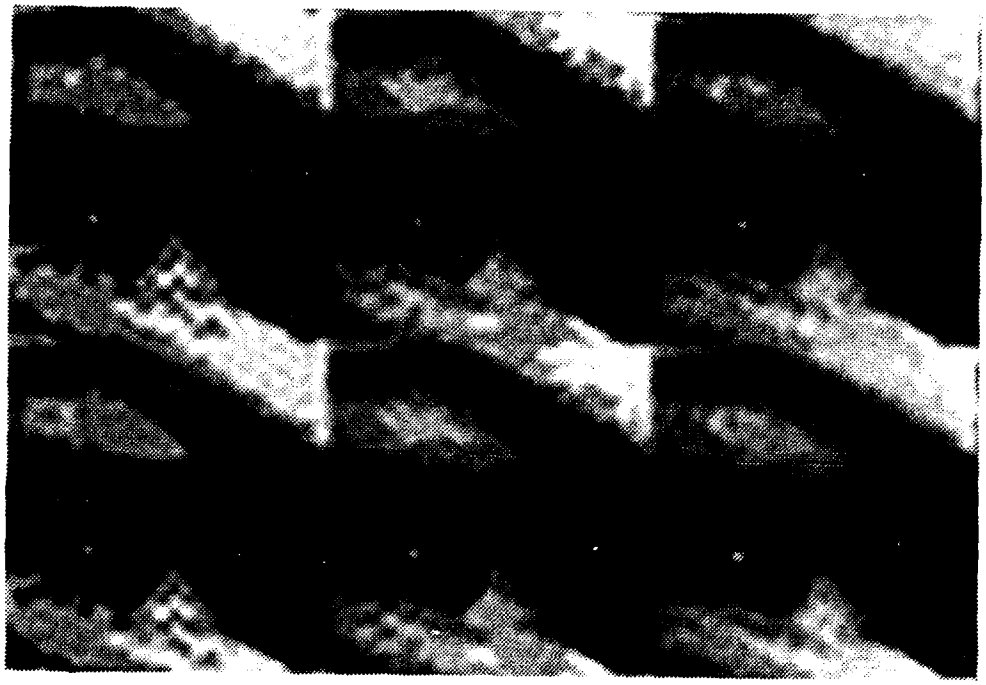

(a)

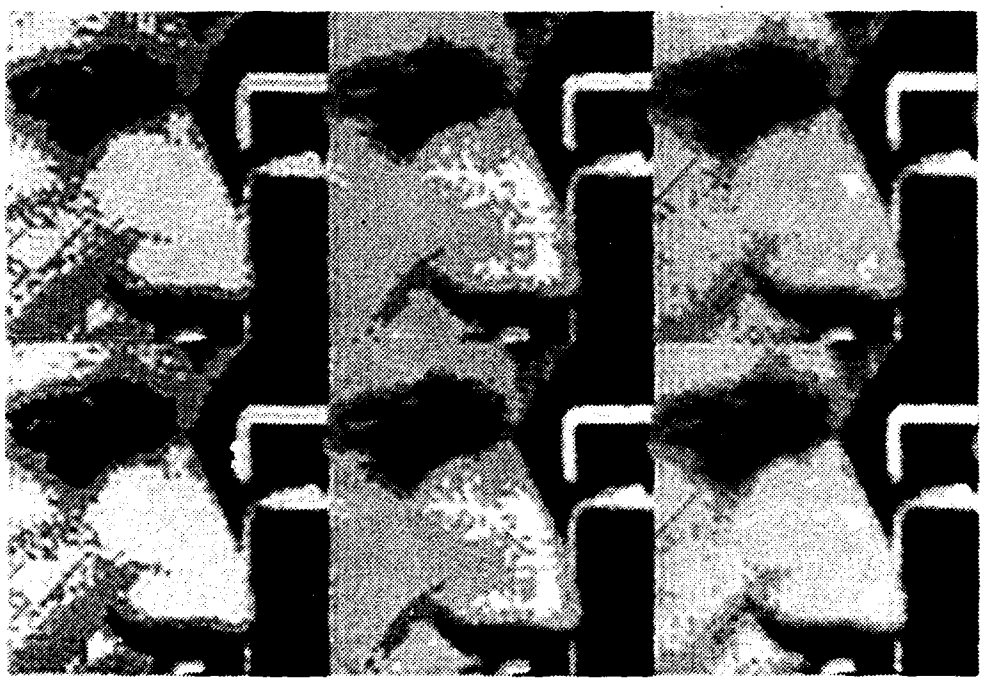

(b)

Figure 3.17: *Reconstructed version of the eye and cman pictures via the iterative algorithm. The numbers of thresholds are 4,6 and 8, increasing from left to right. The number of equally spaced samples on the lines increases from top to bottom, and are 64, 128 for the eye picture, and 128 and 256 for the cman picture.*

to accelerate convergence. Recall that the sixth step of the algorithm projects the sequence $\tilde{g}$ onto C_2, the set of M point real sequences satisfying the space domain constraint. This implies that if the value of the unknown function is constrained to be smaller than $t_u(n)$ and larger than $t_l(n)$, and $\tilde{g}(\frac{n}{M})$ is outside the interval $[t_l(n), t_u(n)]$, its projected value is either $t_u(n)$ or $t_l(n)$, depending on the value of $\tilde{g}(\frac{n}{M})$. Although the the scheme shown in equation (3.7) is not a projection and although the mean square error does not always decrease from one iteration to the next, by "projecting" onto $\frac{t_l(n)+t_u(n)}{2}$ instead of $t_l(n)$ or $t_u(n)$, we can somewhat speed up the convergence. This can be explained by formulating the problem in a statistical framework [49], but we shall not go over it here. The important point here is that, although in most reconstructions, carried out via the above modified version the algorithm, converged to a sequence satisfying both the space and frequency domain constraints, the mean square error of the solution was almost identical to the solution obtained via the over relaxation method. This suggests that the reason behind the poor quality of the reconstruction for a small number of thresholds is not the fact that the algorithm did not converge, but that there are many signals satisfying the space and frequency domain constraints; the algorithm has simply converged to one of them. Increasing the number of thresholds or increasing M, imposes more constraints on the signal, thus reducing the number of sequences satisfying both the space and frequency domain requirements. As we said earlier, if the number of crossings on a sampling line exceeds the number of Fourier harmonics of the one-dimensional signal associated with it, the solution, obtained via the iterative algorithm, becomes unique as $M \to \infty$.

Before we end this section, let us briefly compare the iterative algorithm with other reconstruction algorithms proposed in this chapter. Unlike the iterative approach which needs all the intersections of sampling lines with the crossings of the signal in order to derive the space

domain constraint correctly, all of our other algorithms can use a subset of the intersections for successful reconstruction. Clearly, the quality of reconstruction via the iterative algorithm is not as high as the least-squares approach or the non-iterative line-by-line reconstruction; However, one must bear in mind that reconstructions using the latter techniques use, at least in principle, the *exact* location of the crossings, whereas the iterative algorithm, in effect, uses the rather coarsely quantized version of the crossings as long as M is finite. We will study these quantization issues in more depth in Chapter 5. Finally, the iterative algorithm is free of many limitations of the other schemes proposed earlier in this chapter. More specifically,

- Its storage requirement is not as stringent as the QR decomposition, thus, enabling us to process much larger images. In fact, it is the only algorithm in this chapter which can reconstruct large images from multiple level crossings (as opposed to sinusoid crossings).
- It is not as computationally intensive as the QR decomposition, conjugate gradient or the non-iterative line-by-line reconstruction scheme.
- It is considerably more robust than the recursive algorithm of section (3.2), which is only capable of reconstruction from sinusoid crossings.
- It is more robust than the other algorithms in the sense that if the number of thresholds is not large enough to result in a sufficient number of crossings, it can still carry out approximate reconstruction. Indeed, this graceful degradation in the quality of reconstruction is a feature which is lacking in all the other algorithms we have discussed so far.

In Chapter 5, we will discuss the quantization characteristics of the iterative algorithm and the linear least-squares approach in detail.

3.4 Discussion

In this chapter, we proposed three major reconstruction algorithms for the semi-implicit sampling strategy of Chapter 2. Our first approach involved solving a linear system of equations via QR decomposition or the conjugate gradient algorithm. Reconstruction via QR decomposition is more stable than all of our other algorithms. However, its storage requirements are large enough to limit its applicability to reconstruction problems with a large number of Fourier coefficients. In fact, for a signal with $N \times N$ region of support in the Fourier domain, the storage requirement of the QR decomposition is proportional to N^6, and its computation requirements are proportional to N^6. The conjugate gradient algorithm does not need to store the entire linear least-squares matrix. It is, therefore, less storage intensive. However, its major drawback is that unless the reconstruction problem is extremely well conditioned, it does not result in satisfactory reconstruction. Thus, we have only been able to use it for recovery of signals from their sinusoid crossings.

The recursive algorithm proposed in section (3.2) takes advantage of the geometry of the interpolation points obtained via the semi-implicit sampling strategy. It is not as general as the linear least-squares approach, since it only deals with sampling situations in which all the sampling lines have fixed integer slopes. Furthermore, since it computes the coefficients recursively, small errors in the coefficients obtained in the initial stages of the algorithm are propagated and magnified in the final steps, resulting in instability. Although it is somewhat more stable than the conjugate gradient algorithm, it can only be applied to well conditioned problems such as reconstruction from sinusoid crossings.

The non-iterative line-by-line reconstruction scheme of section (3.3) is more stable than the

conjugate gradient or the recursive algorithm, and its computation and storage requirements are not as demanding as the QR decomposition. Its major drawback however, is that the number of crossings it needs for reconstruction exceeds the theoretical requirements of Chapter 2. Thus for reconstruction from multiple level crossings, the number of thresholds required by this algorithm is generally larger than our other algorithms.

Finally, the iterative algorithm of section (3.3.1) shares many of the characteristics of the non-iterative line-by-line reconstruction algorithm except that it is capable of approximate reconstruction in situations where the number of crossings do not satisfy the theoretical requirements of Chapter (2). However, it requires all the intersections of sampling lines with the crossings of the signal in order to derive the space domain constraint correctly.

In spite of the variety of reconstruction algorithms proposed in this chapter, the major drawback of the semi-implicit sampling scheme is the fact that, in general, we are never guaranteed to get enough intersections between the sampling lines and the level crossings in order to satisfy the minimum theoretical requirements of the Chapter 2. Of course, we can propose various guidelines in order to increase the number of intersections as much as possible. For instance, one way would be to choose the slopes of our sampling lines perpendicular to the general direction of the crossing contours. More specifically, if the harmonic content of a real signal at spatial frequency (p, q) is very strong, we would expect the signal to vary with frequency (p, q) along lines of slope $\frac{q}{p}$ and thus choosing the sampling lines with slope $\frac{q}{p}$ would result in large number of intersections.

Another way to increase the likelihood of satisfying the theoretical requirements is to choose sampling lines which result in the least stringent sampling requirements. For instance, in situations where all the sampling lines have equal slope $\frac{n}{m}$, the ratio between the maximum

number of points on a sampling line and its length is given by:

$$\rho_{max}^2 = \frac{[2N(m + n) + 1]^2}{n^2 + m^2} \approx 4N^2 \left[1 + 1 + \frac{n/m}{1 + (n/m)^2}\right]$$

Thus for $\frac{n}{m} > 1$, larger slopes result in less stringent sampling requirements whereas for $0 < \frac{n}{m} < 1$, smaller slopes result in less stringent sampling requirements.

Clearly, both of the above guidelines are somewhat qualitative and by no means do they guarantee that the number of intersections of the sampling lines with the level crossings satisfies the theoretical requirements of Chapter 2. The major drawback of the semi-implicit approach still remains, since it is incapable of providing us with sufficient conditions for unique reconstruction from an arbitrarily small number of thresholds. Indeed, this has been our main motivation for deriving the implicit sampling scheme of the next chapter.

Chapter 4

Implicit Approach to Reconstruction

In Chapter 2, we proposed a variety of semi implicit sampling strategies for the reconstruction of multidimensional signals from their crossings with arbitrary functions. More specifically, the intersection of sampling lines of rational slope with crossing contours was used to interpolate the bivariate polynomial associated with the signal. As we mentioned earlier, the major drawback of the line sampling strategy for reconstruction from function crossings is the fact that, in general, one is never guaranteed to get enough intersections between the sampling lines and signal crossings to satisfy the conditions of Corollaries (2.1), (2.2) and (2.3). As we saw in section (3.4), we can improve the likelihood of satisfying the sampling requirements of these theoretical results by careful choice of the slope and position of sampling lines. In addition, in section (3.4), we found that under certain conditions, the number of intersections of sampling lines with certain functions such as sinusoids, becomes predictable. In spite of these observations, the basic problem still exists; that is, for arbitrary functions, the intersections of sampling lines and level crossings might not result in a sufficient number of interpolation points to satisfy our theoretical results of Chapter 2. Therefore, it seems natural to search for more general strategies for reconstruction of multidimensional signals from their crossings with an *arbitrary*

AD-A195 561 RECONSTRUCTION OF MULTIDIMENSIONAL SIGNALS FROM MULTIPLE LEVEL THRESHOLD CROSSINGS(U) MASSACHUSETTS INST OF TECH CAMBRIDGE RESEARCH LAB OF ELECTRON.. 2/2

UNCLASSIFIED A ZAKHOR JAN 88 TR-534 N00014-81-K-0742 F/G 12/1 NL

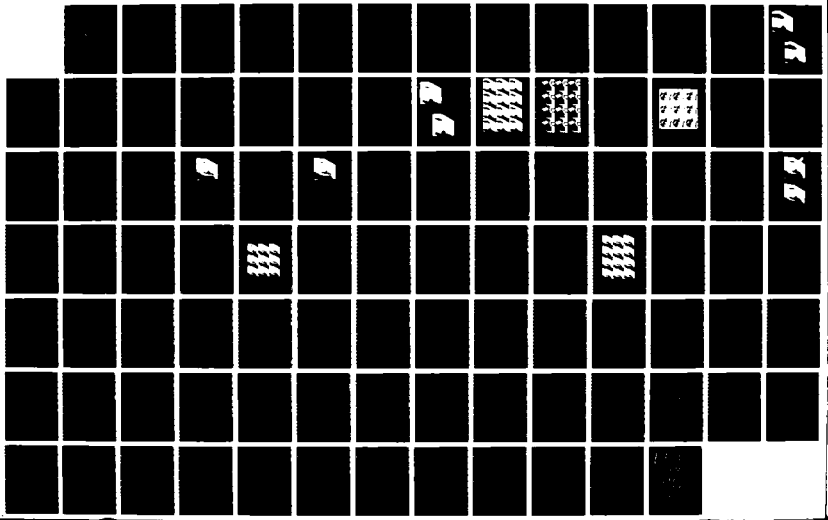

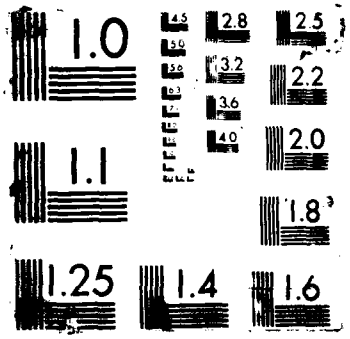
1.0
2.8
2.5
3.2
2.2
3.6
4.0
2.0
1.1
1.8
1.25
1.4
1.6

number of thresholds. The derivation of such a scheme will be our major goal in this chapter.

As we mentioned in Chapter 2, the inherent difficulty in bivariate interpolation is the lack of existence of Chebychef systems in R^2. Our approach in Chapter 2 was to constrain the location of our interpolation points. Another approach, which will be the basis for our implicit sampling strategy of this chapter, consists of conditionally regular interpolation methods. An interpolation method is called regular if it is uniquely solvable for *any* selection of interpolation points. Conditionally regular interpolation methods are solvable not for all selection of points, but only for most of them [31]. Roughly speaking, they are uniquely solvable with probability one. For methods of this type, if one has a concrete problem, and selects the interpolation points at random, it will be extremely likely that the problem will be solvable.

In section (4.1), we will take the above approach to derive sufficient conditions under which the problem of reconstruction from level crossings is almost always uniquely solvable. Section (4.2), describes two reconstruction algorithms for the results of section (4.1). It is worthwhile to mention that while the results of Chapter 2 are applicable to the more general problem of reconstruction from crossings with *arbitrary* functions, the results of this section are specifically tailored to reconstruction from level crossings or crossings with any pre-specified function that lies in the band of the signal under consideration. On the other hand, unlike the semi-implicit approach, the implicit approach of this chapter is capable of reconstruction from an *arbitrary* number of level crossings.

4.1 Theoretical Results

In this section, we apply algebraic geometric concepts to derive conditions under which multidimensional signals can be reconstructed from their level crossings with an arbitrary num-

ber of thresholds. More specifically, we will show that under mild conditions, a signal with $(2N+1) \times (2N+1)$ region of support in the Fourier domain can be uniquely reconstructed from almost any k points from its α level crossings, and $(2N+1)^2 - k$ points from its β level crossings. As we will see, the extension of the above result to the problem of reconstruction from more than two threshold crossings is rather straightforward. Furthermore, we can extend our basic result to the problem of reconstruction from sinusoid crossings, provided the frequency of the sinusoid under consideration lies within the bandwidth of our signal.

Consider a two-dimensional, real, BLP signal, $f(x,y)$ with periods T_x and T_y in x and y directions respectively. The Fourier series representation of $f(x,y)$ is given by:

$$f(x,y) = \sum_{k_1=-N_1}^{N_1} \sum_{k_2=-N_2}^{N_2} F(k_1,k_2)\, e^{j2\pi(\frac{k_1 x}{T_x} + \frac{k_2 y}{T_y})} \tag{4.1}$$

For simplicity we will assume $F(k_1,k_2)$ to have a square region of support of size $(2N+1) \times (2N+1)$, and T_x and T_y, the periods in x and y directions to be equal to 1. Our results can be easily modified for cases when T_x and T_y are not equal to 1 and $F(k_1,k_2)$ has a rectangular region of support.

Since $f(x,y)$ is real, its Fourier series coefficients are conjugate symmetric. That is:

$$F(k_1,k_2) = F^*(-k_1,-k_2) \qquad |k_1|,|k_2| < N \tag{4.2}$$

Using this relationship, we can rewrite our signal as a trigonometric function with real coefficients in the following manner:

$$\begin{aligned} f(x,y) = \; & Re[F(0,0)] + \\ & 2\left\{ \sum_{k_2=1}^{N} Re[F(0,k_2)]cos(2\pi k_2 y) - Im[F(0,k_2)]sin(2\pi k_2 y) + \right. \\ & \left. \sum_{k_1=1}^{N} \sum_{k_2=-N}^{N} Re[F(k_1,k_2)]cos[2\pi(k_1 x + k_2 y)] - Im[F(k_1,k_2)]sin[2\pi(k_1 x + k_2 y)] \right\} \end{aligned} \tag{4.3}$$

Thus, $f(x,y)$ can be uniquely specified with $(2N+1)^2$ real numbers which represent the real and imaginary part of its Fourier series coefficients. Therefore unique reconstructibility of $f(x,y)$ from $(2N+1)^2$ samples of it given by:

$$(x_i, y_i) \quad i = 1, ..., (2N+1)^2$$

is equivalent to non-singularity or full rank of the $(2N+1)^2 \times (2N+1)^2$ matrix M whose ith row, r_i is given by:

$$r_i^T = \begin{bmatrix} 1 \\ cos(2\pi y_i) \\ cos(4\pi y_i) \\ \cdots \\ cos(2N\pi y_i) \\ sin(2\pi y_i) \\ \cdots \\ sin(2N\pi y_i) \\ cos[2\pi(x_i - Ny_i)] \\ \cdots \\ cos[2\pi(Nx_i + Ny_i] \\ sin[2\pi(x_i - Ny_i)] \\ \cdots \\ sin[2\pi(Nx_i + Ny_i)] \end{bmatrix} \tag{4.4}$$

We will refer to M as the matrix associated with the points (x_i, y_i), $\quad i = 1, ..., (2N+1)^2$, and denote its determinant by the trigonometric polynomial $p(x_1, y_1, ..., x_{(2N+1)^2}, y_{(2N+1)^2})$. In general, the $J \times (2N+1)^2$ matrix associated with the points (x_i, y_i), $\quad i = 1, ..., J$ is rectangular

as opposed to square.

As we mentioned earlier, our main goal is to show that almost any $0 < k < (2N+1)^2$ points from the set of α level crossings and $(2N+1)^2 - k$ points from the β level crossings are sufficient for unique specification of $f(x,y)$ provided $\alpha \neq \beta$. In order to express this in a mathematical framework, let us define the sets A_α and A_β as α and β level crossings of f, in the following manner:

$$A_\alpha(C) = \left\{(x,y) \in C^2 \mid f(x,y) = \alpha\right\}$$

$$\begin{aligned} A_\alpha(R) &= \left\{(x,y) \in R^2 \mid f(x,y) = \alpha\right\} \\ &= A_\alpha(C) \cap R^2 \end{aligned} \tag{4.5}$$

$$A_\beta(C) = \left\{(x,y) \in C^2 \mid f(x,y) = \beta\right\}$$

$$\begin{aligned} A_\beta(R) &= \left\{(x,y) \in R^2 \mid f(x,y) = \beta\right\} \\ &= A_\beta(C) \cap R^2 \end{aligned} \tag{4.6}$$

Furthermore, let $B(R) \subset R^{2(2N+1)^2}$ denote the cross product

$$B(R) = A_\alpha^k(R) \times A_\beta^{(2N+1)^2-k}(R)$$

where $A_\alpha^k(R)$ is k times the cross product of $A_\alpha(R)$ with itself, and $A_\beta^{(2N+1)^2-k}(R)$ is $(2N+1)^2-k$ times the cross product of $A_\beta(R)$ with itself.

Having made the above definitions, we can now state our goal as finding the conditions under which real zeros of the trigonometric polynomial $p(x_1, y_1, \ldots, x_{(2N+1)^2}, y_{(2N+1)^2})$ become of measure zero in the set $B(R) \subset R^{2(2N+1)^2}$. To formulate our problem in an algebraic geometric framework, we must change some variables to express our trigonometric polynomials

as algebraic ones. This is primarily because algebraic geometry only deals with zeros of algebraic polynomials rather than trigonometric ones. To this end, let

$$sin(2\pi x) = w$$

$$cos(2\pi x) = z$$

$$sin(2\pi y) = u$$

$$cos(2\pi y) = v$$

so that the trigonometric polynomials $f(x,y)$ and $p(x_1, y_1, \ldots, x_{(2N+1)^2}, y_{(2N+1)^2})$ can be rewritten as:

$$f(x,y) = \tilde{f}(w,z,u,v)$$

$$p(x_1, y_1, \ldots, x_{(2N+1)^2}, y_{(2N+1)^2}) = \tilde{p}(w_1, z_1, u_1, v_1, \ldots, w_{(2N+1)^2}, z_{(2N+1)^2}, u_{(2N+1)^2}, v_{(2N+1)^2})$$

With these new variables, the sets A_α and A_β can be rewritten in the following way:

$$\tilde{A}_\alpha(C) = \left\{ \begin{array}{rl} (w,z,u,v) \in C^4 \mid & \tilde{f}(w,z,u,v) = \alpha \\ & w^2 + z^2 = 1 \\ & u^2 + v^2 = 1 \end{array} \right\}$$

$$\tilde{A}_\alpha(R) = \tilde{A}_\alpha(C) \cap R^4$$

$$\tilde{A}_\beta(C) = \left\{ \begin{array}{rl} (w,z,u,v) \in C^4 \mid & \tilde{f}(w,z,u,v) = \beta \\ & w^2 + z^2 = 1 \\ & u^2 + v^2 = 1 \end{array} \right\}$$

$$\tilde{A}_\beta(R) = \tilde{A}_\beta(C) \cap R^4$$

$$\tilde{B}(C) = \tilde{A}_\alpha^k(C) \times \tilde{A}_\beta^{(2N+1)^2-k}(C) \tag{4.7}$$

$$\begin{aligned}\tilde{B}(R) &= \tilde{B}(C) \cap R^{2(2N+1)^2} \\ &= \tilde{A}_\alpha^k(R) \times \tilde{A}_\beta^{(2N+1)^2-k}(R)\end{aligned}$$

Since there is a one to one correspondence between elements of the sets A_α and $\tilde{A}_\alpha$, A_β and $\tilde{A}_\beta$, and B and $\tilde{B}$, our major goal, which was to find conditions under which real zeros of $p(x_1, y_1, ..., x_{(2N+1)^2}, y_{(2N+1)^2})$ have measure zero in $B(R)$, becomes equivalent to finding conditions under which real zeros of $\tilde{p}(w_1, z_1, ..., u_{(2N+1)^2}, v_{(2N+1)^2})$ have measure zero in $\tilde{B}(R)$. The major implication of changing variables is the fact that, unlike A_α, A_β and B, the sets $\tilde{A}_\alpha$, $\tilde{A}_\beta$ and $\tilde{B}$ are *algebraic sets*. Algebraic sets are important elements in algebraic geometry, and we will take full advantage of their properties in proving the major result of this chapter. Thus, before we state our major theorem, it is worthwhile to go over few definitions in algebraic geometry [50].

Definition 4.1 *Let K be any field and $A^n(K)$ or simply A^n denote the Cartesian product of K with itself n times. That is $A^n(K)$ is the set of $n-$tuples of elements of K. If the coefficients of a polynomial F are in K, i.e. $F \in K[X_1, ..., X_n]$, a point $P = (a_1, ..., a_n) \in A^n(K)$ is a zero of F if $F(P) = F(a_1, ..., a_n) = 0$. If S is any set of polynomials in $K[X_1, ..., X_n]$, we define $V(S)$ to be the set of common zeros of all the polynomials in S. That is:*

$$V(S) = \{P \in A^n \mid F(P) = 0, \quad \forall F \in S\}$$

A subset $X \subset A^n(K)$ is an affine algebraic set or simply an algebraic set, if $X = V(S)$ for some S.

Thus $\tilde{A}_\alpha(R)$ and $\tilde{A}_\beta(R)$ are algebraic sets in R^4, and $\tilde{A}_\alpha(C)$ and $\tilde{A}_\beta(C)$ are algebraic sets in C^4. An algebraic set may be the union of several smaller algebraic sets. An algebraic set $V \subset A^n$ is *reducible* if

$$V = V_1 \cup V_2$$

where V_1 and V_2 are algebraic sets in A^n and

$$V_i \neq V \quad i = 1, 2$$

V_1 and V_2 are referred to as *components* of V. If V is not reducible, it is *irreducible*. It can be shown that an algebraic set is the union of a finite number of irreducible algebraic sets. More specifically, we have:

Theorem 4.1 *[50]: Let V be an algebraic set in $A^n(K)$. Then there are unique irreducible algebraic sets $V_1, ..., V_m$ such that*

$$V = V_1 \cup ... \cup V_m$$

and

$$V_i \not\subset V_j, \quad \forall\, i \neq j$$

The proof is straightforward and is included in [50]. An important consequence of the above theorem is the fact that given an irreducible algebraic set V in $A^n(K)$, the zeros of the polynomial $F \in K[X_1, ..., X_n]$ are either of measure zero in V, or contain all the points in V. As we will see, this fact will be crucial in proving our major theorem which can be stated in the following manner:

Theorem 4.2 *The set of real zeros of the polynomial $\tilde{p}(w_1, ..., v_{(2N+1)^2})$ is of measure zero in the set $\tilde{B}(R)$ provided the following conditions hold:*

1. *$\tilde{A}_\alpha(R)$ and $\tilde{A}_\beta(R)$ have maximal topological dimensions.*
2. *The polynomials*

$$g_\alpha(W_1, W_2) = \sum_{k_1=0}^{2N} \sum_{k_2=0}^{2N} F_\alpha(k_1 - N, k_2 - N) W_1^{k_1} W_2^{k_2}$$

$$g_\beta(W_1, W_2) = \sum_{k_1=0}^{2N} \sum_{k_2=0}^{2N} F_\beta(k_1 - N, k_2 - N) W_1^{k_1} W_2^{k_2}$$

with

$$F_\alpha(k_1, k_2) = \begin{cases} F(0,0) - \alpha & k_1 = k_2 = 0 \\ F(k_1, k_2) & elsewhere \end{cases}$$

$$F_\beta(k_1, k_2) = \begin{cases} F(0,0) - \beta & k_1 = k_2 = 0 \\ F(k_1, k_2) & elsewhere \end{cases}$$

are irreducible over the set of complex numbers.

Proof:

The outline of the proof is as follows: We will first use the first condition to show that $\tilde{B}(R)$ is an irreducible algebraic set over reals. Then either zeros of $\tilde{p}$ are of measure zero in $\tilde{B}(R)$ or all the points in $\tilde{B}(R)$ are zeros of $\tilde{p}$. Since our objective is to prove that real zeros of $\tilde{p}$ are of measure zero in $\tilde{B}(R)$, all we have to show is that there is at least one point in $\tilde{B}(R)$ at which $\tilde{p}$ does not vanish. As we will see, the second condition of the theorem will be used to show this.

To begin, notice that the polynomials $g_\alpha(W_1, W_2)$ and $g_\beta(W_1, W_2)$ are related to our BLP signal $f(x, y)$ via the change of variables

$$\begin{aligned} W_1 &= e^{j2\pi x} \\ W_2 &= e^{j2\pi y} \end{aligned}$$

in the following manner:

$$\begin{aligned} f(x,y) - \alpha &= W_1^{-N}\, W_2^{-N}\, g_\alpha(W_1, W_2) \\ f(x,y) - \beta &= W_1^{-N}\, W_2^{-N}\, g_\beta(W_1, W_2) \end{aligned}$$

Thus, there is a one to one correspondence between zeros of $g_\alpha(W_1, W_2)$ (resp. $g_\beta(W_1, W_2)$) and $\tilde{A}_\alpha(C)$ (resp. $\tilde{A}_\beta(C)$. Therefore, the second condition of the theorem implies that $\tilde{A}_\alpha$ and $\tilde{A}_\beta$ are also irreducible. Considering equation (4.7), since $\tilde{B}(C)$ is the Cartesian product of $\tilde{A}_\alpha(C)$s and $\tilde{A}_\beta(C)$s, we can conclude that $\tilde{B}(C)$ is also irreducible over complex numbers.

Similarly, since $\tilde{A}_\alpha(R)$ and $\tilde{A}_\beta(R)$ have maximal topological dimensions, so does $\tilde{B}(R)$. Therefore considering Theorem (C.1) of Appendix (C), and taking into account that $\tilde{B}(C)$ is irreducible, we can conclude that $\tilde{B}(R)$ is Zariski dense in $\tilde{B}(C)$. This means that every polynomial that vanishes on $\tilde{B}(R)$ vanishes on all of $\tilde{B}(C)$. This, together with the fact that $\tilde{B}(C)$ is irreducible, implies that $\tilde{B}(R)$ is irreducible over complex numbers and thus the reals. Therefore, in order to show that the real zeros of $\tilde{p}(w_1, \ldots, v_{(2N+1)^2})$ are of measure zero in $\tilde{B}(R)$, we merely have to show that there exists at least one point in $\tilde{B}(R)$ at which $\tilde{p}$ does not vanish. That is, $\tilde{p}$ does not vanish identically on $\tilde{B}(R)$.

Since, by hypothesis, $g_\alpha(W_1, W_2)$ and $g_\beta(W_1, W_2)$ are irreducible over complex numbers, taking into account modified version of Bezout's theorem of Appendix (B), we can conclude that *any* $8N^2+1$ samples of A_α will enable us to specify $f(x, y)-\alpha$ to within a scale factor [51]. This means the $(8N^2+1)\times(2N+1)^2$ matrix associated with *any* $8N^2 + 1$ points of A_α, D_α has rank $(2N + 1)^2 - 1$, and its null vector is specified by the coefficients of $f(x, y) - \alpha$. Similarly, D_β, the $8N^2 + 1 \times (2N + 1)^2$ matrix associated with *any* $8N^2 + 1$ points of A_β has rank $(2N + 1)^2 - 1$, and its null vector is given by the coefficients of $f(x, y) - \beta$. Since by hypothesis $\alpha \neq \beta$, the direction of the null vectors of D_α and D_β are different from each other. Therefore, there exists at least one combination of k rows from D_α and $(2N + 1)^2 - k$ rows from D_β which result in a full rank $(2N + 1)^2 \times (2N + 1)^2$ matrix with non zero determinant $\tilde{p}$. Hence $\tilde{p}$ does not vanish identically on $\tilde{B}(R)$.

Since $\tilde{B}(R)$ is irreducible over reals and $\tilde{p}$ does not vanish on it identically, the real zeros of $\tilde{p}$ must be of measure zero in $\tilde{B}(R)$. QED.

□

The above theorem implies that two-dimensional signals with $(2N + 1) \times (2N + 1)$ region of support in the Fourier domain can be uniquely specified from almost any $0 < k < (2N + 1)^2$ points from their α crossings and $(2N + 1)^2 - k$ points from their β crossings, provided they satisfy the conditions of the theorem. Thus, it is natural to question the strictness of these

conditions in practical situations. The first condition of the theorem requires $\tilde{A}_\alpha(R)$ and $\tilde{A}_\beta(R)$ to have maximal topological dimensions. Since the complex topological dimension of $\tilde{A}_\alpha(C)$ (resp. $\tilde{A}_\beta(C)$) is 1, and its real topological dimension is 2, maximal dimension for $\tilde{A}_\alpha(R)$ (resp. $\tilde{A}_\beta(R)$) is 1. This implies that the points (x, y) satisfying $f(x, y) = \alpha$ (resp. $f(x, y) = \beta$) must contain at least a curve and can not simply be isolated points in the $x - y$ plane. In practice, this condition can be easily satisfied by choosing our threshold α (resp. β) in such a way that the corresponding threshold contours form curves and not isolated points.

The second condition of Theorem (4.2) is also easily satisfied in practice. Since throughout our derivation we assumed $f(x, y)$ to be real and $F(k_1, k_2)$ to be conjugate symmetric, our approach is to show that the set of reducible polynomials is of measure zero in the space of all the bivariate polynomials of the form:

$$p(w, z) = \sum_{i=0}^{2N} \sum_{j=0}^{2N} a(i, j)\, w^i z^j$$

$$a^*(i, j) = a(2N - i, 2N - j)$$

As it turns out, this is a simple extension of the fact that the set of reducible polynomials are of measure zero in the space of all the bivariate polynomials with complex coefficients [52,53].

Theorem (4.2) can be easily extended to recovery of multidimensional signals from more than two threshold crossings. More specifically, we can show that given m distinct thresholds, $t_1, ..., t_m$, almost any distribution of $(2N+1)^2$ points among the thresholds will result in unique reconstruction of the signal under consideration provided

1. Not all the points are chosen on one threshold.

2. For $1 < i < m$, the set of points satisfying

$$f(x, y) = t_i$$

has maximal topological dimension (i.e. consists of curves as opposed to isolated points).

3. For $1 < i < m$, the polynomial associated with

$$f(x, y) = t_i$$

is irreducible over complex numbers.

Furthermore, Theorem (4.2) implies that almost any $(2N+1)^2$ samples of one level crossings of a signal with $(2N+1) \times (2N+1)$ region of support in the Fourier domain is sufficient for its unique reconstruction to within a scale factor, provided the polynomial associated with the signal is irreducible. This is in contrast with $(16N^2+1)$ samples required by the theoretical results of Curtis [51], or $8N^2+1$ samples required by the application of the modified form of Bezout's theorem as in [39].

Finally, it is not hard to see that the basic idea in Theorem (4.2) can be extended to reconstruction from crossings with BLP functions, whose bandwidth lie within the bandwidth of the signal. Examples of reconstruction via the implicit sampling scheme, described in this section, are included in the next section.

4.2 Reconstruction Algorithms

In the previous section, we found that most multidimensional signals can be uniquely reconstructed from samples on contours corresponding to two or more level crossings. Unlike the semi-implicit line sampling strategy of Chapter 2, the sampling scheme described in section (4.1) is truly implicit. In other words, whereas the interpolation points of the semi-implicit approach must lie on lines of rational slope, for the implicit approach, there is no pre-imposed

pattern or structure to the samples.

In this section, we will propose two methods to reconstruct multidimensional signals from their level crossings, via the implicit sampling approach of the previous section. The most straightforward way, is to solve a linear (possibly overdetermined) system of equations of the form:

$$f(x_i, y_i) = \sum_{k_1=-N}^{N} \sum_{k_2=-N}^{N} F(k_1, k_2) e^{j2\pi(k_1 x_i + k_2 y_i)} = t_j \quad 1 \le i \le M, \quad 1 \le j \le p$$

where (x_i, y_i) correspond to the threshold values t_j. Theoretical results of the previous section guarantee the uniqueness of the solution provided the signal under consideration satisfies the mild conditions of Theorem (4.2). An example of reconstruction of the original eye picture of figure (2.10) from samples of its two-level crossings is shown in figures (4.1) and (4.2). Figure (4.1) shows the two-level, non-uniform, amplitude quantized version of the eye picture and the crossing contours associated with thresholds 75 and 145. Since the eye picture has 961 coefficients, invoking Theorem (4.2), almost any k points from its 75 level crossings and $961 - k$ samples from its 145 level crossings are sufficient for its unique reconstruction. The reconstructed version of the eye picture using the linear least-squares approach is shown in figure (4.2). QR decomposition was used with 526 samples on the threshold contour corresponding to 75, and 426 samples on the 145 contour. Although other linear least-squares algorithms such as conjugate gradient algorithm need less storage than QR decomposition, they are generally not stable enough for the problem of reconstruction from multiple level threshold crossings, unless the number of thresholds is very large. Our second approach to reconstruction is similar to the iterative algorithm of section (3.3.1). The remaining part of this section is devoted to this algorithm.

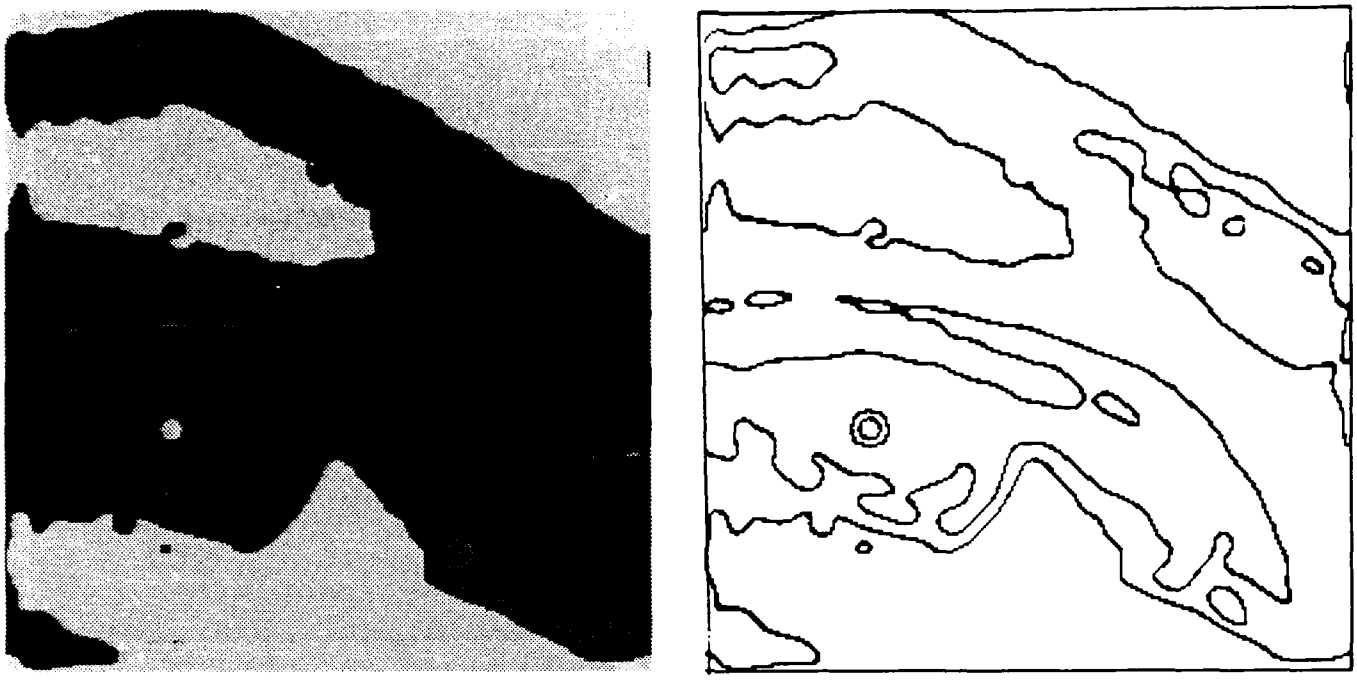

(a) (b)

Figure 4.1: *(a) 2 level non uniform amplitude quantized version of the original eye picture; (b) Threshold contours associated with the 2 level crossings.*

Figure 4.2: *Reconstructed version of the eye picture from its level crossings at 75 and 145 via the QR decomposition.*

4.2.1 The Iterative Approach

Our second approach to the problem of reconstruction from implicit samples of level crossings is iterative and is based on Theorem (3.1) of section (3.3.1). Intuitively, this strategy is based on imposing the space and frequency domain constraints successively. The space domain constraint is derived from the quantized threshold contours; the frequency domain constraint is due to the bandlimitedness of the signal under consideration. We will now describe the algorithm for reconstructing a BLP signal with $(2N+1) \times (2N+1)$ region of support in the Fourier domain. We assume that all the crossing contours of the signal associated with p thresholds $t_1 < t_2 < \ldots < t_p$ are quantized on an $M \times M$ grid where $M > 2N+1$, and that the intensity of the signal lies in the range $[t_0, t_{p+1}]$. The steps of the algorithm are as follows:

1. Deduce the range of intensity of the signal on the nodes of the $M \times M$ grid using the position quantized threshold crossings. The quantization process is shown pictorially in figure (4.3). As shown, quantized threshold contours trace outside of the boundary of level crossings on the nodes of the grid. Thus, as long as there are a minimum of two contours corresponding to two different thresholds, the intensity range for the nodes on the $M \times M$ grid can be found[1]. Therefore, if $t_l(n_1, n_2)$ and $t_u(n_1, n_2)$ denote the lower and upper bound for the (n_1, n_2)th point on the grid, we have:

$$t_l(n_1, n_2) \leq f(\frac{n_1}{M}, \frac{n_2}{M}) \leq t_u(n_1, n_2), \qquad n_1, n_2 = 0, \ldots, M-1$$

It is worthwhile to mention that the quantized threshold contours can also be chosen to be inside of the actual contours. In general, our quantization scheme must be chosen so

[1]The fact that we need at least two thresholds is a direct consequence of Theorem (4.2). Intuitively, if we only have contours associated with one threshold, there is no way to determine which parts of the signal are smaller than the threshold and which parts are larger.

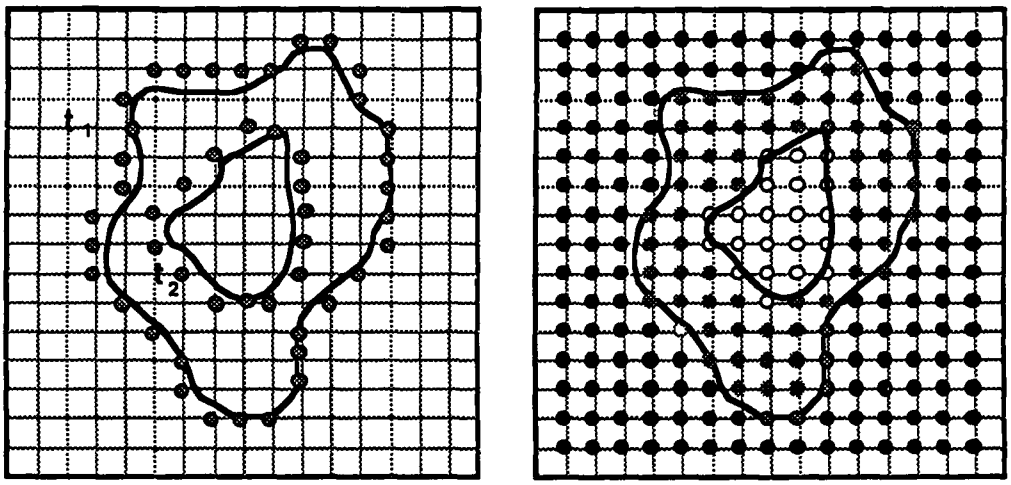

$t_1 < t_2$

● points with intensity $< t_1$

⊙ points with intensity $> t_1$ and $< t_2$

○ points with intensity $> t_2$

(a)

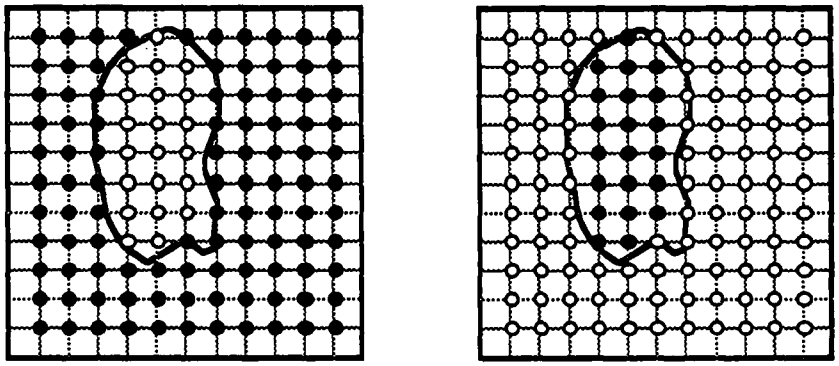

● points with intensity smaller than the threshold

○ points with intensity larger than the threshold

(b)

Figure 4.3: *(a) Deriving the space domain constraint for the two-dimensional iterative algorithm; (b) Ambiguous range information via samples of the contour associated with one threshold.*

that there is no ambiguity which grid points are inside or outside of a given threshold contour.

2. Let $f^{(l)}(\frac{n_1}{M}, \frac{n_2}{M})$ denote the value of f in the lth iteration at the point $(\frac{n_1}{M}, \frac{n_2}{M})$. Then the initial guess becomes:

$$f^{(0)}(\frac{n_1}{M}, \frac{n_2}{M}) = \frac{t_l(n_1, n_2) + t_u(n_1, n_2)}{2}, \qquad n_1, n_2 = 0, \ldots, M-1$$

Similar to the iterative algorithm of section (3.3.1), the convergence of this algorithm is independent of the initial guess.

3. Take the discrete Fourier transform (DFT) of f in the lth step:

$$F^{(l)}(k_1, k_2) = DFT\ [\ f^{(l)}(\frac{n_1}{M}, \frac{n_2}{M})\ ], \quad 0 \le k_1, k_2 < M$$

4. Impose the bandlimited constraint:

$$\tilde{F}^{(l+1)}(k_1, k_2) = \begin{cases} F^{(l)}(k_1, k_2) & , \quad 0 \le k_1, k_2 \le N\ ,\ M-N \le k_1, k_2 < M \\ 0 & , \quad elsewhere \end{cases}$$

5. Inverse discrete Fourier transform of $\tilde{F}^{(l+1)}(k_1, k_2)$:

$$\tilde{f}^{(l+1)}(\frac{n_1}{M}, \frac{n_2}{M}) = DFT^{-1}\ [\ \tilde{F}^{(l+1)}(k_1, k_2)\ ]$$

6. Impose the space domain constraint:

$$f^{(l+1)}(\frac{n_1}{M}, \frac{n_2}{M}) = \begin{cases} \tilde{f}^{(l+1)}(\frac{n_1}{M}, \frac{n_2}{M}) & , \quad t_l(n_1, n_2) \le \tilde{f}^{(l+1)}(\frac{n_1}{M}, \frac{n_2}{M}) \le t_u(n_1, n_2) \\ t_l(n_1, n_2) & , \quad \tilde{f}^{(l+1)}(\frac{n_1}{M}, \frac{n_2}{M}) < t_l(n_1, n_2) \\ t_u(n_1, n_2) & , \quad \tilde{f}^{(l+1)}(\frac{n_1}{M}, \frac{n_2}{M}) > t_u(n_1, n_2) \end{cases}$$

7. If all the nodes of the $M \times M$ grid satisfy the space domain constraint, we are done. Otherwise go to step (3) and repeat steps (3) through (7).

The above algorithm is very similar to the one-dimensional iterative algorithm, described in section (3.3.1). Similar to the one-dimensional case, we can show that the mean square error between the unknown signal, which satisfies the space and frequency domain constraints, and the solution obtained via successive iterations decreases. Furthermore, we can apply Theorem (3.1) to prove that the algorithm is guaranteed to converge to a solution which satisfies both the space and frequency domain constraint, if such a solution exists. More specifically, the algorithm described in this section is a special case of the iteration described in Theorem (3.1) where:

- The Hilbert space H is the finite dimensional space of all $M \times M$ point real sequences.
- The inner product between two $M \times M$ point sequences $x(n_1, n_2)$ and $y(n_1, n_2)$ is given by:

$$(x, y) = \sum_{n_1=0}^{M-1} \sum_{n_2=0}^{M-1} x(n_1, n_2)\, y(n_1, n_2)$$

- C_1 is a convex, closed subset of H, and includes all $M \times M$ point real, bandlimited sequences whose DFT is 0 in the range $N < k < M - N$. Furthermore, C_2 is a convex, closed subset of H containing all $M \times M$ point real sequences, $y(n_1, n_2)$, which satisfy the space domain constraint, derived from the level crossing information as described in the first step of the algorithm. In other words, any $M \times M$ sequence which satisfies

$$t_l(n_1, n_2) \leq y(n_1, n_2) \leq t_u(n_1, n_2), \qquad \forall\ 0 \leq n_1, n_2 < M \tag{4.8}$$

  belongs to the set C_2. Note that for C_2 to be closed, it is necessary to define it exactly the way is is shown above. For instance, if in inequality (4.8), the $\leq$ were replaced with $<$, then C_2 would not be closed.

- P_1 is the bandlimiting operator which operates onto the set C_1, and P_2 is the projection operator which imposes the space domain constraint by projecting onto C_2.

- The relaxation parameters are chosen to be 1.

Thus, the iterative algorithm described in this section, is a special case of the iterative scheme described by Theorem (3.1). Consequently, it converges strongly to an element of $C_0 = C_1 \cap C_2$, the set of two-dimensional $M \times M$ sequences satisfying both the space and frequency domain constraints. Since in practice M is finite, there might be many $M \times M$ point real sequences in the set C_0. However, in the limit as $M \to \infty$, our theoretical results of section (4.1) guarantee that the set C_0 will contain exactly one sequence. Under these circumstances, H will not be finite dimensional, and one might begin to wonder whether strong convergence is guaranteed any longer. However, as it is mentioned in Theorem (3.1), since at least one of our convex closed subsets, namely C_1, is finite dimensional, we are still guaranteed of strong convergence as long as we set $\lambda_1 = 1$.

In order to generalize our algorithm to the case where the relaxation parameters are not equal to one, we must modify its 6th step in the following way:

- Having found the projection of $f^{(l)}(\frac{n_1}{M}, \frac{n_2}{M})$ onto C_1 given by:

$$\tilde{f}^{(l+1)}(\frac{n_1}{M}, \frac{n_2}{M}) = P_1 \left[f^{(l)}(\frac{n_1}{M}, \frac{n_2}{M}) \right]$$

apply the operator

$$T_1 = 1 + \lambda_1 (P_1 - 1)$$

to $f^{(l)}(\frac{n_1}{M}, \frac{n_2}{M})$ to get:

$$f^{(l+1)}(\frac{n_1}{M}, \frac{n_2}{M}) \equiv f^{(l)}(\frac{n_1}{M}, \frac{n_2}{M}) + \lambda_1 \left[\tilde{f}^{(l+1)}(\frac{n_1}{M}, \frac{n_2}{M}) - f^{(l)}(\frac{n_1}{M}, \frac{n_2}{M}) \right]$$

- Now impose the space domain constraint by projecting $\acute{f}^{(l+1)}(\frac{n_1}{M}, \frac{n_2}{M})$ onto C_2 to get:

$$\begin{aligned}
\check{f}^{(l+1)}(\tfrac{n_1}{M}, \tfrac{n_2}{M}) &\equiv P_2 \left[\acute{f}^{(l+1)}(\tfrac{n_1}{M}, \tfrac{n_2}{M}) \right] \\
&= \begin{cases} \acute{f}^{(l+1)}(\frac{n_1}{M}, \frac{n_2}{M}) \quad , & t_l(n_1, n_2) \le \acute{f}^{(l+1)}(\frac{n_1}{M}, \frac{n_2}{M}) \le t_u(n_1, n_2) \\ t_l(n_1, n_2) \quad , & \acute{f}^{(l+1)}(\frac{n_1}{M}, \frac{n_2}{M}) < t_l(n_1, n_2) \\ t_u(n_1, n_2) \quad , & \acute{f}^{(l+1)}(\frac{n_1}{M}, \frac{n_2}{M}) > t_u(n_1, n_2) \end{cases}
\end{aligned}$$

- Apply the operator T_2 given by:

$$T_2 = 1 + \lambda_2 \left(P_2 - 1 \right)$$

to $\check{f}^{(l+1)}(\frac{n_1}{M}, \frac{n_2}{M})$ to get:

$$\begin{aligned}
f^{(l+1)}(\tfrac{n_1}{M}, \tfrac{n_2}{M}) &\equiv T_2 \left[\check{f}^{(l+1)}(\tfrac{n_1}{M}, \tfrac{n_2}{M}) \right] \\
&= \acute{f}^{(l+1)}(\tfrac{n_1}{M}, \tfrac{n_2}{M}) + \lambda_2 \left(\check{f}^{(l+1)}(\tfrac{n_1}{M}, \tfrac{n_2}{M}) - \acute{f}^{(l+1)}(\tfrac{n_1}{M}, \tfrac{n_2}{M}) \right)
\end{aligned}$$

The main advantage of the generalized version of the iterative algorithm is that its convergence properties can be modified by adjusting the relaxation parameters λ_1 and λ_2. In fact, there has been great deal of research on the "optimum" choice of relaxation parameters; we will only mention the simplest such technique, over-relaxation, which essentially consists of choosing the relaxation parameters in the range $(1, 2)$. We have found experimentally that convergence rates do not present serious enough problems to seek other means of accelerating convergence.

4.2.2 Examples of the Iterative Algorithm

An example of the reconstruction of the original eye picture of figure (2.10), is shown in figures (4.4) and (4.5). Figure (4.4) shows the 5 level non-uniform amplitude quantized version of figure (2.10) and the threshold contours associated with these levels. The reconstructed

version of figure (4.4) is shown in figure (4.5); the quantizing grid was 256×256, relaxation parameters were $\lambda_1 = 1$ and $\lambda_2 = 1.7$, and the number of iterations was 20. We have found experimentally that in order to reconstruct the image from fewer than 5 thresholds, the grid size has to be much finer than 512×512. We will investigate the trade off between number of thresholds and the size of the quantizing grid in more detail in Chapter 5. In this section, however, we will only show three examples of reconstruction for different number of thresholds and various values of M. Figures (4.6), (4.7), and (4.8) show the reconstructed version of the eye, cman and vegas picture from $4, 6$ and 8 thresholds via the iterative algorithm for different values of M. The relaxation parameters for all the reconstructions were chosen to be $\lambda_1 = 1, \lambda_2 = 1.75$. As shown, increasing the number of thresholds affects the quality of reconstruction in a more substantial way than increasing M. In addition, comparing figures (4.6) and (3.17) we can see that the quality of reconstruction via the two-dimensional iterative algorithm of this section is superior to the one-dimensional iterative algorithm of section (3.3.1).

Similar to the one-dimensional case, we have found experimentally that altering the 6th step of the algorithm in the following manner:

$$f^{(l+1)}(\frac{n_1}{M}, \frac{n_2}{M}) = \begin{cases} \tilde{f}^{(l+1)}(\frac{n_1}{M}, \frac{n_2}{M}) & , \quad t_l(n_1, n_2) \leq \tilde{f}^{(l+1)}(\frac{n_1}{M}, \frac{n_2}{M}) \leq t_u(n_1, n_2) \\ \frac{t_l(n_1,n_2) + t_u(n_1,n_2)}{2} & , \quad otherwise \end{cases}$$

reduces the mean square error faster than the generalized version of the iterative algorithm where relaxation parameters are used to accelerate convergence. This is true, in spite of the fact that the mean square error does not necessarily decrease from one iteration to the next and that the convergence of this technique can not even be guaranteed by applying Theorem (3.1). Although this faster convergence can be explained by formulating the problem in a statistical

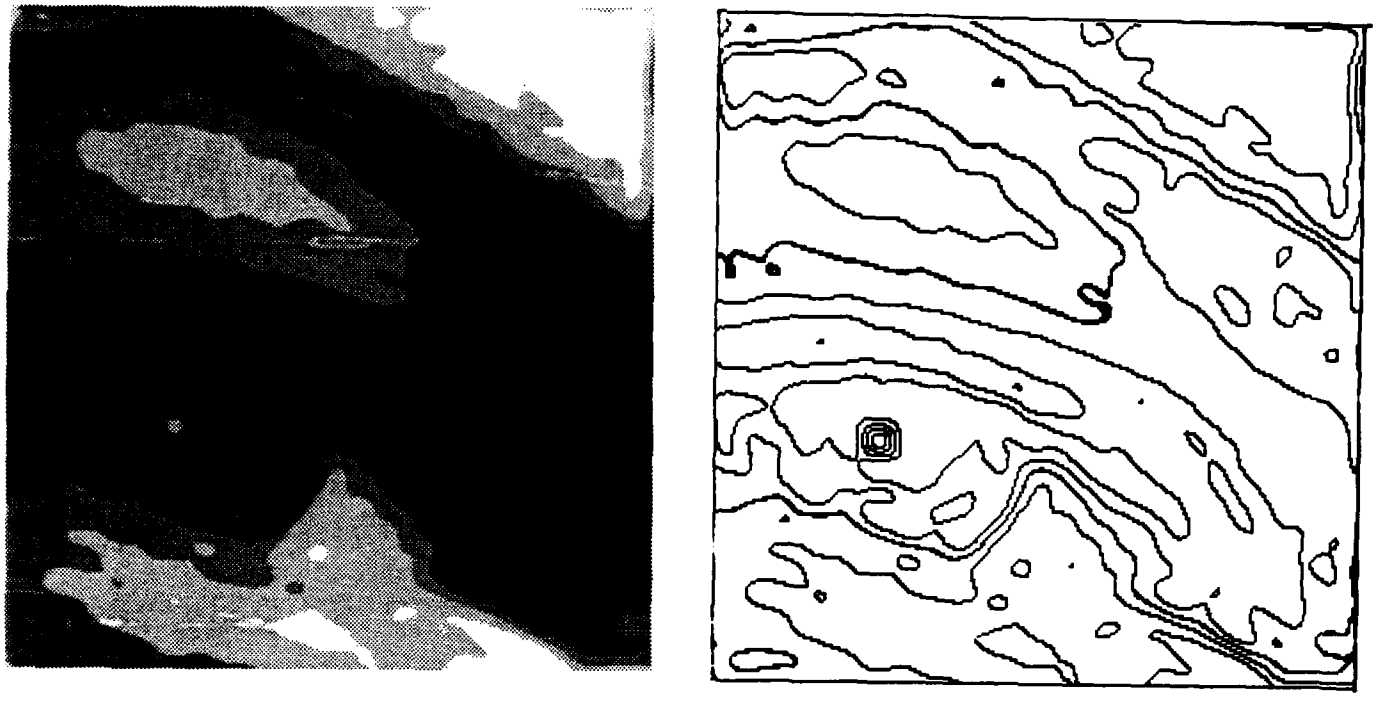

(a) (b)

Figure 4.4: *(a) 5 level non uniform amplitude quantized version of the original eye picture; (b) Threshold contours associated with the 5 level crossings.*

Figure 4.5: *Reconstructed version of the eye picture from its 5 level crossings via the iterative algorithm with $M = 256$.*

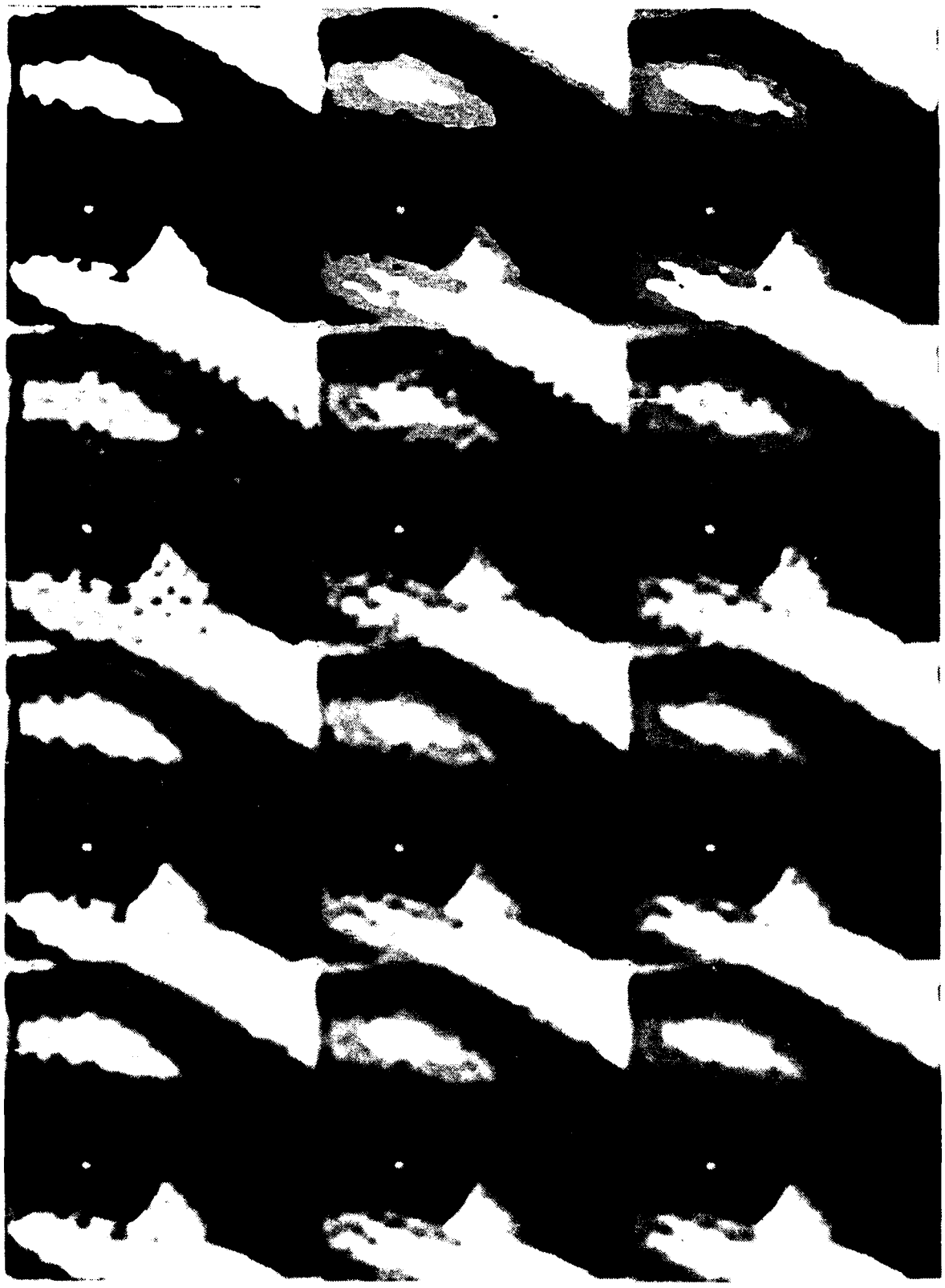

Figure 4.6: *Reconstructed version of the original eye picture via the two-dimensional iterative algorithm. The number of thresholds are 4,6, and 8, increasing from left to right, and the number of equally spaced samples on lines, M are 31 (no reconstruction), 32, 64, 128, increasing from top to bottom.*

Figure 4.7: *Reconstructed version of the cman picture via the two-dimensional iterative algorithm . The number of thresholds are 4,6 and 8, increasing from left to right, and the number of equally spaced samples on lines, M are 63 (no reconstruction), 64, 128, 256 increasing from top to bottom.*

framework [49], we will not develop it here. The important point is that, although in most reconstructions carried out via the above modified version, the algorithm converges to a sequence satisfying both the space and frequency domain constraints, the quality of the reconstructed image was almost identical to the one obtained via the over relaxation method. This suggests that the reason behind poor quality of reconstruction for small number of thresholds is not the fact that the algorithm did not converge, but that, as with the semi-implicit iterative scheme, there are many signals satisfying the space and frequency domain constraints, and the algorithm has simply converged to one of them. Increasing the number of thresholds or increasing M imposes more constraints on the signal, thereby reducing the number of sequences satisfying both the space and frequency domain requirements. As we said earlier, the solution via the iterative algorithm becomes unique as $M \to \infty$.

Before we end this section, let us briefly compare the iterative and linear least-squares approach for reconstruction via the implicit sampling strategy, described in this chapter. Unlike the iterative approach, which needs all the quantized threshold contours, the linear least-squares approach only needs *samples* of the threshold contours. While, the iterative algorithm is less storage and computation intensive, the quality of reconstruction via the iterative algorithm is not as high as the least-squares approach. However, one must keep in mind the fact that reconstructions using the latter technique use, at least in principle, the *exact* location of the crossings, whereas the iterative algorithm uses the rather coarsely quantized version of the crossings, as long as M is finite. Thus, in situations where the location of the level crossings is quantized too coarsely, unlike the linear least-squares algorithm, which is completely unsuccessful in carrying out reconstruction, the iterative algorithm is capable of producing approximate reconstructions. We will study these quantization issues at length in Chapter 5.

Figure 4.8: *Reconstructed version of the vegas picture via the two-dimensional iterative algorithm of this section. The number of thresholds are 4,6 and 8, increasing from left to right, and the number of equally spaced samples on lines, M are 127 (no reconstruction), 128, 256 increasing from top to bottom.*

Chapter 5

Preliminary Speculations on Quantization Properties

In the past three chapters, we have proposed various approaches to the problem of reconstruction from level crossings. As we mentioned in Chapter 1, our main motivation for solving this problem has been to find sampling strategies whose characteristics lie in between the explicit Nyquist sampling and the implicit zero crossing strategy as defined by Curtis [51]. More specifically, in Nyquist sampling, the amplitude of the signal is specified to infinite precision at prespecified points, and all the bits used to represent the signal are essentially amplitude bits. On the other hand, for successful reconstruction from zero crossings, the position of the crossings need to be known extremely accurately, whereas only one bit is needed to quantize the amplitude information. Similarly, while the bandwidth used in representing signals via their Nyquist samples is minimal and the dynamic range is maximal, the zero crossing representation requires maximal bandwidth and minimal dynamic range. As will see in this chapter, in representing signals via their samples of multiple level threshold crossings, the required bandwidth and dynamic range are in between those of the zero crossing and Nyquist representations.

To demonstrate this more quantitatively, we need to investigate position and amplitude quantization requirements of our sampling/reconstruction schemes as a function of the number

of thresholds. A rigorous and thorough investigation of these quantization characterizations involves extensive dealing with coding issues and experiments, both of which are beyond the scope of this thesis. Therefore, the nature of discussions in this chapter tends to be rather preliminary, and most of the conclusions are somewhat tentative. However, these speculative results can be used as a starting point for further research in the areas of multidimensional signal representation and image coding.

Since we have proposed numerous sampling and reconstruction strategies in the last three chapters, even a preliminary investigation of their quantization properties is a formidable task. Thus, our approach in this chapter has been to study a subset of these schemes. More specifically, we will study the quantization properties of the linear least-squares approach in section (5.1), and the iterative algorithms in section (5.2). The reason behind choosing the linear least-squares approach is that, if it is implemented via stable algorithms such as QR decomposition, it can result in extremely robust reconstructions for both the semi-implicit and implicit sampling strategies. The main reason for studying the iterative algorithms is that their quantization characteristics are substantially different from our other algorithms.

The organization of this chapter is as follows. In sections (5.1) and (5.2), we will examine the quantization requirements of the linear least-squares approach and iterative algorithms as a function of the number of thresholds and the sampling strategy. As we will see in section (5.1), the number and geometric distribution of the level crossings play an important role in the robustness of linear least-squares reconstruction via the QR decomposition. In addition, for both the QR decomposition and iterative algorithms, increasing the number of thresholds, which in effect corresponds to an increase in the number of amplitude bits, leads to a decrease in the required number of position bits. Thus, there is a tradeoff between the number of thresholds

and total number of amplitude and position bits. Finally, in section (5.3), we show that under certain circumstances Nyquist sampling simply becomes a special case of our semi-implicit and implicit sampling strategies; this will bridge the conceptual gap between explicit, semi-implicit and implicit sampling strategies, unify seemingly unrelated sampling schemes and provide us with a spectrum of sampling techniques for multidimensional signals.

5.1 Linear Least-Squares Approach

This section includes a preliminary investigation of the quantization properties of reconstruction via the linear least-squares approach and the QR decomposition. Before approaching this problem however, we need to address a few issues.

The first issue has to do with the fact that quantization procedures for the implicit and semi-implicit sampling approaches are *somewhat different from each other*. As we will see in section (5.1.1), while for the implicit approach, level crossing samples are quantized on a square grid, for the semi-implicit approach, we exploit the geometric constraint of the sample positions to quantize their locations.

The second issue that needs to be addressed is how the number of reconstruction samples influences reconstruction robustness. As we will see in section (5.1.2), increasing the number of samples will result in fewer position bits per sample, although beyond a certain level, it increases the *total* number of bits used to represent a signal.

Having discussed these two issues in sections (5.1.1) and (5.1.2), in section (5.1.3), we will investigate how the number of thresholds affect position and amplitude quantization characteristics of reconstruction via the linear least-squares approach and the QR decomposition. Our experimental results seem to suggest that, although increasing the number of thresholds

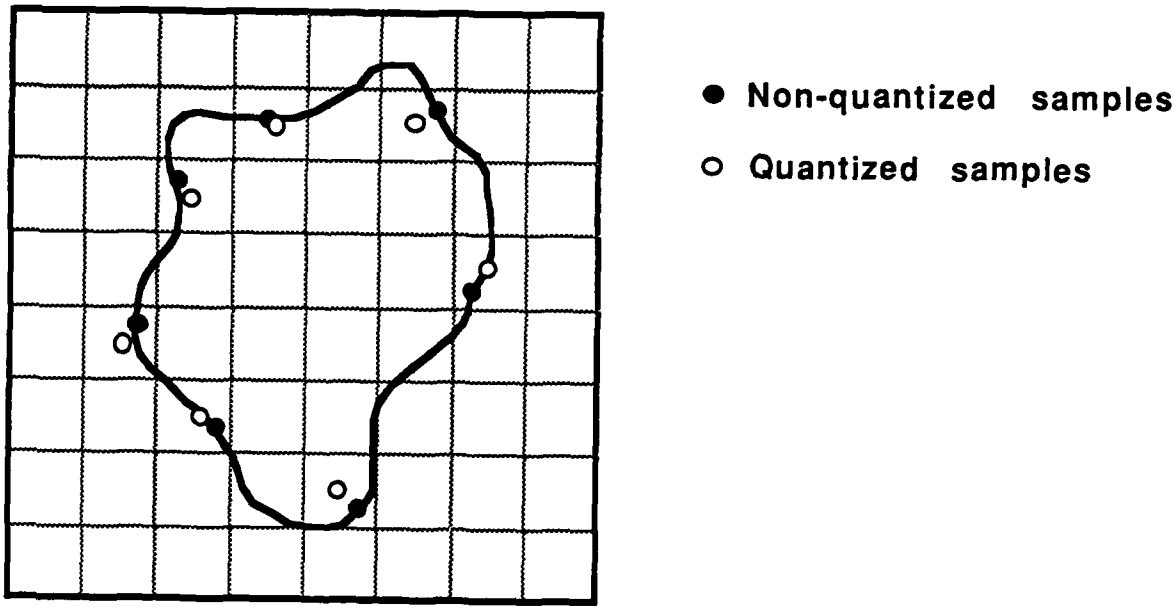

Figure 5.1: *Quantization procedure for the implicit sampling strategy via the linear least-squares approach.*

initially decreases the number of position bits, beyond a certain point, it increases the total number of position and amplitude bits required for representing a two dimensional signal.

5.1.1 Quantization Procedures

Quantization procedures which we used for the implicit and semi-implicit sampling strategies are slightly different from each other. Figure (5.1) shows quantization of samples of threshold contours obtained via the implicit sampling approach. As shown, we used a simple quantization algorithm in which the quantized coordinates of a given sample are chosen to be the coordinates of the center point of the square the sample falls in. In addition, for situations in which two or more samples fall into the same quantizing square, the sample closest to the center of the square is kept and the remaining ones are discarded.

For the semi-implicit approach, we can take advantage of the geometry of the sampling lines. More specifically, in a sampling scenario with n_l sampling lines, our strategy for specifying the location of a given sample has been to:

1. Use $\log_2 n_l$ bits to specify the line it falls on.

2. Use b bits to specify the location of sample along its sampling line.

It is worthwhile to point out that there are many other ways to quantize the position of our samples, and our proposed coding schemes are almost certainly not optimal. In fact, a rigorous investigation of the quantization properties involves dealing with coding issues which are well beyond the scope of this thesis. Since we have chosen unsophisticated and simple quantization strategies, it is important to bear in mind that the nature of our conclusions tend to be rather speculative and preliminary.

5.1.2 Choice of the Number of Samples

Although the theoretical results of Chapters 2 and 4, provide us with a variety of sufficient conditions under which samples of level crossings of a BLP signal can be used to uniquely specify it, using more interpolation points than the minimum required by these theoretical results should improve the robustness of reconstruction, and thus decrease the required number of position bits for specifying the location of the crossings. Although for a fixed quality of reconstruction, increasing the number of samples will initially decrease the number of position bits per sample, beyond a certain point, it increases the total number of bits used to represent a signal. Thus, our goal in this section is to find the extent to which oversampling signals will reduce the total number of bits necessary for representing them. To this end, we carried out

Figure 5.2: *The original eye.lp picture which is the low pass version of the* 31×31 *eye picture.*

a series of experiments on a picture shown in figure (5.2) with 15×15 region of support in the Fourier domain. This picture which is more or less the low pass version of the original eye picture of figure (2.10), will be referred to as *eye.lp*.

For the semi-implicit approach, we first found all the intersections of 7 level crossing contours with 15 equidistant lines of unity slope, and then chose five subsets of these intersections, with a different number of samples in each subset. To guarantee unique reconstructibility, the distribution of the interpolation points among various sampling lines for each subset was chosen in such a way that the conditions of Theorem (2.3) were satisfied. As it turns out, for a small number of thresholds, the quality of recovered images via the QR decomposition deteriorates very rapidly once the number of bits used for quantizing the location of samples drops below a certain level. Hence, it is rather straightforward to find the minimum number of

For the semi-implicit approach, we can take advantage of the geometry of the sampling lines. More specifically, in a sampling scenario with n_l sampling lines, our strategy for specifying the location of a given sample has been to:

1. Use $\log_2 n_l$ bits to specify the line it falls on.

2. Use b bits to specify the location of sample along its sampling line.

It is worthwhile to point out that there are many other ways to quantize the position of our samples, and our proposed coding schemes are almost certainly not optimal. In fact, a rigorous investigation of the quantization properties involves dealing with coding issues which are well beyond the scope of this thesis. Since we have chosen unsophisticated and simple quantization strategies, it is important to bear in mind that the nature of our conclusions tend to be rather speculative and preliminary.

5.1.2 Choice of the Number of Samples

Although the theoretical results of Chapters 2 and 4, provide us with a variety of sufficient conditions under which samples of level crossings of a BLP signal can be used to uniquely specify it, using more interpolation points than the minimum required by these theoretical results should improve the robustness of reconstruction, and thus decrease the required number of position bits for specifying the location of the crossings. Although for a fixed quality of reconstruction, increasing the number of samples will initially decrease the number of position bits per sample, beyond a certain point, it increases the total number of bits used to represent a signal. Thus, our goal in this section is to find the extent to which oversampling signals will reduce the total number of bits necessary for representing them. To this end, we carried out

Figure 5.2: *The original eye.lp picture which is the low pass version of the* 31×31 *eye picture.*

a series of experiments on a picture shown in figure (5.2) with 15×15 region of support in the Fourier domain. This picture which is more or less the low pass version of the original eye picture of figure (2.10), will be referred to as *eye.lp*.

For the semi-implicit approach, we first found all the intersections of 7 level crossing contours with 15 equidistant lines of unity slope, and then chose five subsets of these intersections, with a different number of samples in each subset. To guarantee unique reconstructibility, the distribution of the interpolation points among various sampling lines for each subset was chosen in such a way that the conditions of Theorem (2.3) were satisfied. As it turns out, for a small number of thresholds, the quality of recovered images via the QR decomposition deteriorates very rapidly once the number of bits used for quantizing the location of samples drops below a certain level. Hence, it is rather straightforward to find the minimum number of

position bits required for successful reconstruction. Nevertheless, it is important to emphasize that our evaluation of the reconstructed images were purely subjective and rather informal. A plot of the minimum number of position bits per sample versus the number of reconstruction samples is shown in figure (5.3). As shown, the number of position bits drops very rapidly as the number of samples is increased from 225 to 250. However, this drop becomes considerably less significant as the number of samples is further increased to 399. Figure (5.3) also contains the plot of the position bits versus the number of samples for the implicit sampling approach of Chapter 4. Like the semi-implicit approach, the number of position bits drops considerably as the number of samples is increased from 225 to 256; however, increasing the number of samples from 256 to 576 does not seem to decrease the number of position bits any further.

The shape of the curves in figure (5.3) suggests that a plot of *total* number of position bits versus the number of samples must exhibit a minimum. Indeed, as shown in figure (5.4), the minimum occurs when the number of samples is around 250. It is important to note that the vertical axis in figure (5.3) indicates the number of position bits *per sample*, whereas in figure (5.4) it stands for the *total* number of position bits normalized to the number of Fourier coefficient i.e.:

$$\frac{number\ of\ position\ bits\ per\ sample \times number\ of\ samples}{number\ of\ Fourier\ coefficients}$$

The curves in figure (5.4) suggest that for a fixed number of thresholds, (in this case 7), oversampling the level crossings by approximately 10 percent results in lowest total number of position bits. In the next section, we will investigate how the number of thresholds and the number of reconstruction samples affect the quantization requirements of reconstruction via the QR decomposition.

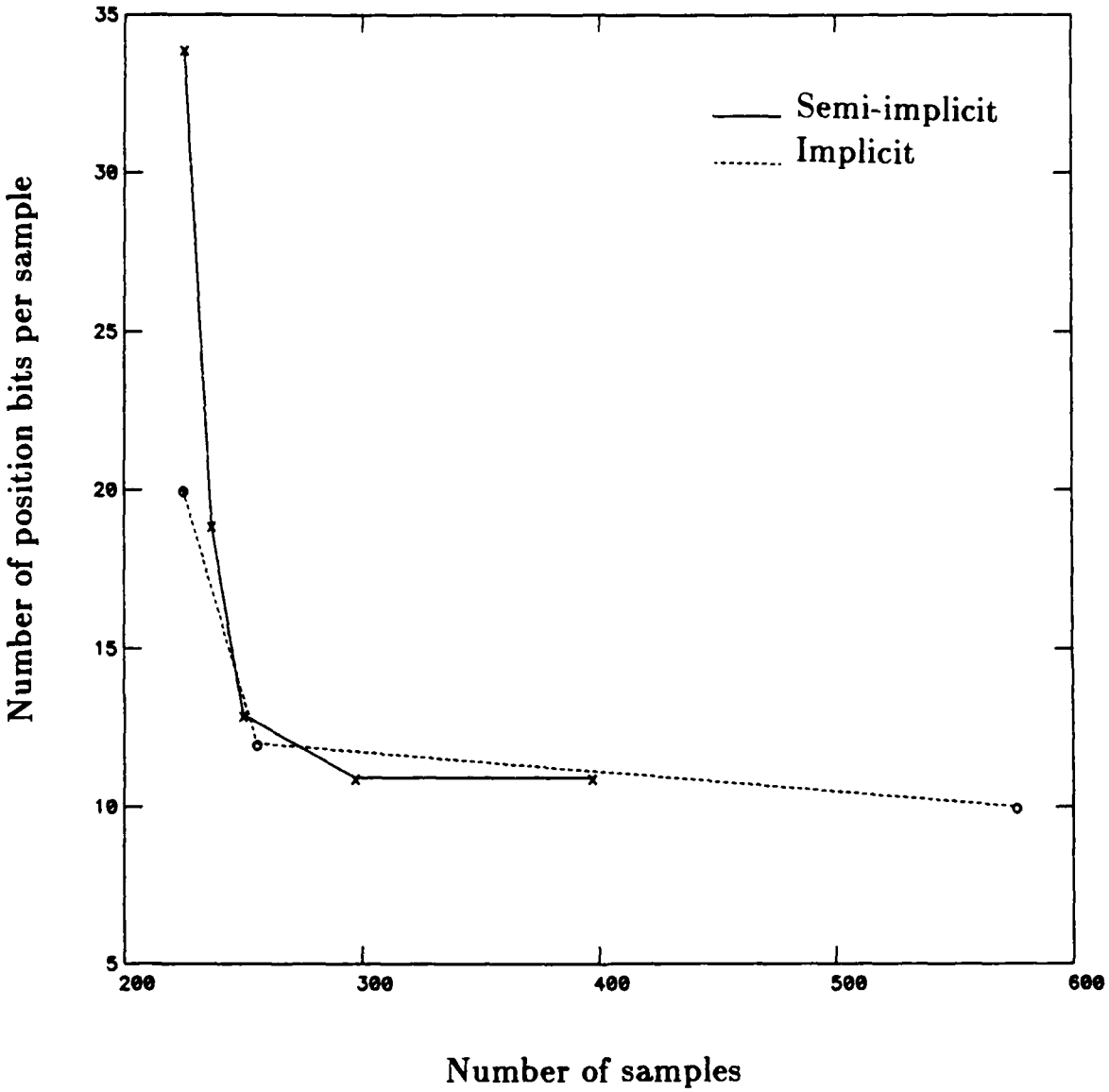

Figure 5.3: *Number of position bits per sample used for successful reconstruction of the eye.lp picture versus the number of samples. Each curve represents more or less constant quality as judged subjectively and informally.*

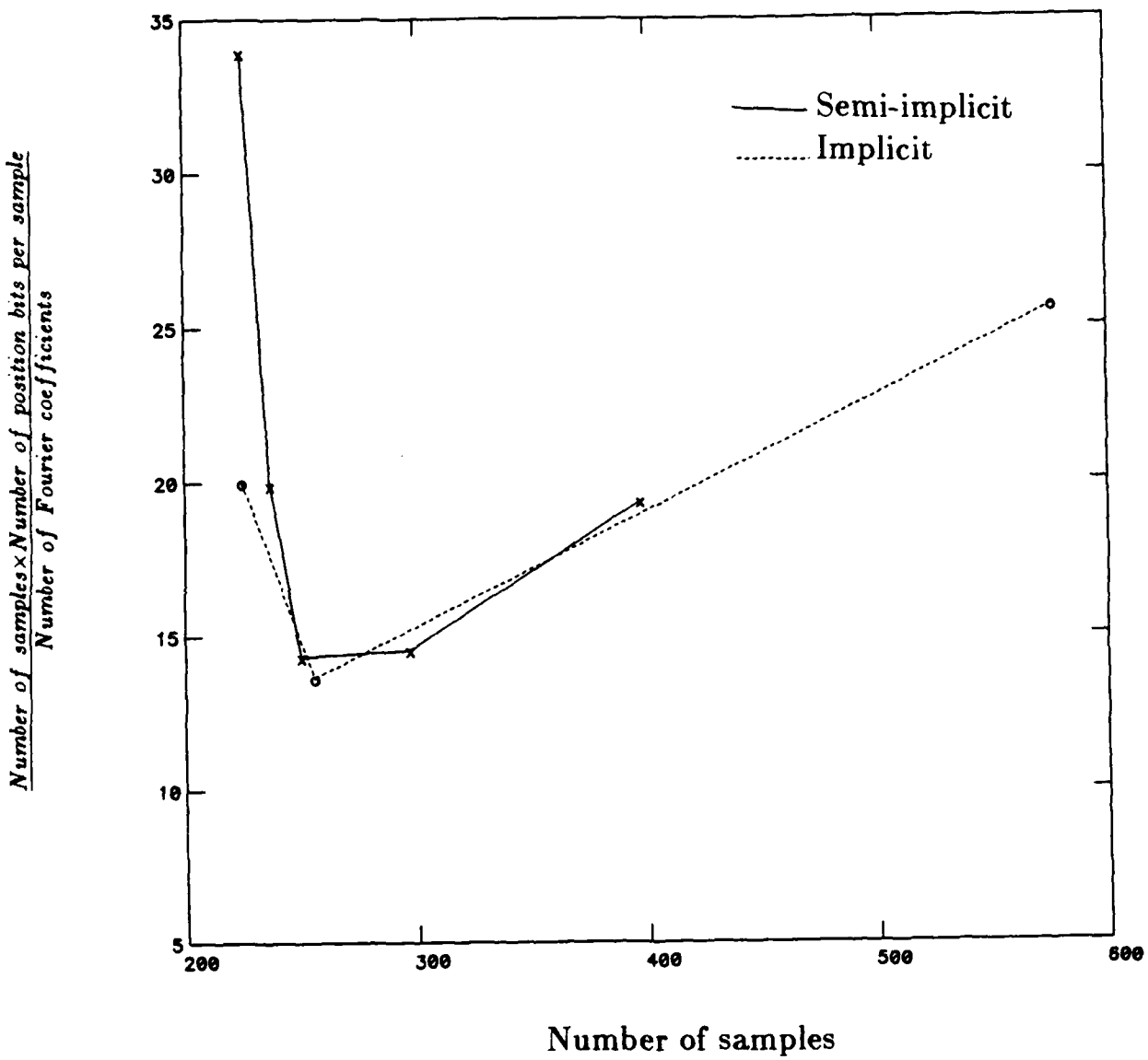

Figure 5.4: *Normalized number of position bits used for successful reconstruction of the eye.lp picture versus the number of samples. Each curve represents more or less constant quality as judged subjectively and informally.*

5.1.3 Quantization Requirements

As we mentioned earlier, position and amplitude quantization requirements of various reconstruction strategies depend on factors such as sampling strategy and the number of reconstruction samples. Having discussed the effect of number of reconstruction samples in section (5.1.2), we are now ready to investigate quantization requirements of semi-implicit and implicit sampling strategies as a function of the number of thresholds.

Figure (5.5) shows the plot of mean square error (mse) versus the total number of amplitude and position bits as a function of the number of thresholds. The mean square error between the original and reconstructed image is given by:

$$mse = \frac{1}{(2N+1)^2} \sum_{k_1=-N}^{N} \sum_{k_2=-N}^{N} [F(k_1,k_2) - \tilde{F}(k_1,k_2)]^2$$

where $F(k_1,k_2)$ and $\tilde{F}(k_1,k_2)$ correspond to the Fourier coefficients of the original and reconstructed image respectively. We have found experimentally that the quality of the reconstructed image becomes almost indistinguishable from the original one when $mse \leq .1$. Figure (5.5b) corresponds to the implicit sampling strategy and (5.5a) corresponds to semi-implicit sampling strategy with equidistant lines of unity slope. In both cases, the number of samples used for reconstruction was 225 i.e. the minimum number required by our theoretical results. As we would expect, the slope of the curves shown in figure (5.5) are negative, indicating that the quality of the reconstruction is improved as the the number of position bits is increased. In addition, the spacing between the curves decreases from right to left, indicating that the improvement in the quality of reconstruction decreases as the the number of thresholds gets larger. In fact, as shown in figure (5.5b), for $mse < .05$ the quantization characteristics of the curve corresponding to 16 thresholds is slightly more favorable than that of 32 thresholds.

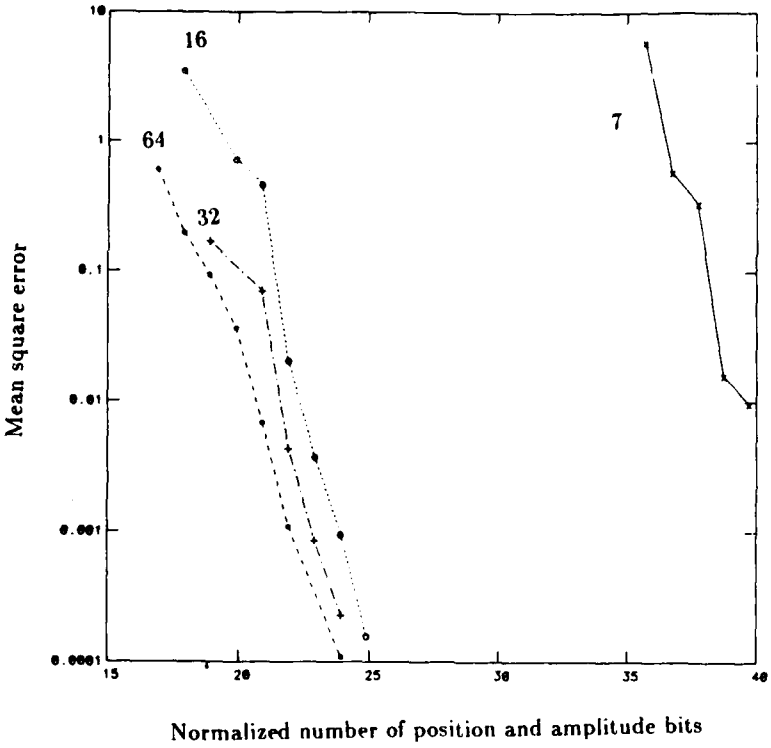

(a)

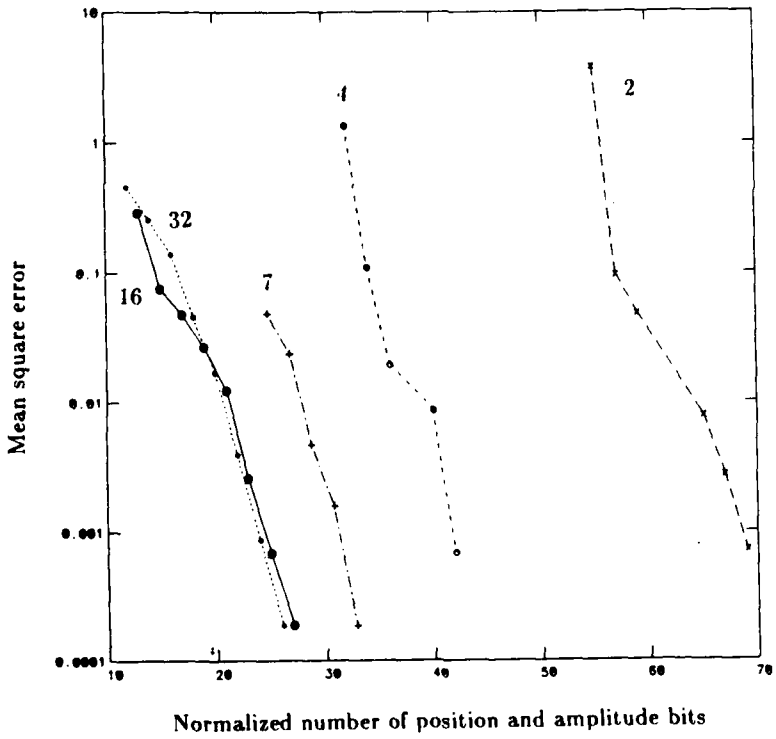

(b)

Figure 5.5: *Plot of mse versus total normalized number of position and amplitude bits as a function of the number of thresholds for: (a) semi-implicit sampling; (b) implicit sampling. The number of reconstruction samples was fixed at 225.*

Superimposing curves of figures (5.5a) and (5.5b), we obtain figure (5.6) which shows the semi-implicit and implicit curves corresponding to 7, 16, and 32 thresholds. As shown, the slope of the semi-implicit curves are more negative than the slope of implicit ones. In addition, it appears that for $mse > .1$, the implicit curves exhibit more favorable quantization characteristics than the semi-implicit ones. This is primarily due to the fact that for semi-implicit sampling situations in which the number of reconstruction samples does not exceed the required minimum value, the geometric distribution of samples is constrained by the conditions of theorems of Chapter 2, whereas the interpolation points of the implicit sampling are more or less chosen at random and can be more evenly distributed across the image. As an example, consider semi-implicit sampling scenarios where all the sampling lines have identical integer slopes m. In this case, the ratio between the maximum and minimum number of required samples on the sampling lines is given by:

$$\rho = \frac{\textit{maximum number of points on a line}}{\textit{minimum number of samples on a line}} = \frac{1 + 2(|m| + 1)\,N}{1 + 2(|m| + 1)\,N - 4N} \tag{5.1}$$

which can be approximated by:

$$\rho \approx \frac{|m| + 1}{|m| - 1} \tag{5.2}$$

Clearly, an even distribution of samples corresponds to small values of ρ. Therefore, for $|m| > 1$ increasing $|m|$, and for $|m| < 1$, decreasing $|m|$ will result in smaller value of ρ, and thus, a more favorable distribution of samples. To verify this experimentally, a reconstructed version of the *eye.lp* picture using samples on lines of slopes 3 and 1 are shown in figure (5.7). The artifacts in figure (5.7a) occur at a place where two neighboring sampling lines of unity slope have 15 and 1 points respectively. Indeed, the value of ρ is 15 for sampling lines of unity slope and approximately 2 for lines of slope 3.

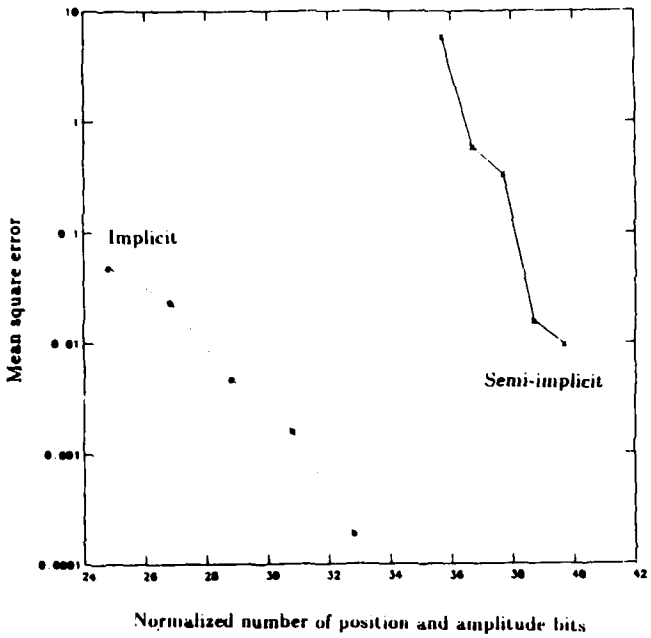

(a)

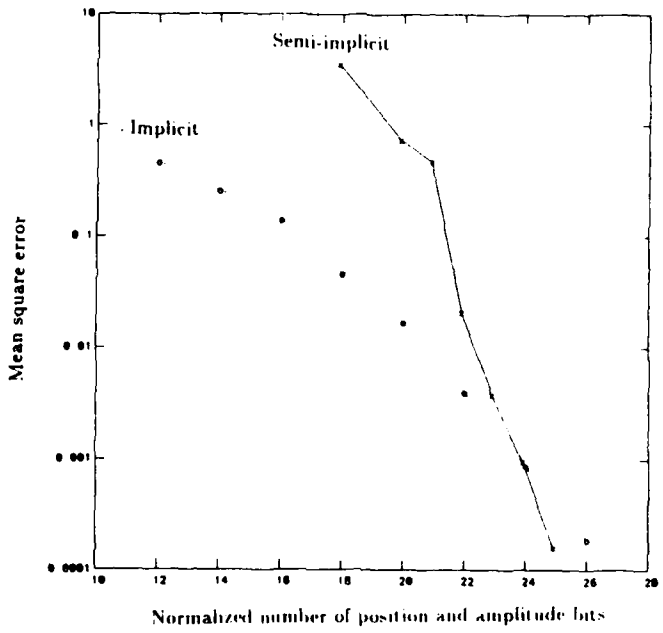

(b)

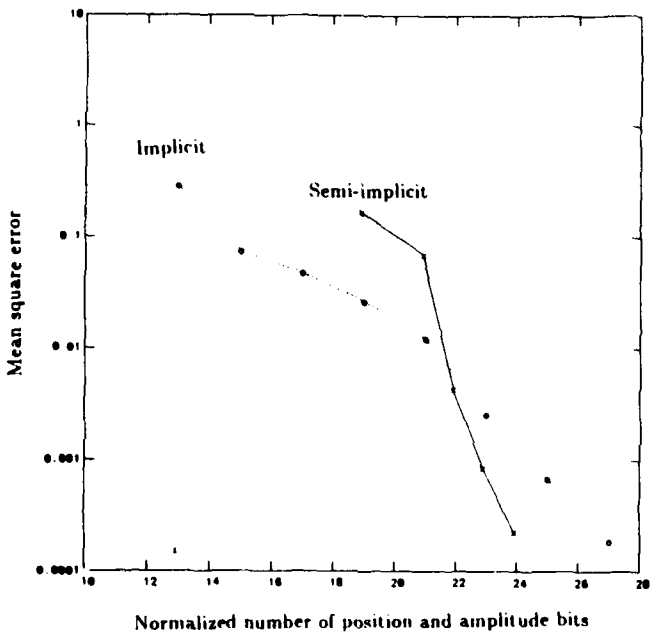

(c)

Figure 5.6: *Plot of mse versus total normalized number of position and amplitude bits for semi-implicit and implicit sampling. The number of reconstruction samples was fixed at 225 and the number of thresholds was 7 in (a), 16 in (b), and 32 in (c).*

(a)

(b)

Figure 5.7: *Reconstructed version of the eye.lp picture from 225 intersections of 7 level crossings with lines of: (a) unity slope; (b) slope 3.*

As the number of reconstruction samples is increased beyond the minimum required by our theoretical results, the distribution of interpolation points becomes more even, thus resulting in fewer position bits. Figure (5.8) shows the plot of mse versus total number of position and amplitude bits as a function of the number of thresholds. The curves shown in figure (5.8) were generated in a similar fashion to those of figure (5.5) except that the number of reconstruction samples was 256 instead of 225. Notice that for the semi-implicit curves of figure (5.8a), increasing the number of thresholds from 7 to 16 improves the quantization characteristics, while further increase from 32 to 64 thresholds degrades it. As far as implicit sampling curves of figure (5.8b) go, the "optimum" number of thresholds which results in minimum number of bits varies as a function of mse. For instance, for $.2 \leq mse \leq 1$ it is 7, for $.06 \leq mse \leq .2$ it is 16, and for $.02 \leq mse \leq .06$ it is 32.

Although it is rather difficult to draw strong conclusions from figures (5.5) and (5.8), the plots seem to suggest that for both semi-implicit and implicit sampling strategies, there exists an "optimum" number of thresholds which results in the least number of amplitude and position bits. This "optimum" number appears to be a function of mse, the sampling strategy and the number of reconstruction samples.

5.2 Iterative Approach

As we mentioned earlier, the quantization properties of the iterative algorithms of sections (3.3.1) and (4.2.1) are substantially different from our other algorithms. In this section, we will present some preliminary results on the quantization properties of these iterative algorithms. More specifically, sections (5.2.1) and (5.2.2) include amplitude and position quantization re-

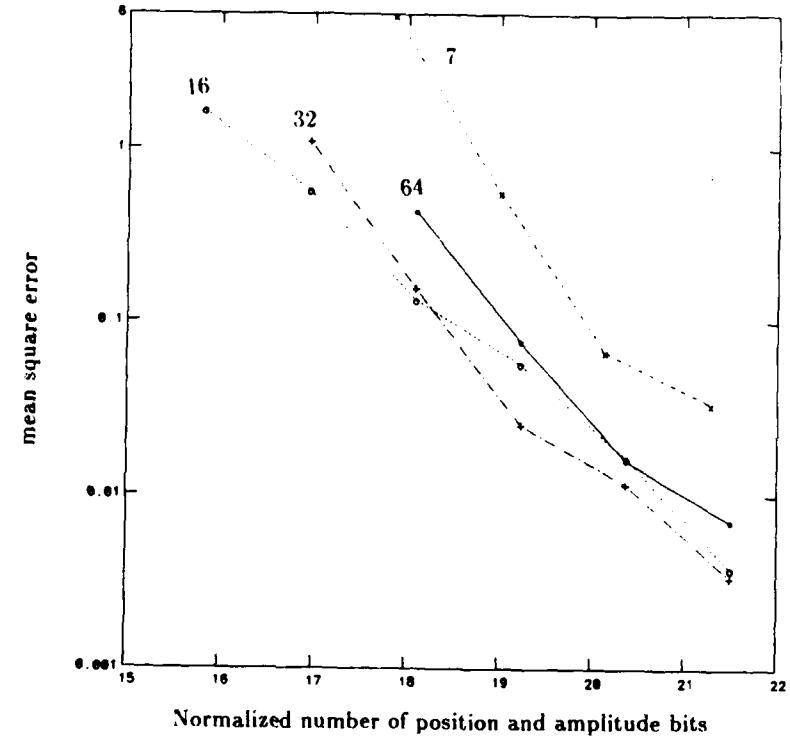

(a)

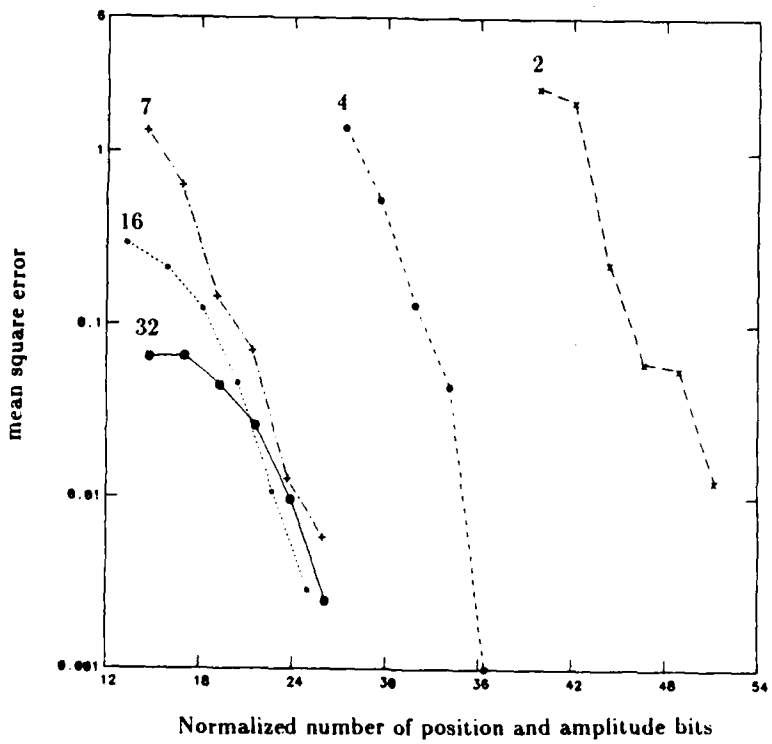

(b)

Figure 5.8: *Plot of mse versus total normalized number of position and amplitude bits as a function of the number of thresholds for: (a) semi-implicit sampling; (b) implicit sampling. The number of reconstruction samples was fixed at 256.*

quirements of the semi-implicit and the implicit sampling strategies respectively.

5.2.1 Quantization Requirements for Semi-implicit Sampling

In this section, we will present a preliminary investigation of the quantization properties of the iterative algorithm for the semi-implicit sampling strategy. Figure (5.9) shows the mean square error between the original *eye.lp* picture and its reconstructed version, versus the number of position and amplitude bits. The number of thresholds associated with the four curves shown in figure (5.9) is 6, 8, 12, and 16. For each curve the thresholds were chosen with equal spacing between 0 and 256. The four points on each curve correspond to different number of equally spaced points on the sampling lines, i.e. $M = 32, 64, 128$. In addition, the sampling lines were chosen to be equidistant and of unity slope. Although our theoretical results of Chapter 2 only require 15 sampling lines of unity slope, to be able to use the FFT with a power of 2 for the interpolation part of the iterative algorithm (i.e. interpolation from recovered one-dimensional signals to a square grid on the two-dimensional one), we chose 16 equally spaced sampling lines. The y axis in figure (5.9) corresponds to mse, and for completeness we have also included the actual reconstructed images for different values of M and different number of thresholds in figure (5.10). As shown in figure (5.10), the quality among the reconstructed images with approximately equal mse is comparable. Also, the quality of reconstruction certainly improves as mse is decreased. Finally, the x axis in figure (5.9) indicates the total number of position and amplitude bits used for the particular reconstruction at hand. Because of the inherent structure of the samples used by the iterative algorithm, there are a variety of ways to represent the signal under consideration and to arrive at the number of quantization bits. The most straightforward way is to quantize the location of threshold crossings on the sampling lines to $\log_2 M$ bits, so

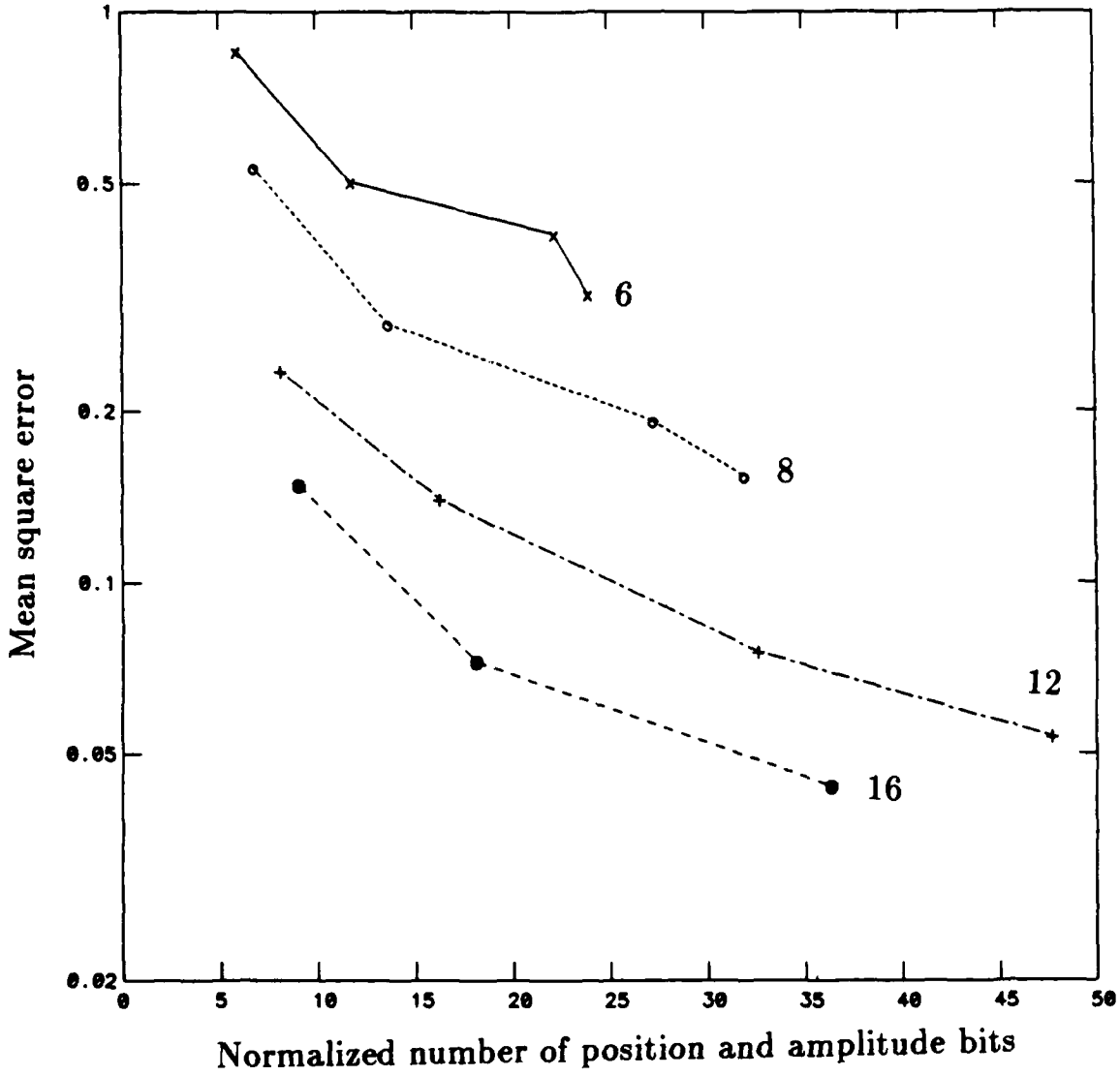

Figure 5.9: *Plot of mean square error versus normalized number of position and amplitude quantization bits as a function of the number of thresholds for the eye.lp picture.*

Figure 5.10: *Reconstructed images of the eye.lp picture via the semi-implicit sampling strategy with lines of unity slope. The number of thresholds is increased in the sequence 4,6,8 from top to bottom, and M is increased in the sequence 32,64,128 from left to right.*

that the space domain constraint for the M equally spaced points on each of the sampling lines can be derived easily. Using this strategy, the total number of amplitude and position bits for representing the signal can be written as:

$$(\log_2 M + \log_2 n_t + \log_2 n_l) \sum_{i=1}^{n_t} N_i$$

where

- N_i denotes the number of intersections of the ith threshold crossings with all the sampling lines.
- n_t denotes the number of thresholds.
- n_l denotes the number of sampling lines.
- M denotes the number of equally spaced points on each of the sampling lines.

An alternative strategy for representing the signal is to specify the range of intensity for each of the equally spaced points on the sampling lines. More specifically, if the number of thresholds is n_t, and the signal is known to be in the range $[0, 256]$, then the value of the signal at any given point lies in one of the $(n_t + 1)$ intervals corresponding to our n_t thresholds. In this case, the total number of bits used to represent the signal is given by $M n_l \log_2(n_t + 1)$. Clearly, this second quantization strategy outperforms the first one for large values of n_t and small values of M. Our strategy in determining the total number of position bits for the abscissa of figure (5.9) has been to choose the minimum of the above two quantization strategies. As it turns out, we would reach the same conclusions if we choose either of the quantization strategies described above.

Having discussed the details of generating the curves shown in figure (5.9) and the images of figure (5.10), it is now appropriate to make a few observations and comments regarding

their shapes. As we would expect, the slope of each curve is negative indicating that for fixed number of thresholds the mean square error decreases as M is increased. In addition, for fixed M, the mean square error is decreased as the number of thresholds is increased. The decreasing distance between the curves shown in figure (5.9) is indicative of the fact that as the number of thresholds increases, the resulting drop in mse is less. Thus, the decrease in mse as the number of thresholds changes from 6 to 8 is more substantial than when it changes from 12 to 16. An interesting question to address, however, is whether or not there is an "optimum" number of thresholds for which the lowest number of amplitude and position quantization bits is achieved. As figure (5.9) shows, this "optimum" number varies as a function of the mean square error. For instance, for the value of mse in the range $[0.53, 0.85]$, it is between 6 to 8, and for mse in the range $[0.15, 0.23]$, it is between 12 and 16. Thus, for iterative reconstruction via semi-implicit sampling, it appears that the "optimum" number of thresholds, resulting in least number of amplitude and position bits, is a decreasing function of mse. In the next section, we will investigate iterative reconstruction via implicit sampling.

5.2.2 Quantization Requirements for Implicit Sampling

Our main goal in this section is to investigate quantization properties of the iterative reconstruction algorithm for the implicit sampling strategy. The basic idea behind this algorithm, is to iterate between the space domain constraints derived from the quantized threshold contours, and the frequency domain constraints derived from the bandlimitedness of the signal.

Similar to the iterative reconstruction algorithm of the semi-implicit sampling, there are several strategies one might take to arrive at the total number of amplitude and position

quantization bits for representing a given image via the implicit sampling scheme. Since in each of these strategies, we are encoding the quantized contours corresponding to different thresholds, almost all of the efficient coding schemes for two tone images proposed and studied by many researchers [54,55] can be used for representing our images. The most obvious way of encoding the boundary points of a threshold contour quantized to b bits is to use $2b$ bits for x and y coordinates of each point. Using this strategy, the total number of bits required to specify n_t threshold contours is given by:

$$(\log_2 n_t + 2b)(\sum_{i=1}^{n_t} N_i(b))$$

where $N_i(b)$ denotes the number of quantized boundary points on a $2^b \times 2^b$ quantization grid for the ith threshold. A second and more efficient way of representing the boundary points is to follow the boundary i.e. to do contour tracing. Since the image is quantized on a $2^b \times 2^b$ square grid, each pel has only eight neighbors. Therefore, it is sufficient to use 3 bits to indicate where the next boundary point is. Of course, to get on each boundary, we need to specify the position of an initial point. Thus, ignoring the additional bits required to get to the initial points on the boundaries and to specify their associated threshold value, total number of points required for specifying an image is given by

$$3\sum_{i=1}^{n_t} N_i(b)$$

Our third encoding strategy involves specifying the range of the signal for each node of the $2^b \times 2^b$ quantization grid. This strategy is suitable for sampling schemes with large number of thresholds and coarse quantization of the contours. The total number of bits required for specifying an image via this encoding technique is given by

$$2^{2b} \log_2(n_t + 1)$$

As far as efficiency of these encoding strategies goes, clearly the second strategy outperforms the first one, and the relative efficiencies of the second and third encoding schemes depend on the form of $N_i(b)$. Intuitively, we would expect $N_i(b)$ to be proportional to 2^b, since the number of boundary points of quantized threshold contours is doubled as the size of quantizing grid is increased from $2^b \times 2^b$ to $2^{b+1} \times 2^{b+1}$. Thus, for small values of b and large values of n_t, the third strategy outperforms the second one. As it turns out, our major conclusions are more or less independent of the actual encoding strategy used; so our adopted strategy has been to choose the minimum of second and third quantization strategies for representing images.

Having described our quantization strategy, we will now examine how the number of thresholds affect the required number of position bits and the quality of reconstruction. Figure (5.11) shows the plot of the mean square error between the *eye.lp* picture and its reconstructed version versus the total number of position and amplitude bits. The four curves shown in figure (5.11) correspond to four different values of the grid size, i.e 16, 32, 64 and 128. Various points on each curve correspond to reconstruction from different numbers of thresholds. The reconstructed images corresponding to different points on the curves of figure (5.11) are shown in figure (5.12). The reconstruction was carried out via the iterative algorithm of section (4.2) with $\lambda_1 = 1.5$ and $\lambda_2 = 1.95$. These values of λ's were found to result in the smallest values of the mean square error. The following observations can be made about the plots shown in figure (5.11):

- The slopes of the curves are negative indicating that the quality of reconstruction is improved as the number of thresholds is increased or equivalently as the number of position and amplitude bits used for representing the image is increased.
- Smallest number of position and amplitude bits is achieved when the grid size is at its minimum value i.e. 16, or equivalently for $b = 4$.

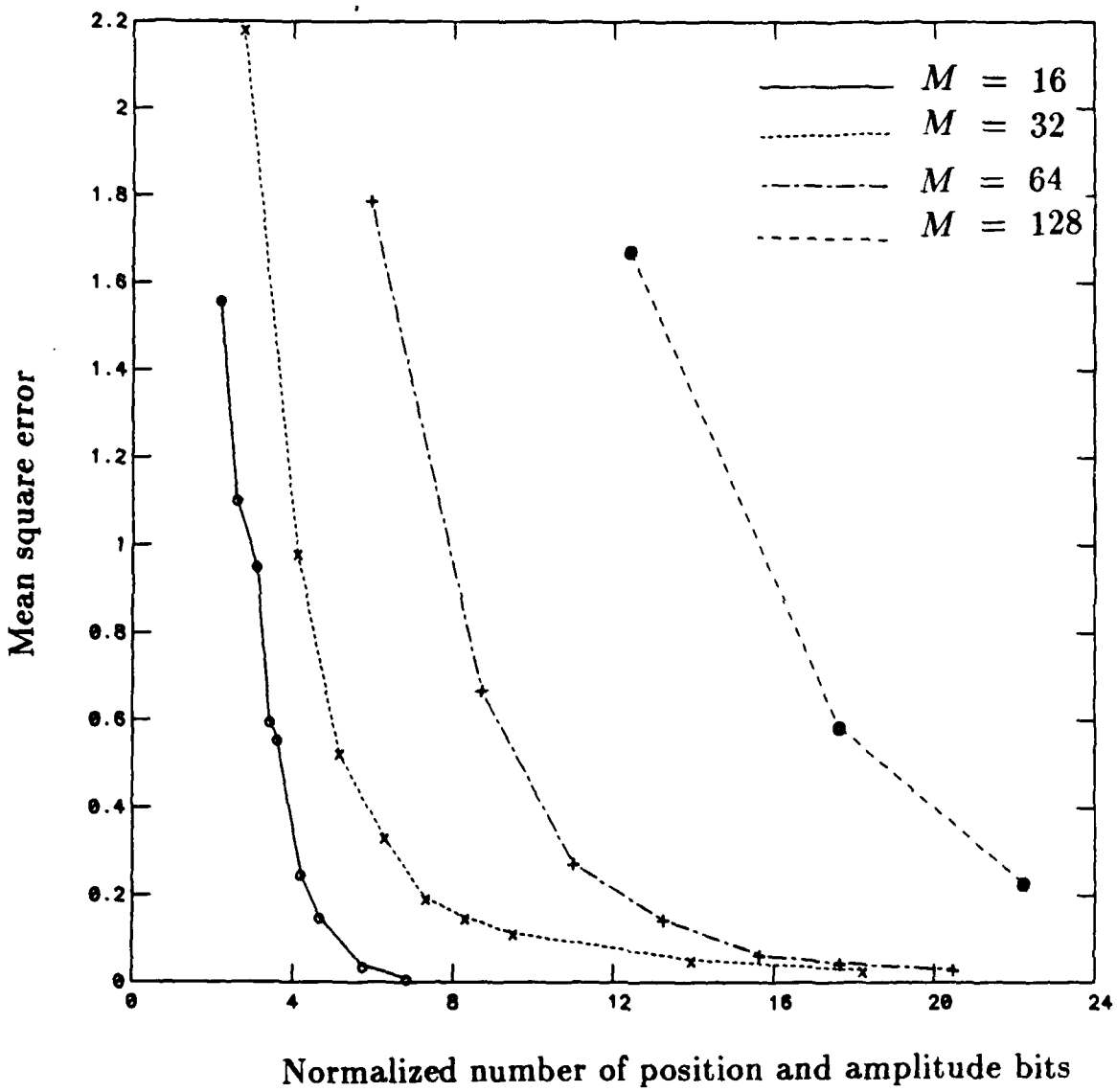

Figure 5.11: *Plot of mean square error between the eye.lp picture and its reconstructed version versus normalized number of position and amplitude quantization bits for different values of grid size.*

Figure 5.12: *Reconstructed images of the eye.lp picture via the implicit sampling strategy and the iterative algorithm. The number of thresholds is increased in the sequence 4,6,8 from top to bottom, and the grid size is increased in the sequence 16,32,64,128 from left to right.*

- The number of thresholds which results in smallest number of quantization bits is a decreasing function of the mse. For the curve corresponding to $b = 4$, the "optimal" number of thresholds for $mse = 1, .1, .01$ are $6, 32$, and 128 respectively.

- Beyond a certain point, an increase in the number of thresholds does not result in further decrease in the mse, but merely increases the total number of bits. For the curves corresponding to $b = 5, 6$, this phenomenon is reached at $n_t = 16, 8$ respectively. Thus, the larger the grid size is, the smaller the number of thresholds which result in this "saturation" phenomenon.

Another way to present the quantization results of figure (5.11) is to plot the mean square error versus normalized number of position and amplitude bits as a function of the number of thresholds. This is shown in the curves of figure (5.13), which correspond to reconstruction from a different number of thresholds. Various points on each curve correspond to reconstruction with different values of grid size. As we would expect, the slopes of the curves are negative, indicating that the quality of reconstruction improves as the quantization grid becomes finer. In addition, the number of thresholds which results in smallest number of quantization bits is a function of mse. For instance, if we are interested in reconstructed signals with $mse \leq .556$, then the optimal number of thresholds is between 8 and 16. Finally, comparing figures (5.13) and (5.9), it seems that for fixed quality of reconstruction via iterative algorithms, implicit sampling results in lower number of bits than semi-implicit sampling with lines of unit slope.

5.3 Relationship to Nyquist Sampling

As we mentioned in Chapter 1, explicit sampling refers to schemes in which a function is

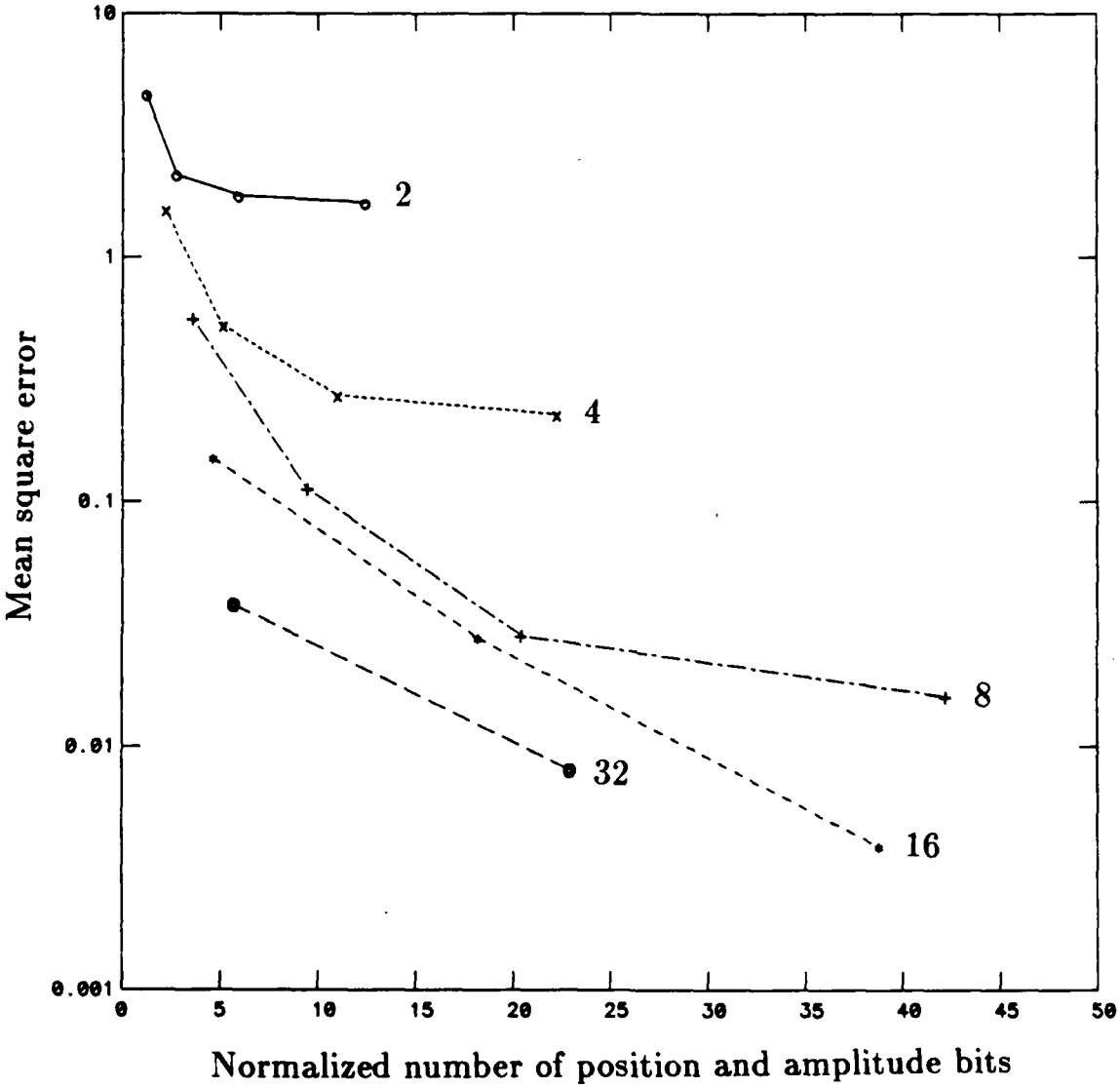

Figure 5.13: *Plot of mean square error between the eye.lp picture and its reconstructed version versus normalized number of position and amplitude quantization bits for reconstruction from different number of thresholds.*

represented by its samples or derivatives at prespecified points. An example of such a technique is Nyquist sampling where the amplitude of a signal is given at equally spaced points. Thus, for a two-dimensional BLP signal with $N \times N$ region of support in the Fourier domain, Nyquist sampling involves amplitude specification at the nodes of a $N \times N$ grid. Our main goal in this section is to explore the relationship between Nyquist sampling/reconstruction and reconstruction from level crossings via implicit or semi-implicit sampling strategies. We shall begin with the implicit sampling strategy of Chapter 4.

5.3.1 Implicit Sampling

Recall from section (5.1.1) that reconstruction of an $N \times N$ signal from implicit samples of its n_t level crossings via the linear least-squares approach consists of the following steps:

1. Find the level crossing contours associated with n_t thresholds.
2. Quantize the threshold contours to b bits by
   - Superimposing a $2^b \times 2^b$ grid over the signal in the space domain.
   - Assigning to the center point of all the $\frac{1}{2^b} \times \frac{1}{2^b}$ squares which contain some piece of one or more threshold contours, the value of the threshold whose contour comes closest to the center of the square.
3. Choose M of the above $\frac{1}{2^b} \times \frac{1}{2^b}$ squares with their center points becoming our quantized reconstruction samples.
4. Reconstruct the signal from its quantized samples by finding its Fourier series coefficients.

The above process is shown pictorially in figure (5.14a). As seen in figure (5.14b), for sufficiently large number of thresholds, all the 2^{2b} squares associated with the $2^b \times 2^b$ grid

will have a threshold value associated with them. Moreover, if the grid size is the same as the signal size i.e. $2^b = N$, the number of reconstruction samples, M, becomes equal to N^2, and we will end up with quantized samples of our signal on a $N \times N$ grid. Under these circumstances, the position of our sampling points are identical to that of Nyquist samples, and their amplitude corresponds to the threshold associated with them. Thus, there seems to be a duality between the above sampling set and $\log_2 n_t$ bit amplitude quantized Nyquist samples. However, it is important to bear in mind that these two sampling sets are inherently different from each other. In Nyquist sampling, the amplitude information is quantized at the nodes of a $N \times N$ grid, whereas, in reconstruction from threshold crossings, the nodes of this $N \times N$ grid correspond to position quantized samples of level crossings. In other words, Nyquist sampling corresponds to amplitude quantization at prespecified points, and reconstruction from level crossings corresponds to position quantization at prespecified amplitudes.

We will now turn our attention to the iterative algorithm of section (4.2.1). Recall from section (5.2.2) that the quantization procedure for iterative reconstruction of an $N \times N$ signal from n_t level crossings via the implicit sampling strategy consists of the following steps:

1. Find all the level crossing contours associated with n_t thresholds.

2. Quantize the threshold contours to b bits by finding nodes of a $2^b \times 2^b$ grid corresponding to the boundary points of the contours.

3. Derive the range of the signal for each of the nodes of a $2^b \times 2^b$ grid by utilizing the quantized threshold contours of the previous step. This will be used as the space domain constraint of the algorithm.

4. Impose the bandlimited constraint and the space domain constraint of the previous step

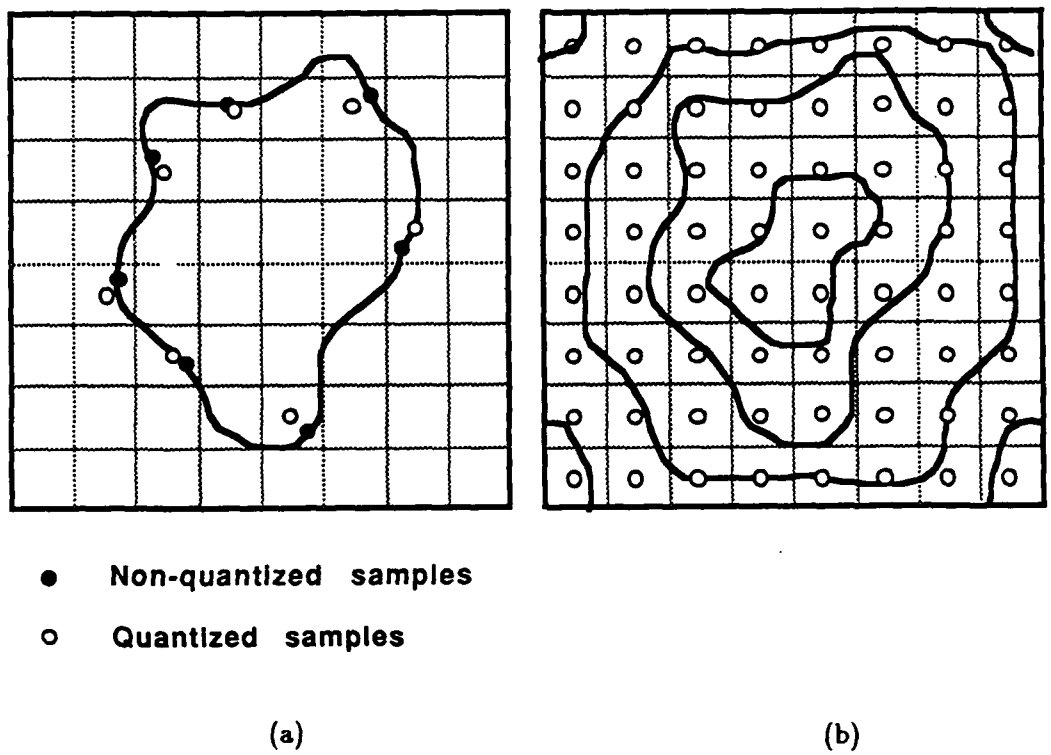

Figure 5.14: *(a) Position quantized samples obtained via implicit sampling; (b) Position quantized samples occupy all the N^2 nodes of a $N \times N$ grid if the number of thresholds are large enough.*

iteratively.

Thus, the iterative algorithm derives the amplitude range for the nodes of a $2^b \times 2^b$ grid by utilizing the quantized threshold contours. Therefore, the input to the iterative algorithm can be either represented by quantized threshold contours, or by the space domain constraint obtained from them. Indeed, as we saw in section (5.2.2), representation via the former strategy involves tracing the boundary of threshold contours, and representation via the space domain constraint involves specifying the range information for the nodes of a $2^b \times 2^b$ grid. In the case where all the contours associated with all the thresholds are used for reconstruction, the

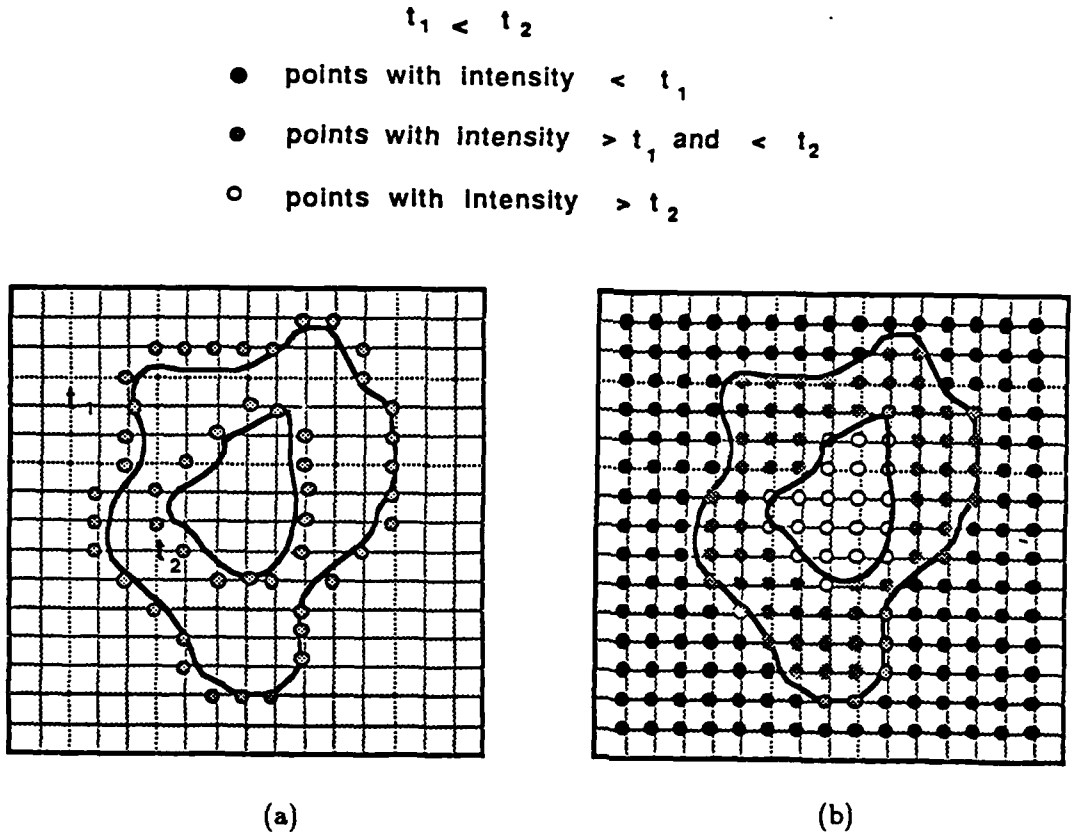

Figure 5.15: *(a) Contours corresponding to two thresholds t_1 and t_2; (b) Amplitude quantized samples derived from quantized threshold contours are identical to amplitude quantized Nyquist samples.*

intensity of each node of the grid lies in one of the $n_t + 1$ intervals defined by the n_t thresholds. Thus, as shown in figure (5.15), we can think of the nodes of the grid being amplitude quantized to $\log_2(n_t + 1)$ bits. In addition, if the size of the grid, 2^b, assumes its minimum possible value i.e. N, then our sampling set becomes identical to $\log_2(n_t + 1)$ bit amplitude quantized Nyquist samples.

5.3.2 Semi-implicit Sampling

The discussion for the semi-implicit sampling is somewhat similar to implicit sampling.

Recall from section (5.1.1) that reconstruction of an $N \times N$ signal from its crossings with n_t arbitrary functions, via the semi-implicit sampling strategy of Chapter 2, consists of the following steps:

1. Find all the crossings of the signal with the n_t crossing functions.
2. Sample the crossings along lines of rational slope.
3. Choose M samples from the intersections of the sampling lines and function crossings in such a way that conditions of Corollary (2.3) are satisfied.
4. Quantize the position of the chosen samples to b bits.
5. Reconstruct the signal from its quantized samples by finding its Fourier series coefficients.

The above process is shown pictorially in figure (5.16a). Suppose that the following conditions are satisfied:

- The crossing functions are chosen to be constants, so that function crossings become level crossings.
- The sampling lines are chosen to be horizontal or vertical and equally spaced.
- The number of reconstruction samples is N^2.
- The number of quantization bits is $\log_2 N$.

As seen in figure (5.16b), under these circumstances, the location of our N^2 position quantized samples corresponds to the nodes of a $N \times N$ grid, or equivalently the location of Nyquist samples, and their amplitudes correspond to the threshold crossing associated with them. Note that for the above conditions to hold, the number of thresholds used for reconstruction must be large enough so that each of the N horizontal (or vertical) lines contain N samples after

quantizing the x (or y) position of the samples to $\log_2 N$ bits. Thus, similar to the implicit sampling case, there seems to be a duality between the samples obtained in the above manner and $\log_2 n_t$ bit amplitude quantized Nyquist samples. However, it is important to bear in mind that these sampling sets are inherently different from each other. In Nyquist sampling, the amplitude information is quantized at the nodes of a $N \times N$ grid, whereas, in semi-implicit reconstruction from threshold crossings, the nodes of this $N \times N$ grid correspond to samples of level crossings position quantized along the sampling lines. In other words, Nyquist sampling corresponds to amplitude quantization at prespecified points, and reconstruction from level crossings corresponds to position quantization along sampling lines at prespecified amplitudes.

We will now turn our attention to the iterative algorithm of section (3.3.1). As shown in figure (5.17a) , the iterative algorithm utilizes the position quantized semi-implicit samples in order to derive the space domain constraint. Therefore, the input to the iterative algorithm can be represented either by position quantized samples, i.e. in a similar fashion to the linear least-squares and recursive approach, or by the intensity range of equally spaced points on the sampling lines. In the latter case, since all the intersections of sampling lines with the threshold contours are utilized, the intensity of the equally spaced points lie in one of $n_t + 1$ intervals defined by the n_t thresholds. In addition, suppose that the following conditions are satisfied:

- We have N equally spaced horizontal or vertical sampling lines.
- The number of equally spaced points on sampling lines, M, is equal to N.

As figure (5.17b) shows, under these circumstances, the N equally spaced samples on N horizontal or vertical lines correspond to nodes of a $N \times N$ grid, and since the amplitude of each node is in one of the $(n_t + 1)$ intervals corresponding to n_t thresholds, our sampling set becomes

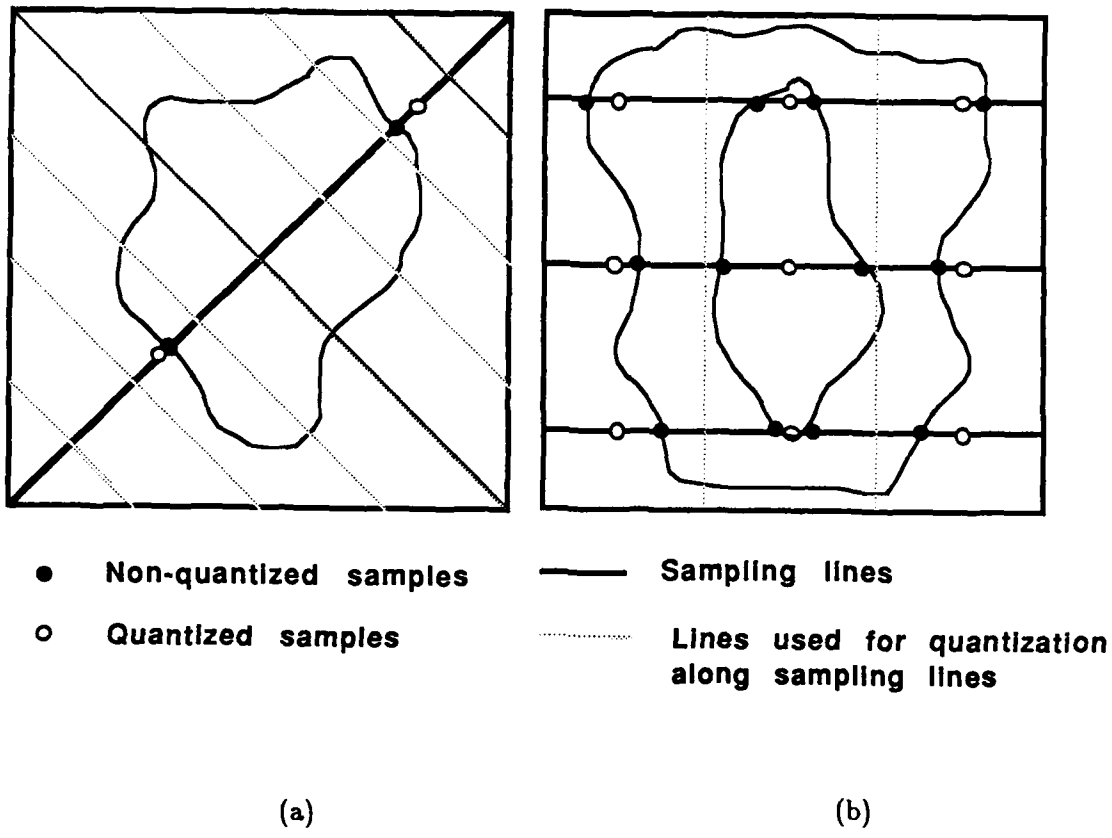

Figure 5.16: *(a) Position quantized samples obtained via semi-implicit sampling; (b) If we have N equidistant horizontal or vertical sampling lines, and the number of thresholds is large enough, the position quantized samples will occupy all the N^2 nodes of a $N \times N$ grid.*

identical to $\log_2(n_t + 1)$ bit amplitude quantized Nyquist samples.

To summarize this section, we have found conditions under which the location of position quantized samples obtained via semi-implicit and implicit sampling become identical to those of Nyquist samples. In addition, under certain circumstances, the range information used as an input to the iterative algorithms can be considered to be identical to amplitude quantized Nyquist samples. Thus, it appears that representation of two-dimensional signals via their amplitude quantized explicit samples is intimately related to their position quantized semi-implicit or implicit samples, and that reconstruction from multiple level threshold crossings has

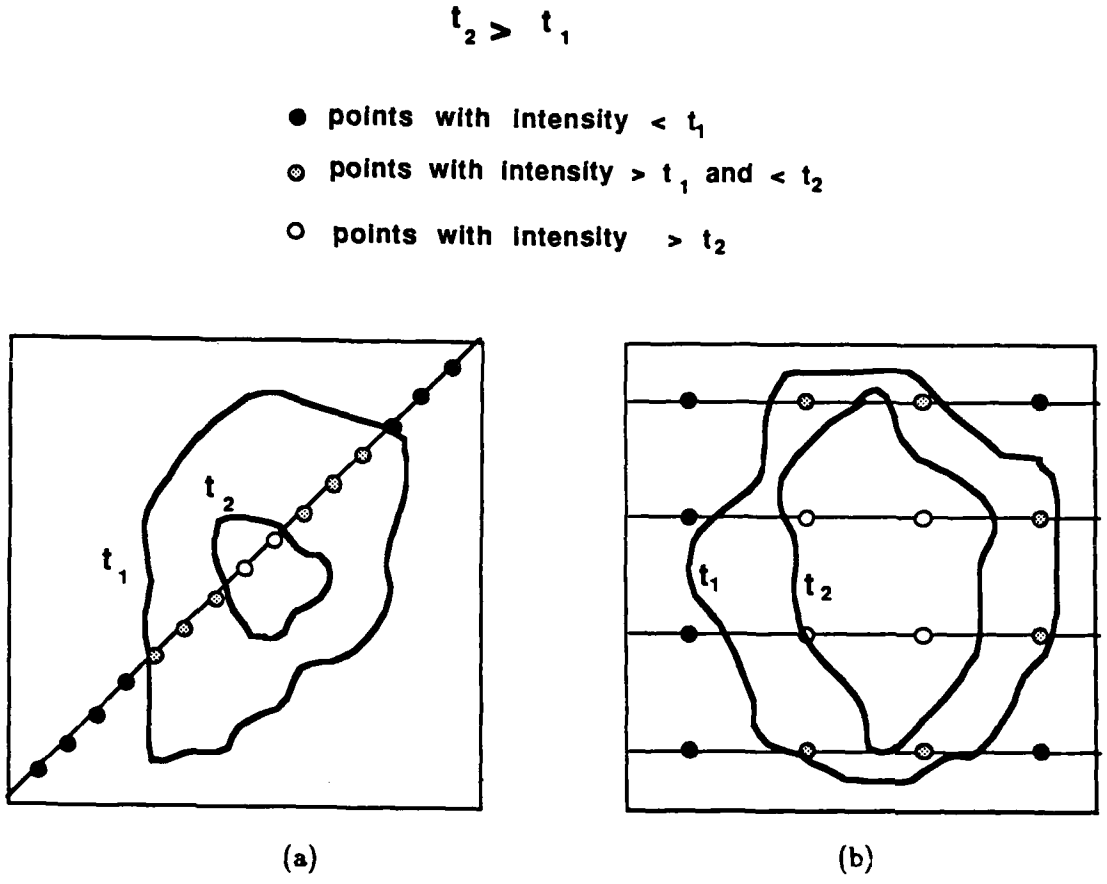

Figure 5.17: *(a) Derivation of space domain constraint for the iterative algorithm of semi-implicit sampling; (b) If we have N equidistant horizontal or vertical sampling lines, together with N equally spaced samples on each line, our sampling set corresponds to amplitude quantized Nyquist samples.*

bridged the gap between explicit, semi-implicit and implicit sampling strategies.

5.4 Summary

In this chapter, we have presented a preliminary investigation of quantization properties of various sampling and reconstruction schemes as a function of the number of thresholds. We started with the linear least-squares approach via the QR decomposition, which is our most stable reconstruction algorithm for both the semi-implicit and implicit sampling strategies.

There are a variety of factors influencing the robustness of reconstruction via the linear least-squares approach. In section (5.1.2), we found that for fixed number of thresholds and a given sampling strategy, the number of position bits is initially decreased as the number of reconstruction samples is increased from its minimum value. However, as seen in figure (5.4), increasing the number of samples beyond a certain point will merely result in an increase in total number of bits used for representing the signal. In section (5.1.3), we found that for fixed number of reconstruction samples, the quantization characteristics initially improve as the number of thresholds is increased. However, for large number of thresholds, further increase in the number of thresholds does not necessarily lead to more favorable quantization characteristics.

As far as iterative algorithms go, the "optimum" number of thresholds, which results in smallest number of position and amplitude bits, *is highly dependent on the quality of the* reconstructed images. More specifically, as seen in figures (5.9) and (5.11), for smaller values of the mean square error, the "optimum" number of thresholds is larger.

Recall that our goal in this chapter has been to demonstrate that the quantization characteristics of our sampling and reconstruction algorithms lie in between Nyquist and zero crossing sampling and reconstruction. While recovery of an $N \times N$ signal from its Nyquist samples requires minimum number of position bits, i.e. $\log_2 N$, and maximum number of amplitude bits, i.e. infinite, and recovery from zero crossings requires maximum number of position bits, i.e. infinite, and minimum number of amplitude bits, i.e. 1, the position and amplitude quantization requirements of our sampling strategies for reconstruction from multiple level crossings lie in between these two extremes. In fact, the experimental results of this chapter seem to suggest that the optimal number of thresholds, which results in minimum number of total amplitude

tion requirements of our sampling strategies for reconstruction from multiple level crossings lie in between these two extremes. In fact, the experimental results of this chapter seem to suggest that the optimal number of thresholds, which results in minimum number of total amplitude and position bits, is neither infinite, as it is with Nyquist sampling, nor is it one, as is the case with zero crossing sampling. Indeed, this optimum number depends on a variety of factors such as:

- Quality of reconstruction.
- The specific sampling strategy used i.e. semi-implicit or implicit sampling.
- The specific reconstruction strategy.
- The number of reconstruction samples.

Finally, as we saw in section (5.3), representation of two-dimensional signals via their amplitude quantized, explicit, Nyquist samples is intimately related to their position quantized implicit or semi-implicit samples. The preliminary results of this chapter seem to indicate that reconstruction from multiple level threshold crossings, has bridged the gap between explicit, semi-implicit, and implicit sampling strategies, unified seemingly unrelated sampling schemes, and provided us with a spectrum of sampling techniques for multidimensional signals.

Chapter 6

Summary, Conclusions, and Future Directions of Research

Our main goal in this thesis has been to derive sampling and reconstruction schemes whose characteristics lie in between Nyquist sampling and zero crossing sampling as proposed by Curtis [51]. As we mentioned in Chapter 1, while the required bandwidth for representing signals via their Nyquist samples is minimal, to be able to recover the signal exactly, the dynamic range or equivalently the number of amplitude bits must be infinite. On the other hand, since in representing multidimensional signals via their one level threshold crossings the location of the level crossings must be known with large accuracy, the required bandwidth is extremely large, while the dynamic range is minimum. Thus our objective has been to derive sampling strategies whose bandwidth and dynamic range characteristics lie in between these two extremes, and can be used for reconstruction of signals from their multiple level crossings.

Our approach to solving this problem has been to formulate it in terms of multivariate interpolation theory. The reasons behind this formulation are two-fold. First, BLP signals which encompass a fairly large, general class of signals, can be represented in terms of polynomials. Second, a rather large body of the mathematical results in polynomial interpolation theory can be applied directly to the problem at hand. As we mentioned in Chapter 2, although univariate

polynomial interpolation is relatively straightforward, the inherent difficulty in multivariate interpolation is the fact that unlike the univariate case, there are no Chebychef systems in R^s for $s \geq 2$. Indeed, our main theoretical results in this thesis deal with two major strategies for overcoming this difficulty.

Our first strategy, described in Chapter 2, consisted of imposing restrictions on the location of interpolation points, used for recovery of the bivariate polynomial associated with the signal under consideration. To this end, we developed several theoretical results on multivariate polynomial interpolation theory using algebraic geometric concepts. We then used these results to derive a variety of semi-implicit sampling strategies to provide us with sufficient conditions under which multidimensional BLP signals can be recovered from their non-uniform samples on lines of rational slope. To utilize these results in the context of reconstruction from level crossings, the non-uniform samples were chosen at the intersection of sampling lines with level crossings. As we saw in section (2.3), the semi-implicit sampling strategy can also be applied to a variety of other problems such as reconstruction from crossings of the signal with arbitrary functions, and reconstruction of multidimensional signals from their projections.

The major drawback of the line sampling strategy for reconstruction from level crossings is the fact that in general, we are never guaranteed to get enough intersections between the sampling lines and level crossings to satisfy the conditions of the theorems in Chapter 2. As we saw in section (3.4), although we can improve the likelihood of satisfying these conditions by careful choice of the slope and position of sampling lines, the basic problem still remains in the sense that the semi-implicit sampling strategy is incapable of reconstructing signals from an *arbitrary* number of thresholds.

To overcome the above difficulty, in Chapter 4, we proposed a second approach to the

problem of reconstruction from level crossings. While the semi-implicit sampling strategy of Chapter 2 can be applied to the more general problem of reconstruction from non-uniformly spaced samples, the implicit sampling strategy of Chapter 4 can only be applied to reconstruction from level crossings or crossings with functions, whose bandwidth lies within the bandwidth of the signal. The main advantage of the implicit sampling scheme, however, is that unlike the semi-implicit approach it can reconstruct signals from an arbitrary number of thresholds. The major result in Chapter 4 states that for almost all signals with $N \times N$ region of support in the Fourier domain, almost all $k > 0$ points from its α level crossings and $N^2 - k$ points from its β level crossings are sufficient to uniquely specify it. This result was extended to situations where the number of thresholds is larger than 2 and to the problem of reconstruction from crossings with sinusoids, whose frequencies lie within the bandwidth of the signal.

Having developed the semi-implicit and implicit sampling strategies, we then proposed a variety of reconstruction algorithms in Chapters 3 and 4. The most straightforward way of carrying out reconstructions for both the semi-implicit and implicit sampling strategies, is to solve a linear system of equations to find the Fourier series coefficients associated with the signal. We proposed two algorithms for solving the linear least-squares problem: QR decomposition and the conjugate gradient algorithm. While QR decomposition is considerably more robust than the conjugate gradient algorithm, its storage requirements for a signal with $N \times N$ region of support in the Fourier domain are of the order of N^4. We also proposed the recursive algorithm of section (3.2) in conjunction with the semi-implicit sampling strategy; the recursive approach is not storage intensive and is efficient computationally, although it is somewhat ill conditioned. To circumvent the problems associated with the recursive and linear least-squares approach, we proposed the line by line iterative algorithm of section (3.3.1) for the semi-implicit sampling

strategy, and the iterative algorithm of section (4.2) for the implicit sampling strategy. As it turns out, these iterative algorithms are relatively stable and their storage and computational requirements are not demanding.

The input requirements of the iterative algorithms however, are somewhat different from our other algorithms, since they utilize *all* the available level crossing information to derive the space domain constraint for the iterations. More specifically, the iterative algorithm of section (3.3.1) requires all the intersections of sampling lines and threshold contours, and the iterative algorithm of section (4.2) requires all the quantized threshold contours. An important feature of the iterative algorithm of section (3.3.1) is the fact that, if the number of threshold crossings on each sampling line exceeds the number of Fourier harmonics of the one-dimensional signal associated with the line, then the solution obtained via the iterative algorithm is unique, only in the limit as the number of equally spaced samples on the sampling lines, M, *tends to infinity*. Since in practice M can only be finite, the solution obtained via the iterative algorithm is only an approximate one. As far as the implicit sampling strategy goes, while the linear least-squares approach requires N^2 samples of threshold crossings in order to recover an $N \times N$ signal, the iterative algorithm requires quantized versions of all the threshold contours themselves. Similar to the semi-implicit case, the solution obtained via the iterative algorithm is unique only in the limit as the size of quantization grid approaches zero. Thus the solution obtained via the iterative algorithm with finite grid size is only an approximate one.

In Chapter 5, we presented a preliminary investigation of the quantization properties of some of our reconstruction algorithms as a function of the number of thresholds. We started with the linear least-squares approach via the QR decomposition, which is our most stable reconstruction algorithm for both the semi-implicit and implicit sampling strategies. As we

saw, there are a variety of factors influencing the robustness of reconstruction via the linear least-squares approach. In section (5.1.2), we found that for a fixed number of thresholds and a given sampling strategy, the number of position bits is initially decreased as the number of reconstruction samples is increased from its minimum value. However, as seen in figure (5.4), increasing the number of samples beyond a certain point will merely result in an increase in total number of bits used for representing the signal. In section (5.1.3), we found that for a fixed number of reconstruction samples, the quantization characteristics of the linear least-squares approach initially improve as the number of thresholds is increased. However, for a large number of thresholds, further increase in the number of thresholds does not necessarily lead to more favorable quantization characteristics. As we saw in section (5.2), the quantization properties of the iterative algorithms suggest that the "optimum" number of thresholds which results in the smallest number of position and amplitude bits is highly dependent on the quality of the reconstructed images. More specifically, as figures (5.9) and (5.11) show, for smaller values of the mean square error, the "optimum" number of thresholds is larger. It is important to mention that the results presented in Chapter 5 are rather preliminary and that the conclusions are somewhat tentative. Our hope is that these speculative results can be used as a starting point for further research in the applications of the theory to areas of multidimensional signal representation and image coding.

Recall that our goal in this thesis has been to derive sampling schemes whose bandwidth and dynamic range characteristics lie in between those of Nyquist and zero crossings sampling. While recovery of an $N \times N$ signal from its Nyquist samples requires minimum number of position bits, i.e. $\log_2 N$, and maximum number of amplitude bits, i.e. infinite, and recovery from zero crossings requires maximum number of position bits, i.e. infinite and minimum

number of amplitude bits, i.e. 1, the position and amplitude quantization requirements of our sampling strategies for reconstruction from multiple level crossings lie in between these two extremes. In fact, the experimental results of Chapter 5 seem to suggest that the optimal number of thresholds, which results in minimum number of total amplitude and position bits, is neither infinite, as it is with Nyquist sampling, nor is it one, as is the case with zero crossing sampling. Indeed, this optimum number depends on a variety of factors such as:

- Quality of reconstruction.
- The specific sampling strategy used i.e. semi-implicit or implicit sampling.
- The specific reconstruction strategy.
- The number of reconstruction samples.

Finally, as we saw in section (5.3), representation of *two-dimensional signals via their amplitude* quantized explicit samples is intimately related to their position quantized implicit or semi-implicit samples. The results of Chapter 5 seem to indicate that not only does the amplitude and position quantization characteristics of our sampling and reconstruction schemes lie in between those of Nyquist and zero-crossings, but also under certain circumstances, semi-implicit and implicit sampling strategies become a special case of Nyquist sampling. In short, reconstruction from multiple level threshold crossings, has bridged the gap between explicit, semi-implicit and implicit sampling strategies, unified seemingly unrelated sampling schemes, and provided us with a spectrum of sampling techniques for multidimensional signals.

6.1 Directions for Future Research

A wide variety of different directions are possible for expanding or extending the results of this thesis. The most natural application of the results are in the area of multidimensional signal representation and coding. As we mentioned earlier, the quantization results of Chapter 5 are rather preliminary, and most of the conclusions are somewhat tentative. However, these speculative results can be used as a starting point for a rigorous and thorough investigation of the quantization characteristics of the various sampling and reconstruction schemes presented in this thesis. Such characterization involves consideration of many coding issues, a large number of experiments and comparison to other existing coding schemes.

Our theoretical results can also be applied to the area of multidimensional signal reconstruction from projections. This problem arises in diverse fields as X-ray tomography, transmission electron microscopy, and radio astronomy. In section (2.3.2), we used Theorem (2.7) to generalize the one-projection theorem due to Mersereau and Oppenheim [45] to a ***multiple-projection*** theorem. The major problem in reconstructing bandlimited functions of order M from a single projection is a computational one, and is due to the high order of the polynomials involved. More specifically, in order to recover all M^2 samples from a single projection, it is necessary to work with a polynomial of degree greater than or equal to M^2. However, reconstruction from multiple projections at angles specified by Corollary (2.5), results in lower degree polynomials and thus, a more stable numerical problem. Extensive simulations are needed to verify this idea experimentally, and to compare it with the existing reconstruction schemes.

Our results in bivariate polynomial interpolation can also be applied to a variety of other problems. An example of such problems is multidimensional FIR filter design, where the fre-

quency response of the filter is expressed in terms of a two-dimensional polynomial. If the frequency response of the filter is specified at points located on lines of rational slope, we can apply a variety of the techniques described in Chapter 3 to determine the impulse response of the filter. Another application of the multivariate polynomial interpolation is surface interpolation from scattered data. This problem arises frequently in fields such as geology, astronomy, oceanography, and machine vision where it is necessary to recover a signal or function whose values are known along certain contours, paths, or curves. For instance in machine vision, primal sketch descriptions of several images are matched, either by stero or motion computation, to obtain a description of surface information at the zero crossings contours of the convolution of the image with the Laplacian of a Gaussian.

As we saw in section (2.3.1), the theoretical results of Chapter 2 can be used to reconstruct signals from their crossings with arbitrary functions. A potential application of this result is in the conversion of halftone images to contone ones. The halftone process has been used for more than a century to convert continuous tone pictures into a regular patterns of black and white dots which can then be printed. Mathematically speaking, the halftone version of a continuous tone image can be obtained by comparing the value of the signal with a two-dimensional periodic function, called the screen function, and producing a white or black pixel on a high contrast medium depending on whether the signal value is higher or lower than the screen function. In effect, the boundary of black and white pixels in the halftone image corresponds to the crossing of the signal with the screen function. Thus, the theoretical results of Chapter 2 can be applied to reconstruct the continuous signal from its crossings. Few examples of such reconstructions via the conjugate gradient and recursive algorithms were shown in Chapter 3. In these examples,

the screen function was chosen to be

$$A\ \{1\ +\ cos[2\pi(px\ +\ qy)]\}$$

Thus, future work must focus on the applicability of these results to more general screen functions, numerical robustness of reconstruction in practical situations, and comparison with existing conversion techniques.

As we mentioned in Chapter 1, a major drawback of reconstruction from one-level crossings is that the location of the crossings need to be known extremely accurately. This accuracy limits the applicability of reconstruction from one-level crossings in many practical situations such as image restoration. More specifically, consider an image which has undergone nonintentional nonlinear processing such as a high contrast recording medium with few intensity levels. If it is distorted in such a way as to preserve one or more of its level crossings, it is possible, at least in principle, to recover it from the level crossings of its distorted version. Since reconstruction from a single threshold needs very accurate location of the one-level crossings, successful recovery of the original image requires an extremely high resolution recording medium. However, considering the results of Chapter 5, we would expect this requirement to be substantially reduced if the original image is reconstructed from multiple level crossings of its distorted version. Thus, the spectrum of sampling/reconstruction techniques described in this thesis enables us to store/retrieve data from a wide variety of recording media with different resolution and dynamic range characteristics. Similar remarks can be made about analog communication channels with different bandwidth and dynamic range characteristics.

From a theoretical point of view, we can extend our results in a number of different ways. We have not addressed the robustness of our sampling and reconstruction schemes with re-

spect to the bandlimitedness and periodicity assumption. We would expect the level crossing contours of an almost BLP signal to be somewhat similar to the threshold contours of its bandlimited, periodic version. Further investigation is needed to determine how violations of these assumptions affect the quality of reconstruction as a function of the number of thresholds. A different problem involves finding sufficient conditions for unique reconstruction of nonperiodic signals. These conditions have already been found for the case of reconstruction from one-level crossings [51].

Finally, the results in this thesis could potentially have a major impact in the area of signal representation and manipulation. In most signal processing applications, multidimensional signals such as images are usually represented by a two-dimensional array consisting of the intensity of the signal on a square or rectangular array, with most of the processing done in the space or frequency domain. In this thesis, we have shown that multidimensional signals can be robustly represented with an arbitrary number of threshold contours or their samples. Thus, one might consider ways of processing signals in the *threshold domain* as opposed to the more conventional space or frequency domains. More specifically, signal processing operations which preserve the bandlimitedness and periodicity of the signal, can be carried out in the threshold domain by simply operating on few threshold contours of the signal in order to obtain a new set of threshold contours of the "processed" signal.

An interesting application of the above idea might be in the area of morphological analysis of images where some of the morphological operations such as erosion and dialation commute with thresholding. One way to carry out these operations on a function f, at least in principle, is to process all the level crossings of f separately in order to "build" the desired signal by stacking its level crossings. Thus, in situations where we know that the dialated or eroded

version of a signal f is bandlimited and periodic, we can perform these operations on few level crossings of f instead of all of them. Clearly, most of the above ideas are rather speculative, and further research is needed to verify them both theoretically and experimentally.

Appendix A

Proof of Theorem 3.8

In this appendix we will prove Theorem (2.4) of section (2.2.2).

Theorem A.1 *Let $l_0, ..., l_p$ be distinct curves with l_i, the ith curve given by:*

$$z = \alpha_i w^m \qquad\qquad \alpha_i \neq 0$$

where $m \leq n$ is an arbitrary integer, p is the smallest integer such that

$$\sum_{i=0}^{p} [(m+1)n - 2mi + 1] \geq (n+1)^2$$

and

$$\{(w_j^{(i)}, z_j^{i)}) | j = 0, ..., (m+1)n - 2mi; \} \tag{A.1}$$

the set of distinct points on l_i. If none of the interpolation points defined by (A.1) are equal to $(0,0)$, the common intersection of all the curves, then for any data set

$$\{t_j^{(i)} | j = 0, ..., (m+1)n - 2mi; \qquad i = 0, ..., p; \}$$

there is a unique bivariate polynomial of the form

$$p(w,z) = \sum_{i=0}^{n} \sum_{j=0}^{n} a(i,j) w^i z^j$$

such that

$$p(w_j^{(i)}, z_j^{(i)}) = t_j^{(i)} \qquad j = 0, ..., (m+1)n - 2mi; \qquad i = 0, ..., n;$$

Proof:

Our approach will be to describe a method of reconstruction of the polynomial $p(w,z)$ which satisfies the conditions described in the theorem. In the process of reconstruction, we will show

that this polynomial exists and is unique. The reconstruction algorithm consists of $p+1$ steps. We will use induction to show that in the ith step we can find the $2mi$ coefficients given by the set

$$\{a(l_1,l_2)|l_1+ml_2=(i-1)m,...,im-1,n(m+1)-im+1,...,n(m+1)\}$$

Before we start the induction, it is worthwhile to mention that sampling the bivariate polynomial $p(w,z)$ along the ith curve, l_i, which is given by

$$z=\alpha_i w^m$$

is equivalent to sampling the univariate polynomial

$$p_i(w)=p(w,\alpha_i w^m)=\sum_{r=0}^{n(m+1)} b_r^{(i)} w^r \tag{A.2}$$

where

$$b_r^{(i)}=\sum_{\substack{l_1=0\\ l_1+ml_2=r}}^{n}\sum_{l_2=0}^{n} \alpha_i^{l_2} a(l_1,l_2) \tag{A.3}$$

In the first step of the algorithm, we can use the points on the curve l_0 given by the set

$$\{(w_j^{(0)},\alpha_0 w_j^{(0)})|j=0,...,(m+1)n\}$$

together with their corresponding data set

$$\{t_j^{(0)}|j=0,...,(m+1)n\}$$

in order to find $b_i^{(0)}$ for $i=0,...,n(m+1)$. This can be done because $p_0(w)$ of equation (A.1) is a one dimensional polynomial of degree $n(m+1)$ and thus any $(m+1)n+1$ distinct samples of it are sufficient to find its coefficients. We can now use the value of the quantities

$$\{b_i^{(0)}|i=0,...,m-1,n(m+1)-(m-1),...,n(m+1);\}$$

together with equation (A.3) to find the coefficients

$$\{a(l_1,l_2)|l_1+ml_2=0,...,m-1,n(m+1)-(m-1),...,n(m+1);\}$$

As we will see later, the values of the remaining coefficients of the polynomial $p_0(w)$, which are found in the first step of the algorithm, will be used in future steps. More specifically, for $j=0,...,m-1$ the quantities $b_{i+mj}^{(0)}$ and $b_{n(m+1)-im-j}^{(0)}$ will be used in the $(i+1)$st step of the algorithm.

Having shown the validity of the induction hypothesis for the first step of the algorithm, we will now show that if in steps 1 through i the quantities

$$\{a(l_1,l_2)|l_1+ml_2=0,...,im-1,n(m+1)-im+1,...,n(m+1);\}$$

and

$$\{b_r^{(j)}|j=0,...,i;\qquad r=jm,jm+1,...,n(m+1)-jm+1;\}$$

are found, then in the $(i+1)$st step the quantities

$$\{a(l_1,l_2)|l-+ml2=mi,...,m(i+1)-1,n(m+1)-(i+1)m,...,n(m+1)-im;\}$$

and

$$\{b_r^{(i+1}|r=im,...,n(m+1)-im;\}$$

can be evaluated. Rearranging the terms in equation (A.1) we get:

$$\begin{aligned}
\tilde{p}(w,\alpha_i w^m) &= p(w,\alpha_i w^m) - \sum_{\substack{l_1=0 \\ l_1+ml_2=0,...,m-1,\, n(m+1)-im+1,...,n(m+1)}}^{n} \sum_{l_2=0}^{n} \alpha_i^{l_2} a(l_1,l_2) w^{l_1+l_2} \\
&= \sum_{\substack{l_1=0 \\ l_1+ml_2=im\,,...,n(m+1)-im}}^{n} \sum_{l_2=0}^{n} \alpha_i^{l_2} a(l_1,l_2) w^{l_1+l_2} \\
&= \sum_{r=im}^{n(m+1)-im} b_r^{(i)} w^r \qquad \text{(A.4)}
\end{aligned}$$

By hypothesis, since the point $(0,0)$ is on the intersection of all the curves $l_0,...,l_p$, it could not possibly be one of the interpolation points. Therefore we have

$$w_j^{(i)} \neq 0 \qquad\qquad j=0,...,n(m+1)-2im;$$

This implies that the points on the ith curve, l_i, given by the set

$$\{(w_j^{(i)},\alpha_i w_j^{(i)})|j=0,...,n(m+1)-2im\}$$

are sufficient to uniquely specify the coefficients

$$\{b_r^{(i)}|r=im,...,n(m+1)-im;\}$$

of the univariate polynomial given by equation (A.4). The values of $b's$ found in the $(i+1)st$ step of the algorithm together with the ones found in previous steps can now be used for finding the coefficients of $p(w,z)$. More specifically, for $j=0,...,m-1$ the quantities

$$\{b_{im+j}^k|k=0,...,i;\}$$

can be used to find the coefficients

$$\{a(l_1,l_2)|l_1+ml_2=mi+j;\}$$

Using equation (A.3) we have

$$b_{im+j}^{(k)} = \sum_{r=0}^{i} \alpha_k^r a(j+im-rm,r)$$

Since the curves $l_0,...,l_p$ are distinct, the $\alpha's$ corresponding to different curves are different from each other. Therefore the coefficients

$$\{a(l_1,l_2)|l_1+ml_2=mi+j;\}$$

can be uniquely found by solving the above Van der Monde system of equations. The same procedure can be applied for finding

$$\{a(l_1, l_2)|l_1 + ml_2 = n(m+1) - im - j;\}$$

from the quantities

$$\{b^k_{n(m+1)-im-j}|k = 0, ..., i;\}$$

Therefore we have shown that in step $i+1$ we can uniquely determine the quantities

$$\{a(l_1, l_2)|l_1 + ml_2 = mi, ..., m(i+1) - 1, n(m+1) - (i+1)m + 1, ..., n(m+1) - im;\}$$

This completes the induction and proves the theorem. It is worthwhile to mention that since in the ith step of the algorithm we find $2mi$ coefficients of $p(w, z)$, for arbitrary values of n and m, there is no guarantee that the number of interpolation points is equal to the number of the unknown coefficients. In fact unless there is an integer p such that

$$\sum_{i=0}^{p}(m+1)n - 2mi + 1 = (n+1)^2$$

we need more data points than unknown coefficients.

□

Appendix B

A Bound on the Number of Finite Common Zeros Based on Polynomial Degree

Recall that Bezout's theorem is concerned with determining the number of common zeros of two bivariate polynomials. It is restated here for convenience,

Theorem B.1 *If $p(w,z)$ and $q(w,z)$ are bivariate polynomials of total degree r and s respectively with no common factors, then there are at most rs distinct pairs (w,z) where*

$$p(w,z) = q(w,z) = 0 \tag{B.1}$$

Since Bezout's theorem is concerned with *total degree* as opposed to degree in each variable, it pertains most generally to polynomials whose coefficients have triangular support as shown in Figure B.1.

In our case of reconstruction from level crossings, this corresponds to an image which has a triangular support. On the other hand, many times one is interested in images with square or rectangular support as shown in Figure B.2.

For the case when the polynomials under consideration have rectangular support, we are able to lower the bound on the number of common finite zeros from the bound set by Bezout's

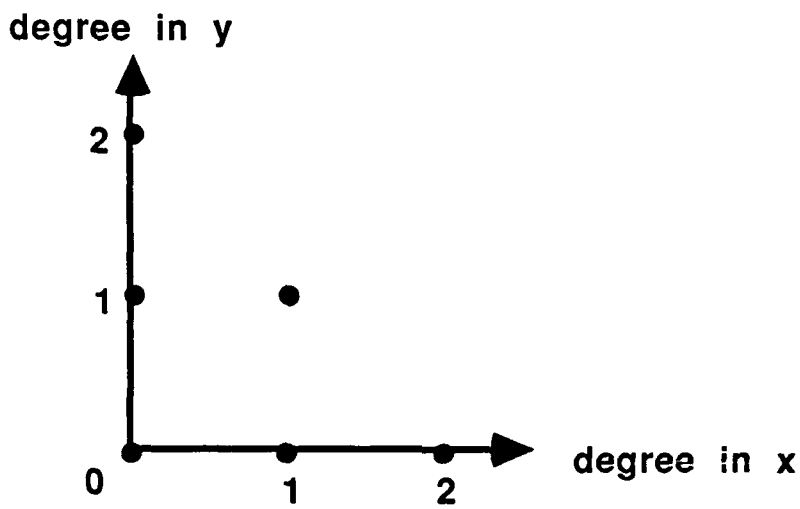

Figure B.1: *Non-zero coefficients for a polynomial of total degree 2.*

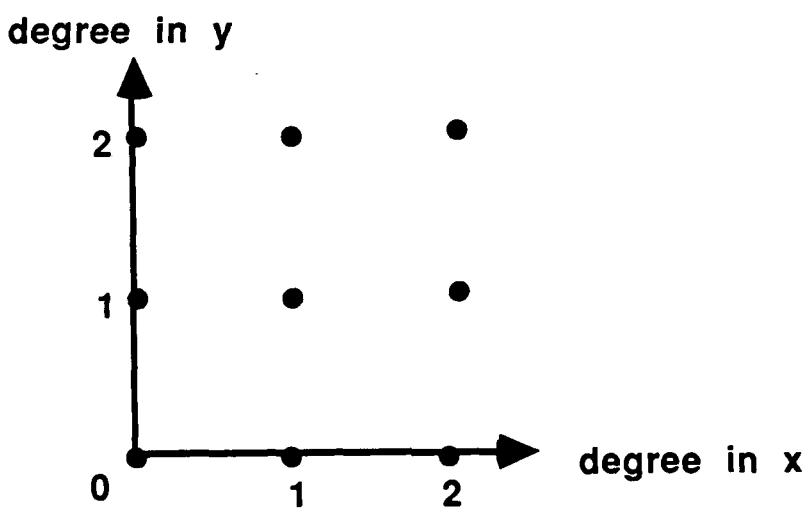

Figure B.2: *Non-zero coefficients for a polynomial of degree (2,2).*

theorem. Specifically if the two relatively prime polynomials $p(w,z)$ and $q(w,z)$ are given by

$$p(w,z) = \sum_{m=0}^{M_p} \sum_{n=0}^{N_p} p_{m,n} w^m z^n \tag{B.2}$$

and

$$q(w,z) = \sum_{m=0}^{M_q} \sum_{n=0}^{N_q} q_{m,n} w^m z^n \tag{B.3}$$

the upper bound on the number of common finite zeros set by Bezout's theorem is $(N_p + M_p)(N_q + M_q)$. Our objective is to establish a tighter upper bound on the number of common finite zeros of $p(w,z)$ and $q(w,z)$.[1]

Before proceeding, we need to review several results concerning the *resultant* of polynomials in one or two variables. The resultant R_{pq} of two one-dimensional polynomials $p(w)$ and $q(w)$

$$p(w) = \sum_{n=0}^{M_p} p_n w^n \tag{B.4}$$

$$q(w) = \sum_{n=0}^{M_q} q_n w^n \tag{B.5}$$

$$\tag{B.6}$$

is defined [37] as the determinant of the $(M_p + M_q)$ by $(M_p + M_q)$ matrix

$$\begin{bmatrix}
p_0 & p_1 & \cdot & \cdot & \cdot & \cdot & \cdot & p_{M_p} & 0 & 0 & \cdot & \cdot & 0 \\
0 & p_0 & p_1 & \cdot & \cdot & \cdot & \cdot & p_{M_p-1} & p_{M_p} & 0 & \cdot & \cdot & 0 \\
\cdot & \cdot & \cdot & \cdot & \cdot & \cdot & \cdot & \cdot & \cdot & \cdot & \cdot & \cdot & \cdot \\
\cdot & \cdot & \cdot & \cdot & \cdot & \cdot & \cdot & \cdot & \cdot & \cdot & \cdot & \cdot & \cdot \\
0 & 0 & \cdot & \cdot & p_0 & \cdot & \cdot & \cdot & \cdot & \cdot & \cdot & \cdot & p_{M_p} \\
q_0 & q_1 & \cdot & \cdot & \cdot & q_{M_q} & 0 & 0 & \cdot & \cdot & \cdot & \cdot & 0 \\
0 & q_0 & q_1 & \cdot & \cdot & q_{M_q-1} & q_{M_q} & 0 & \cdot & 0 & \cdot & \cdot & 0 \\
\cdot & \cdot & \cdot & \cdot & \cdot & \cdot & \cdot & \cdot & \cdot & \cdot & \cdot & \cdot & \cdot \\
\cdot & \cdot & \cdot & \cdot & \cdot & \cdot & \cdot & \cdot & \cdot & \cdot & \cdot & \cdot & \cdot \\
0 & 0 & \cdot & \cdot & \cdot & \cdot & q_0 & \cdot & \cdot & \cdot & \cdot & \cdot & q_{M_q}
\end{bmatrix} \tag{B.7}$$

[1]The derivation presented here is due to a collaboration between D. Izraelivitz and the author and is also described in [39].

A basic property of resultants is stated in the following theorem [37],

Theorem B.2 *When the polynomials $p(w)$ and $q(w)$ have numerical coefficients, a necessary and sufficient condition that they shall have a finite or infinite common root is that $R_{pq} = 0$.*

Consider now the two relatively prime bivariate polynomials $p(w, z)$ and $q(w, z)$, defined in (B.2) and (B.3), expressed as polynomials in w, with coefficients which are polynomials in z,

$$p(w, z) = p_0(z) + p_1(z)w + \cdots + p_{M_p}(z)w^{M_p} \tag{B.8}$$

$$q(w, z) = q_0(z) + q_1(z)w + \cdots + q_{M_q}(z)w^{M_q} \tag{B.9}$$

We can define the resultant of $p(w, z)$ and $q(w, z)$ with respect to w as the determinant of the $(M_p + M_q)$ by $(M_p + M_q)$ matrix, $M(z)$, with polynomial entries:

$$M(z) = \begin{bmatrix} p_0(z) & p_1(z) & . & . & . & . & . & p_{M_p}(z) & 0 & 0 & . & 0 \\ 0 & p_0(z) & p_1(z) & . & . & . & . & p_{M_p-1}(z) & p_{M_p}(z) & 0 & . & 0 \\ . & . & . & . & . & . & . & . & . & . & . & . \\ . & . & . & . & . & . & . & . & . & . & . & . \\ 0 & 0 & . & . & p_0(z) & . & . & . & . & . & . & p_{M_p}(z) \\ q_0(z) & q_1(z) & . & . & . & q_{M_q}(z) & 0 & 0 & . & . & . & 0 \\ 0 & q_0(z) & q_1(z) & . & . & q_{M_q-1}(z) & q_{M_q}(z) & 0 & . & 0 & . & 0 \\ . & . & . & . & . & . & . & . & . & . & . & . \\ . & . & . & . & . & . & . & . & . & . & . & . \\ 0 & 0 & . & . & . & . & q_0(z) & . & . & . & . & q_{M_q}(z) \end{bmatrix} \tag{B.10}$$

This resultant is a function of the remaining variable z and is denoted by $R_{pq}(z)$. Expanding the determinant of the above matrix and taking into account that each $p_i(z)$ and $q_i(z)$ is of degree at most N_p and N_q respectively, we can conclude that $R_{pq}(z)$ is a polynomial of degree $N_pM_q + N_qM_p$ or less. It can be shown [38], that if $p(w, z)$ and $q(w, z)$ are relatively prime then $R_{pq}(z)$ is not identically zero. Moreover, if (w_0, z_0) is a common zero of $p(w, z)$ and $q(w, z)$ then

$R_{pq}(z_0) = 0$. Thus, the zero sets of $p(w,z)$ and $q(w,z)$ have at most $N_pM_q + N_qM_p$ values of z in common.

As our argument stands, we have not yet placed any tight limit on the number of intersections of $p(w,z)$ and $q(w,z)$ since for each z_i which is a root of $R_{pq}(z)$ there could be a large number of w_j, such that for each j,

$$p(w_j, z_i) = q(w_j, z_i) = 0 \tag{B.11}$$

In order to specify the number of w_j for each z_i, we need to study the behavior of $R_{pq}(z)$ in the vicinity of each z_i.

Theorem B.3 *If at each z_0 there are k values of w, w_j, such that*

$$p(w_j, z_0) = q(w_j, z_0) = 0 \text{ for } j = 1, \cdots, k \tag{B.12}$$

then $R_{pq}(z)$ has a zero of multiplicity at least k at z_0.

The above theorem implies that $p(w,z)$ and $q(w,z)$ as defined in equation (B.2) and (B.3) have at most $N_pM_q + N_qM_p$ zeros in common.

In order to prove Theorem B.3 we need to review some results on matrices with polynomial entries, relating to the Smith Normal Form [56],

Theorem B.4 *Let $A(x)$ be an n by n polynomial matrix of normal rank r. We can find unimodular matrices $\{P(x), Q(x)\}$, such that*

$$B(x) = P(x)A(x)Q(x) \tag{B.13}$$

and

1. *$B(x)$ is a diagonal polynomial matrix called the Smith Normal Form of $A(x)$.*
2. *The first r diagonal elements of $B(x)$ are monic polynomials $p_1(x)$, $p_2(x)$, $\cdots$, $p_r(x)$.*
3. *The remaining diagonal elements, if any, are zero.*

4. $p_i(x)$ *divides* $p_{i+1}(x)$ *for* $i = 1, \cdots, r-1$.

Normal rank in the above theorem is defined in [56]. The *unimodular* polynomial matrices of the above theorem are defined to have nonzero constant determinant independent of x. Therefore, if $r = n$, i.e., if $A(x)$ has *full normal rank* then,

$$\det(B(x)) = \prod_{i=1}^{n} p_i(x) \tag{B.14}$$

Also, from part (4) of Theorem B.4 we can conclude that if $p_i(x) = 0$ then $p_k(x) = 0$ for $k \geq i$. From the above theorem, we can derive the following,

Theorem B.5 *Let $A(x)$ be a polynomial matrix of full normal rank. If $A(x_0)$ has rank deficiency of k then* $\det(A(x))$, *has a zero of multiplicity at least k at x_0.*

Proof:

Using Theorem B.4 we can find $B(x)$, the Smith normal form of $A(x)$. Since $P(x)$ and $Q(x)$ are unimodular, $B(x)$ is of full normal rank. Furthermore, the ranks of $B(x)$ and $A(x)$ at each value of x, including x_0, are equal. Therefore $B(x_0)$ has rank deficiency of k. This means that $p_n(x_0) = p_{n-1}(x_0) = \cdots = p_{n-k+1}(x_0) = 0$. Therefore, from (B.14) $\det(B(x))$ has a zero of multiplicity at least k at x_0. Since the determinant of $A(x)$ is within a constant factor of that of $B(x)$, $A(x)$ also has a zero of multiplicity at least k at x_0.

□

Using Theorem B.5, we can return to Theorem B.3,

Proof:

(Theorem B.3) Suppose that for z_0 there are k common finite zeros w_j, $j = 1, \cdots, k$ between $p(w, z)$ and $q(w, z)$. Then the matrix $M(z_0)$ defined by (B.10) must have k linearly independent null vectors given by:

$$[1, w_j, w_j^2, \cdots, w_j^{M_p+M_q-1}]^T \tag{B.15}$$

for $j = 1, \cdots, k$. Thus $M(z_0)$ has rank deficiency of k. Furthermore, since $p(w, z)$ and $q(w, z)$ have no common factors, $R_{pq}(z)$ is not identically zero, so $M(z)$ has full normal rank. From Theorem B.5 then, $R_{pq}(z)$ has a zero of multiplicity of at least k at z_0.

□

From Theorem B.3, and the fact that $R_{pq}(z)$ is a polynomial of degree $N_pM_q + N_qM_p$, we get immediately, the main result of this appendix,

Theorem B.6 *Let $p(w,z)$ and $q(w,z)$ be two polynomials of degree (M_p, N_p) and (M_q, N_q) with no common factors, then there are at most $N_pM_q + N_qM_p$ pairs of finite complex numbers (w,z) such that*

$$p(w,z) = q(w,z) = 0 \tag{B.16}$$

Appendix C

A Result in Algebraic Geometry

In this appendix, we will briefly go over few definitions, and then prove a result in algebraic geometry, which is used in the proof of Theorem (4.2).

Consider the polynomials

$$p_i(x_0, ..., x_n) \;=\; 0 \quad , \quad i = 1, ..., r$$

defining an irreducible algebraic set V over $\mathcal{K}$. Let us denote the $r \times n$ Jacobian matrix associated with V by $(\frac{\partial f_i}{\partial x_j})$. Points xt of V at which the Jacobian matrix assumes is maximum rank are called ***ordinary*** points. Any point of V which is not ordinary is said to be ***singular*** [57]. If the singular points of V are removed, we obtain a manifold whose dimension defines the ***topological dimension*** of V [1]. The dimension of a reducible algebraic set is defined to be the maximum of topological dimensions of its various irreducible components.

The complex topological dimension of $V \subset C^n$, which is defined to be the dimension of its associated complex manifold, is also given by [59]:

$$n - \max_P(\frac{\partial f_i}{\partial x_j})_P$$

[1] Precise definition of manifolds is included in [58]

where P ranges over the points in V. By definition, the real dimension of V is twice its complex dimension. For convenience, we will use the term topological dimension to denote real dimension unless specificed otherwise. If $V(R)$ denotes the real part of $V \subset C^n$, we have [60]:

$$dim_{top}V(R) \leq \frac{1}{2}dim_{top}V$$

where dim_{top} denotes the topological dimension. $V(R)$ is said to be of ***maximal*** topological dimension if its dimension is exactly half the dimension of V.

We are now ready to prove the following theorem [2] which is ultimately used in the proof of Theorem (4.2).

Theorem C.1 *Let $V \subset C^N$ be the set of complex zeros of polynomials $f_1, ..., f_r$. Then if V is irreducible and $V(R)$, the real points of V has maximal topological dimension, then $V(R)$ is Zariski dense in V. That is, every polynomial that vanishes on $V(R)$ must vanish on all of V.*

Proof:

We will prove the above result by contradiction. If a polynomial f vanishes on $V(R)$ and does not vanish on V, then let $W \subset V$ be the set of real and complex zeros of f which are in V. Since V is irreducible, and W is a proper subset of V,

$$dim_{top}W \ < \ dim_{top}V \tag{C.1}$$

Since the real part of W and V are the same, then

$$dim_{top}W(R) \ = \ dim_{top}V(R)$$

Using the above equation and the assumption of maximal topological dimension for $V(R)$, we get

$$dim_{top}W(R) \ = \ \frac{1}{2}\ dim_{top}V \tag{C.2}$$

Furthermore, as we mentioned earlier

$$dim_{top}W(R) \ \leq \ \frac{1}{2}\ dim_{top}W \tag{C.3}$$

[2]This theorem and its proof were suggested by Prof. M. Artin at MIT.

From equations (C.2) and (C.3) we conclude that:

$$dim_{top}V \leq dim_{top}W$$

which contradicts inequality (C.1).

□

Bibliography

[1] G.H. Golub and C.F. Van Loan. *Matrix Computations.* The Johns Hopkins University Press, 1984.

[2] Russell M. Mersereau. *Digital reconstruction of multidimensional signals from their projections.* PhD thesis, Massachusetts Institute of Technology, 1974.

[3] J.S. Lim A.V. Oppenheim and S.R. Curtis. Signal synthesis and reconstruction from partial fourier domain information. *Journal of the Optical Society of America*, 73(11):1413–1420, November, 1983.

[4] J.S. Lim M.H. Hayes and A.V. Oppenheim. Signal reconstruction from phase or magnitude. *IEEE Trans. Acoustics, Speech, and Signal Processing*, ASSP-28(6):672–680, December, 1980.

[5] M.H. Hayes. The reconstruction of a multidimensional sequence from the phase or magnitude of its fourier transform. *IEEE Trans. Acoustics, Speech, and Signal Processing*, ASSP-30(6):145–154, 1982.

[6] J.S. Lim P.L. Van Hove, M. Hayes and A.V. Oppenheim. Signal reconstruction from signed fourier transform magnitude. *IEEE Trans. Acoustics, Speech, and Signal Processing*, ASSP-31(5):1286–1293, October, 1983.

[7] J.L.C. Sanz and T.S. Haung. Unique reconstruction of a bandlimited multidimensional signal from phase or magnitude. *Journal of the Optical Society of America*, 73(11):1446–1450, November, 1983.

[8] A.V. Oppenheim S. R. Curtis and J. S. Lim. Signal reconstruction from fourier transform sign information. *IEEE Trans. Acoustics, Speech, and Signal Processing*, ASSP-33(3):643–657, June 1985.

[9] S. R. Curtis and A.V. Oppenheim. Reconstruction of multidimensional signals from zero crossings. *Journal of the Optical Society of America*, 4:221–231, January, 1987.

[10] S. Ullman D. Marr and T. Poggio. Bandpass chennels, zero crossings, and early visual information processing. *Journal of the Optical Society of America*, 69:914–916, 1979.

[11] F.E. Bond and C.R. Cahn. On sampling the zeros of bandwidth limited signals. *IRE Trans. Information Theory*, IT-4:110–113, 1958.

[12] H.B. Voelcker. Toward a unified theory of modulatio - part ii: zero manipulation. *Proceedings of the IEEE*, 54(5):735–755, May, 1966.

[13] A. Sekey. A computer simulation study of real-zero interpolation. *IEEE Trans. Audio and Electroacoustics*, 18(1):43–54, March, 1970.

[14] I. Bar-David. An implicit sampling theorem for bounded bandlimited functions. *Information and Control*, 24:36–44, 1974.

[15] D. Rotem and Y.Y. Zeevi. Image reconstruction from zero crossings. *IEEE Trans. Acoustics, Speech, and Signal Processing*, ASSP-34(5):1269–1277, October, 1986.

[16] JR. B. F. Logan. Information in zero crossing of bandpass signals. *Bell Syst. Tech. J.*, 56:487–510, April 1977.

[17] Yao-Ming Chao. *An Investigation into the Coding of Halftone Pictures.* PhD thesis, Massachusetts Institute of Technology, 1982.

[18] W.E.L. Grimson. A computational theory of visual surface interpolation. *Phil. Trans. R. Soc. Lond. B*, 298:395–427, 1982.

[19] D. Terzopoulos. *Multi-level Reconstruction of Visual Surfaces.* AI Memo 671, MIT, Cambridge, MA, 1982.

[20] R.W. Hjelmming. *An Introduction to Radio Astronomy Very Large Array.* National Radio Astronomy Observatory, Untited States of America, 1982.

[21] S.X. Pan and A. C. Kak. A computational study of reconstruction algorithms for diffraction tomography: interpolation versus filtered backprojection. *IEEE Trans. Acoustics, Speech, and Signal Processing*, ASSP-31:1262–1275, October, 1983.

[22] F.J. Beutler. Error-free recovery of signals from irregularly spaced samples. *SIAM Rev.*, 8(3):328–335, July, 1966.

[23] J.L. Yen. On the nonuniform sampling of bandwidth limited signals. *IRE Trans. Circuit Theory*, CT-3:251–257, December, 1956.

[24] M.R. Palmer J.J. Clark and P.D. Lawrence. A transformation method for the reconstruction of functions from nonuniformly spaced samples. *IEEE Trans. Acoustics, Speech, and Signal Processing*, ASSP-33(4):1151–1165, October, 1985.

[25] R. W. Hamming. *Numerical Methods for Scientists and Engineers.* McGraw-Hill, 1973.

[26] S. Karlin. *Total Positivity.* Stanford University Press, 1968.

[27] S. Karlin and W. J. Sudden. *Tchebycheff Systems. with Applications in Analysis and Statistics.* Interscience, New York, 1966.

[28] M. G. Krein. The ideas of p. l. chebyshev and a. a. markoff in theory of limiting values of integrals and their further developments. *AMS Transl. Ser.*, 2(12):1–122, 1951.

[29] C. A. Michelli. Algebraic aspects of interpolation. *Approximation Theory Short Course, Amer. Math. Soc.*, 1986.

[30] E.W. Cheney. *Multivariate Approximation Theory: Selected Topics.* CBMS-NSF Regional Conference Series in Applied Mathematics, 1986.

[31] G. G. Lorentz and R. A. Lorentz. Multivariate interpoltion. In E.B. Saff P.R. Graves-Morris and R.S. Varga, editors, *Rational Approximation and Interpolation*, pages 136–144, Springer-Verlag, Tampa, Florida, December 1983. Proceedings of the United Kingdom - United States Conference.

[32] K. C. Chung and T. H. Yao. On lattices admitting unique lagrange interpolations. *SIAM Journal of Numerical Analysis*, 14(4):735–743, September, 1977.

[33] M. Gasca and E. Lebron. A note on recurrence interpolation formulae for certain sets of points in r^k. *ISNM, Vol. 67, Numerical Methods of Approximation theory*, 7:77–85, 1984.

[34] R. A. Nicolaides. On a class of finite elements generated by lagrange interpolation. *SIAM Journal of Numerical Analysis*, 9(3):435–445, September 1972.

[35] F. Stenger. Kronecker product extensions of linear operations. *SIAM Journal of Numerical Analysis*, 5(2):422–435, June 1968.

[36] M. Gasca and J.I. Maeztu. On lagrange and hermite interpolation in r^k. *Numerische Mathematik*, 39:1–14, 1982.

[37] R. J. Walker. *Algebraic Curves.* New York: Springer-Verlag, 1978.

[38] A. Mostowski and M. Stark. *Introducion to Higher Algebra.* New York: Mac-Millan Co., 1964.

[39] A. Zakhor and D. Izraelevitz. A note on the sampling of zero-crossings of two-dimensional signals. Accepted for publication, March 1986.

[40] S. Ullman. *The Interpolation of Visual Motion.* MIT Press, Cambridge, Mass, 1979.

[41] D. Marr and T. Poggio. A theory of human stero vision. *Proc. R. Soc. Lond. B*, 204:301–328, 1979.

[42] D. Marr. Early processing of visual information. *Phil. Trans. R. Soc. Lond.*, 275:483–534, 1976.

[43] D. Marr. *Vision: A Computational investigation in the human representation and processing of visual information.* W.J. Freeman, San Francisco, 1981.

[44] D. Marr and H.K. Nishihara. Representation and recognition of the spatial organization of three dimensional shapes. *Proc. R. Soc. Lond. B*, 200:269–294, 1978.

[45] R.M. Mersereau and A.V. Oppenheim. Digital reconstruction of multidimensional signals from their projections. *IEEE Trans. Acoustics, Speech, and Signal Processing*, 62:1319–1338, 1974.

[46] D. C. Youla and H. Webb. Image restoration by the method of convex projections: part1 - theory. *IEEE Transactions on Medical Imaging*, 1(2):81–94, October, 1982.

[47] Ahmed Abo-Taleb and Moustafa M. Fahmy. Design of fir two-dimensional digital filters by successive projections. *IEEE Trans. Circuits and Systems*, 31(9):801–805, September, 1984.

[48] T. S. Motzkin and I. Shoenberg. The relaxation method for linear inequalities. *Can. Journal of Math.*, 6(3):393–404, 1954.

[49] Meir Feder. *Iterative Algorithms for Parameter Estimation from Incomplete Data with Applications to Signal Processing.* PhD thesis, Massachusetts Institute of Technology, 1987.

[50] William Fulton. *Algebraic Curves.* W.A. Benjamin Inc., 1969.

[51] S. R. Curtis. *Reconstruction of Multidimensional Signals from Zero Crossings.* PhD thesis, Massachusetts Institute of Technology, 1985.

[52] Monson H. Hayes. *Signal reconstruction from phase or magnitude.* PhD thesis, Massachusetts Institute of Technology, 1981.

[53] A. Vistoli. Private communication.

[54] T. S. Haung. Coding of two-tone images. *IEEE Trans. Communications*, 25(11):1406–1424, November 1977.

[55] D. N. Graham. Image transmission by two-dimensional contour coding. *IEEE Trans. Communications*, 55(3):336–346, Proceedings of the IEEE.

[56] T. Kailath. *Linear Systems.* Englewood Cliffs, NJ: Prentice-Hall, 1980.

[57] Solomon Lefschetz. *Algebraic Geometry.* Princeton University Press, 1953.

[58] Victor Guillemin and Alan Pollack. *Differential Topology.* Prentice-Hall, 1974.

[59] W.V.D. Hodge and D. Pedoe. *Methods of Algebraic Geometry.* Cambridge, 1968.

[60] Tom M. Apostol. *Mathematical Analysis.* Addison-Wesley, 1974.

DISTRIBUTION LIST

	DODAAD Code	
Director Defense Advanced Research Project Agency 1400 Wilson Boulevard Arlington, Virginia 22209 Attn: Program Management	HX1241	(1)
Head Mathematical Sciences Division Office of Naval Research 800 North Quincy Street Arlington, Virginia 22217	N00014	(1)
Administrative Contracting Officer E19-628 Massachusetts Institute of Technology Cambridge, Massachusetts 02139	N66017	(1)
Director Naval Research Laboratory Attn: Code 2627 Washington, D.C. 20375	N00173	(6)
Defense Technical Information Center Bldg 5, Cameron Station Alexandria, Virginia 22314	S47031	(12)
Dr. Judith Daly DARPA / TTO 1400 Wilson Boulevard Arlington, Virginia 22209		(1)

END
DATE
FILMED
9-88
DTIC